Electron and Hole Behavior in Powdered TiO_2 – Photoluminescence and Infrared Studies

by

Ana Stevanovic
Belgrade, Serbia

M.S., Physical Chemistry, University of Belgrade, Serbia 2008

A Dissertation presented to the Graduate Faculty
of the University of Virginia in Candidacy for the Degree
of Doctor of Philosophy

Department of Chemistry

University of Virginia
April 2014, Degree **will be Conferred**

UNIVERSITY of VIRGINIA
GRADUATE SCHOOL of ARTS & SCIENCES

Graduate Enrolled Student Office, 101 Randall Hall
P.O. Box 400773
Charlottesville, VA 22904-4773
Phone: 434-924-6741
Fax: 434-924-6737
http://artsandsciences.virginia.edu/grad/

FINAL EXAMINATION FORM

This form is to be completed by a student's department, specifically by a student's major advisory professor, to indicate that the student has passed the final defense of their thesis/dissertation. Students are responsible for making sure this form is submitted to the Enrolled Student Office by the appropriate deadline: **December 1** for December graduation, **May 1** for May graduation, and **August 1** (August graduation.)

Last Name: STEVANOVIC First Name: ANA University/SIS ID: 5 1 7 2 0 3 8 7 4

Program: CHEMISTRY (PhD) Date Final Examination Passed: 04/21/2014

***This examination is in fulfillment of the requirements for a final examination as described in the Record under the appropriate degree.**

Master's Final Examination: A candidate must achieve satisfactory standing in a final examination (oral, written or both) conducted by two or more graduate faculty members designated by the candidate's department.

PhD Final Examination: The PhD committee, chaired by the primary advisor, will consist of a minimum of four members of the graduate faculty. One member of the committee must hold a primary appointment outside of the student's department and will serve as the Dean's representative to affirm that the student has been assessed fairly and in accord with Graduate School policy. Once these minimum requirements have been met, additional committee members from within the University or other institutions may be added.

Committee Role	Name	Department	Signature
1. Major Advisor	John T. Yates, Jr.	Chemistry	
2. Other	Kevin Lehmann	Chemistry	
3. Other (PhD Only)	Ian Harrison	Chemistry	
4. GSAS Rep (PhD Only)	PEIRA REINKE	MSE	
5. Other (if applicable)			

Official or Approved Title of Doctoral Dissertation or Master's Thesis if Required by Master's Degree Program

Electron and Hole Behavior in Powdered TiO_2 - Photoluminescence and Infrared Studies.

John T. Yates, Jr.
Graduate Advisor (if no thesis, Graduate Studies Director) (Print)

Signature

04/21/14
Date

Department Chair or Representative (Print)

Signature

Date

***If Advisor is the Graduate Director, Chair Signature is required. If Chair is advisor, Graduate Director Signature is required.*

When this form has been completed, submit it to the department graduate administrator for milestone completion.

Grad Admin: After verifying title match, complete SIS Milestone PHDDEFENSE or MTHESISDEF and forward completed form to GSAS Enrolled Student Office.

GSAS: Final Exam Milestone Complete

Abstract

This thesis reports the behavior of electrons and holes in photoexcited TiO_2 powder under high vacuum conditions. We studied the effect of UV irradiation and different adsorbates, electron acceptors and electron donor molecules, on the perturbation of the band structure of TiO_2. The electron-hole recombination rate in electronically excited TiO_2 is influenced by band bending at the TiO_2 surface and was studied by photoluminescence (PL) spectroscopy. In addition, we also employed infrared spectroscopy to qualitatively estimate the surface condition and to quantitatively estimate the amount of adsorbates on the surface.

It was found that continuous UV irradiation at 3.88 eV on an n-type TiO_2 surface enhances the photoluminescence emission at ~529 nm (2.34 eV) as UV-induced surface potential causes upward bent bands to flatten. In addition, the adsorption of electron donor molecules such as CO and NH_3 caused downward band bending in TiO_2 and upon their adsorption/desorption, the PL intensity responded reversibly, showing reversible band bending. On the other hand, adsorption of an electron acceptor molecule such as O_2 induces upward band bending and does not respond completely reversibly upon desorption.

We measured the kinetics of transport of adsorbed molecules to and from the outer surface of the TiO_2 powder, in a depth of ~ 20 nm, compared to the molecular transport kinetics in the interior of a 95,000 nm thick porous TiO_2 material. Here, we employed NH_3 and CO as representatives of slow and fast diffusing molecules, respectively. Adsorption of NH_3 at the outer surface of the TiO_2 powder occurs quickly while its distribution in the powder was found to be retarded. In contrast, adsorption of CO molecule shows that the surface coverage in the first ~ 20 nm of the TiO_2 powder lags behind the surface coverage in the bulk due to the fast diffusion into

the interior of the powder. In addition, we found that adsorption/desorption of CO showed a hysteresis effect when viewed by the two spatially sensitive surface spectroscopies.

This thesis presents a new method for measuring charge transport between TiO_2 particles using an optical method, photoluminescence spectroscopy. We found that long continuous UV irradiation of the TiO_2 powder caused photoexcited electrons to percolate deep into the powder inducing changes in the surface photovoltage and band flattening as detected by PL enhancement. The main finding was that in the dark after charging by illumination, the negative charge tends to return back to the surface partially restoring upward band bending as detected by the PL intensity decrease. It was found that the relaxation of the negative charge at 140 K is a very slow process, on a minute time scale. The slow process was assigned to either electron hopping from a TiO_2 surface site to a surface site or from a TiO_2 nanocrystallite to a nanocrystallite in the TiO_2 bed. This electron hopping process is temperature-dependent with an activation energy of 15 meV. We used the rate of the discharging process to estimate the electron mobility ($\sim 10^{-10}$ m^2 V^{-1} s^{-1}) at room temperature. Further, we studied the effect of single wall carbon nanotubes and gold nanoparticles on charge transport between TiO_2 particles. We found that carbon nanotubes act as electron acceptor molecules but do not affect charge transport between TiO_2 particles. In contrast to that, ~ 3 nm gold nanoparticles supported on TiO_2 nanpoarticles act as strong electron acceptors significantly suppressing PL intensity and the buildup of surface photovoltage as measured by PL intensity change.

ACKNOWLEDGMENTS

This thesis condenses the results of research obtained from six years of work as a graduate student at University of Virginia. Although far away from home, this period has been a joyful part of my life and I would like to thank all the people who made me feel like at home.

This work would not be possible without the direction and help of my advisor John T. Yates, Jr. and many other people that I worked with at UVA. Foremost, I sincerely thank John T. Yates, Jr. for being such an enthusiastic teacher and mentor. He has been the source of incredible energy which I admire plenty. I deeply appreciate his guidance, endless patience and dedication he provided during my graduate days. I would like to acknowledge Dr. Michael Büttner for being a great source of information and for patiently teaching me about the work in surface science and ultra-high vacuum technology in the beginning years.

A special thanks to Dr. Ujjwal Raut who made my experience within and beyond the lab colorful and joyful and who enriched my graduate days with plenty of cheerful moments that will stay in my heart forever. I wish to thank my fellow graduate student Jason Navin for being my friend and for teaching me about American culture and language.

To Uros, my husband, I am so grateful for your support through all these years. Thank you for being patient and encouraging, while listening to all my frustrations during difficult times in the lab. I also wish to acknowledge my grandfather and extended family for their love and support. Ultimately, I would like to thank my parents, Vesna and Ivica and my sister Dejana, for all the sacrifices they made to have me pursue my goals. Without you all on my side, I would not be able to accomplish a fraction of this. I devote this piece of work to you all.

TABLE OF CONTENT

Chapter 1

Introduction

Semiconductor materials have attracted significant attention of the scientific and engineering community due to their superb electronic properties. There is a family of semiconductors in oxide form such as TiO_2, ZnO, SnO_2 and others[1-3] that are extensively studied as their energy band gap $E_{bg} \approx 2.0\text{-}3.2$ eV for electronic excitation allows for efficient coupling with the solar spectrum. This class of semiconductors is important for the development of solar-based technologies. These technologies mainly include: (1) sun-light activated remediation of toxic environmental pollutants through photodestruction; and (2) development of superior photovoltaic (PV) cells which convert solar light into electricity.

The subject of this thesis is focused on one particular problem related to the understanding of the behavior of photoexcited charge carriers in a semiconductor (TiO_2). It is of high importance to improve the performance efficiency of both TiO_2- based photocatalyst and photovoltaic devices which primarily depends on the efficiency of the light interaction with the semiconductor and also the charge transport through the semiconductor.

1.1 TiO_2- based Photoactivation Technologies

In this thesis, we study titanium dioxide (TiO_2) in the context of a candidate semiconductor for the aforementioned technologies, as it is robust and inexpensive material that has enormous surface area for adsorption of foreign molecules in its commercially-available form and more importantly, it has a band gap of ~ 3.0 - 3.2 eV for sun-light activation. These characteristics make TiO_2 an excellent photocatalyst, which can be activated via absorption of

the ultraviolet (UV) photons ($\lambda < 390$ nm) of the solar spectrum. Fujushima and Honda used this photocatalytic property of TiO_2 to generate hydrogen and oxygen gas from solar-induced water splitting in a photo-electrochemical cell[4]. Further research on TiO_2 was extended toward water and air purification and also environmental remediation where photo-oxidation of contaminants was the main process studied[5, 6] . In photovoltaic area, upon the development of Grätzel solar cell, which is based on a dye-sensitized TiO_2 electrode excited by sunlight[7-11], TiO_2 became a more popular photo-absorbing material.

This thesis summarizes studies of: (1) The band bending phenomenon in powdered TiO_2 by photoluminescence spectroscopy (Chapter 3); (2) Molecular diffusion by photoluminescence and infrared spectroscopy (Chapter 4); (3) Electron hopping between TiO_2 particles (Chapter 5) and (4) Effect of fullerene and Au nanoparticles on photoluminescence and electron hopping between TiO_2 particles (Chapter 6).

1.2 Electrons and Holes at Work in Photoexcited TiO_2

An important process that determines the performance of these solar-driven devices is the recombination of the electrons and holes in photoexcited TiO_2 powder. In fields of photocatalysis and photovoltaic cells, understanding charge transfer/transport between electronically excited TiO_2 particles and adsorbed electron acceptor/electron donor molecules is vital for: (1) photo-oxidation reactions; and (2) the efficiency of operation of PV cells. The main factor that limits the improvement of the efficiency of operation of TiO_2 photocatalyst and TiO_2-based photovoltaic cell is the recombination of photo-excited electrons and holes in electronically excited TiO_2 powder. A schematic picture of photo-excitation and de-excitation events in TiO_2 is shown in Figure 1. The process of recombination is usually followed by emission of radiation or

heat when photoexcited electrons cascade down to the bottom of the conduction band losing their energy, ultimately finding a defect site within the band gap where they react with a hole.

The research presented in this thesis investigates the factors that affect the electron-hole (e^--h^+) recombination in TiO_2 powder [processes (1) and (3) in Figure 1.]. The overarching goal of this work is to present novel methods to reduce the fraction of electrons and holes that undergo useless recombination by modifying TiO_2 surface with electron acceptor molecules (O_2, Single Wall Carbon Nanotubes (SWNT), SF_6, Au nanoparticles) and electron donor molecules (CO, NH_3, H_2, C_3H_8).

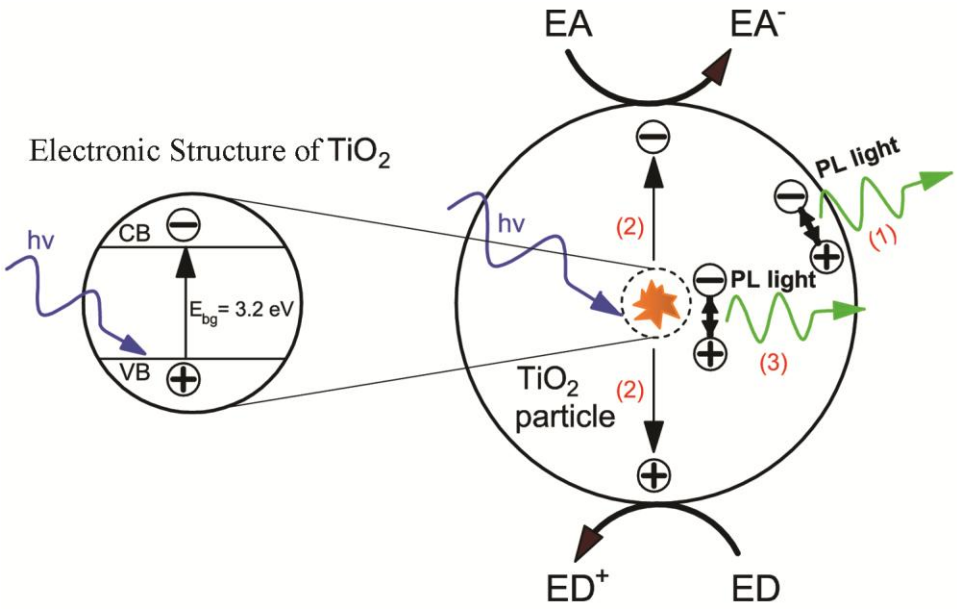

Figure 1. An incident photon on TiO_2 produces an exciton (excited electron coupled to a positive center) which quickly evolves into an electron-hole pair. These charge carriers then evolve in one of the following ways: (1) they can diffuse onto the surface and recombine, (2) react with other electron acceptor or electron donor molecules adsorbed on the surface, or (3) recombine in the bulk of the material.

These studies of electron-hole recombination in TiO_2 powder are performed in a newly constructed high vacuum apparatus with a base pressure of 1.5 x 10^{-9} Torr **(more details in Chapter 2)** which employs: (1) photoluminescence spectroscopy (PL) that serves for directly observing the e^-- h^+ recombination process; and (2) transmission infrared (IR) spectroscopy that serves for estimating the amount of adsorbates on the TiO_2 surface, as well as understanding the chemical bonding modes of molecules on the surface. The apparatus consists of a portable high vacuum cell equipped with turbopump, various pressure gauges and a quadrupole mass spectrometer as well as a quantitative provision for gas dosing. The cell houses an optically transparent tungsten grid which holds the sample that can be cooled to 83 K using ℓ-N_2. It can also be resistively heated to 1000 K. We stress the need to employ high vacuum conditions where the surface of the semiconductor may be freed of adsorbed contaminants.

We have studied the effects of UV irradiation and adsorption of different electron donor or electron acceptor molecules on the electronic structure of TiO_2. We found that both absorption of UV light and adsorption of electron acceptor or electron donor species induce changes in the work function of TiO_2 which results in band bending of the conduction and valance bands. These processes were studied through PL by directly observing recombination of charge carriers. It is of importance to understand how the band bending in solid materials can be manipulated and optimized for purposes of improving both PV cells and photocatalysts. In PV cells, band bending influences the charge transport process between solid-solid interfaces while in photocatalysis, the band bending phenomenon governs the rates of photo-oxidation or photo-reduction reactions when electron or hole is promoted to a surface.

1.3 Band Bending in Semiconductors

The presence of defects and impurities in semiconductors are responsible for changes in electronic structure as they produce filled and unfilled electronic states within the band gap of a semiconductor. A semiconductor surface also possesses defects where the periodicity of the semiconductor lattice is broken (missing atoms, interstitials) at the surface due to the solid-vacuum boundary[12, 13]. These surface defects perturb the local band structure as they can carry both negative or positive charge depending on the type of defect (acceptor or donor, respectively) and the Fermi level. The charge present in a surface state is screened by an opposite image charge induced inside a semiconductor. As a result, conduction and valence bands at a surface of a semiconductor bend forming a space charge layer. In other words, the band bending represents the change in the potential energy of an electron at the surface and in the bulk of a semiconductor. For instance, the defects that carry negative charge on a semiconductor surface induce upward band bending that produces a space charge layer called a depletion region. This type of semiconductor is called n-type (Figure 2a). On the other hand, a defect that carries positive charge causes downward band bending and a space charge layer called the accumulation layer. This type of semiconductor is called a p-type semiconductor (Figure 2b).

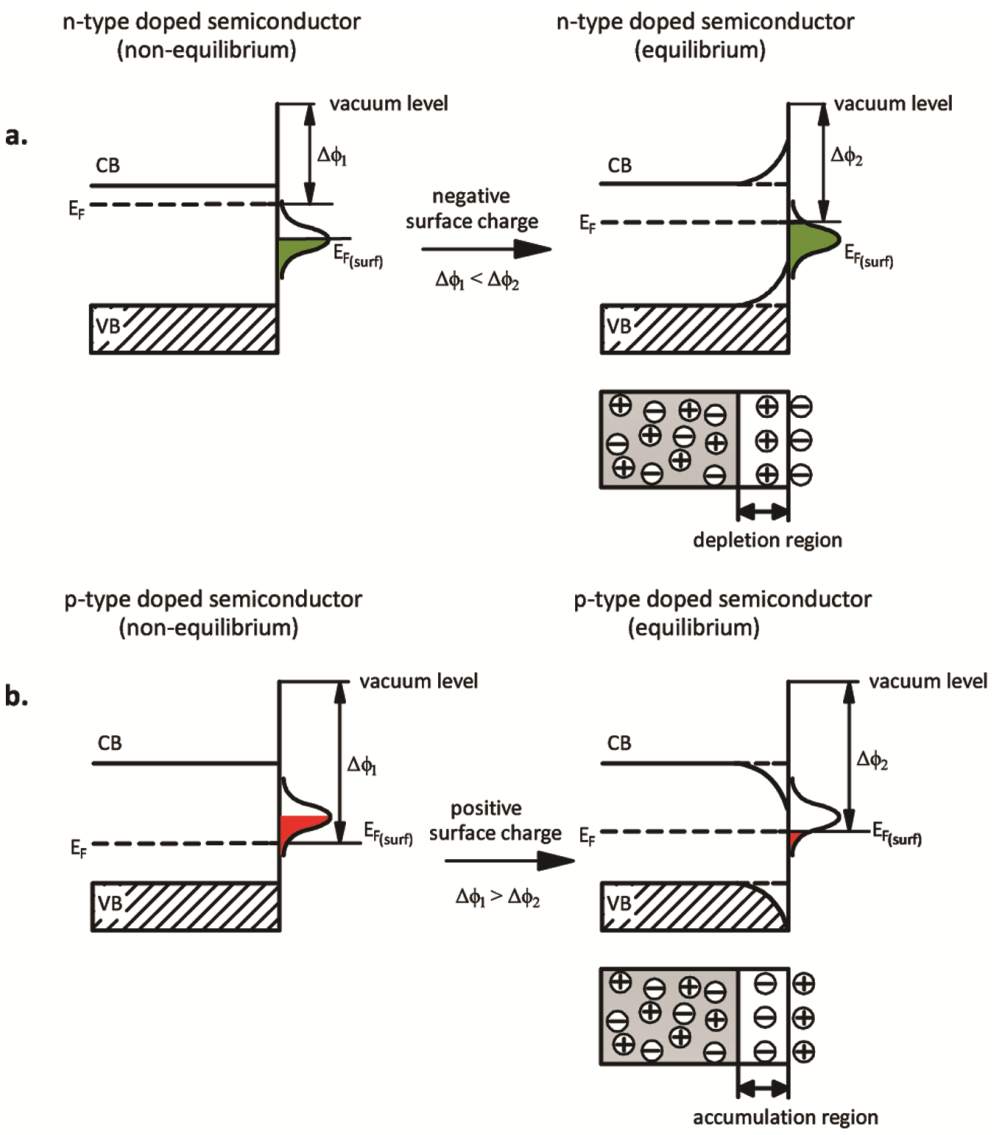

Figure 2. The change in work function ($\Delta\phi$) and band bending (eV_{BB}): (a) Upon adding a negative charge to a surface, the work function increases inducing upward band bending producing an n-type semiconductor; (b) Upon adding a positive charge to a surface, the work function decreases inducing downward band bending and producing a p-type semiconductor.

1.3.1 Origin of Band Bending in TiO_2

The surface of the powdered TiO_2 employed in this work is nonstoichiometric as we create defects by applying cleaning procedures where the sample is annealed in vacuum to high temperatures resulting in oxygen loss. Also the mixture of crystallographic phases exists due to the polycrystalline character of the TiO_2 powder where anatase and rutile coexist in 3:1 anatase/rutile ratio. It has been previously observed by STM[14-16], TPD[17] , XPS[18] and theoretically[19, 20] that upon annealing to 700-800 K, two types of surface TiO_2 defect sites are created: interstitial Ti^{3+} sites and oxygen vacancies. Figure 3A shows a schematic of atomic structure of the most studied rutile -reduced TiO_2 (110) surface[21]. The formation of both types of defects results in excess electrons on the TiO_2 surface. Upon lattice oxygen desorption from the bulk or surface of TiO_2 and/or the reduction of Ti^{4+} to Ti^{3+}, excess electrons are trapped at a vacancy site. This accumulated negative charge on a TiO_2 surface induces upward band bending (increase in surface potential of electrons at the near surface) and maybe thought of as a change in work function ($\Delta\phi$). Thus, oxygen-deficient TiO_2 is an n-type semiconductor. Figure 3B shows a schematic picture of the conduction band, Ti^{3+} defect site, oxygen vacancies and valence band. Figure 3C shows the STM image of a reduced TiO_2 (110) surface where the bright spots (circled in black) are O-vacancies.

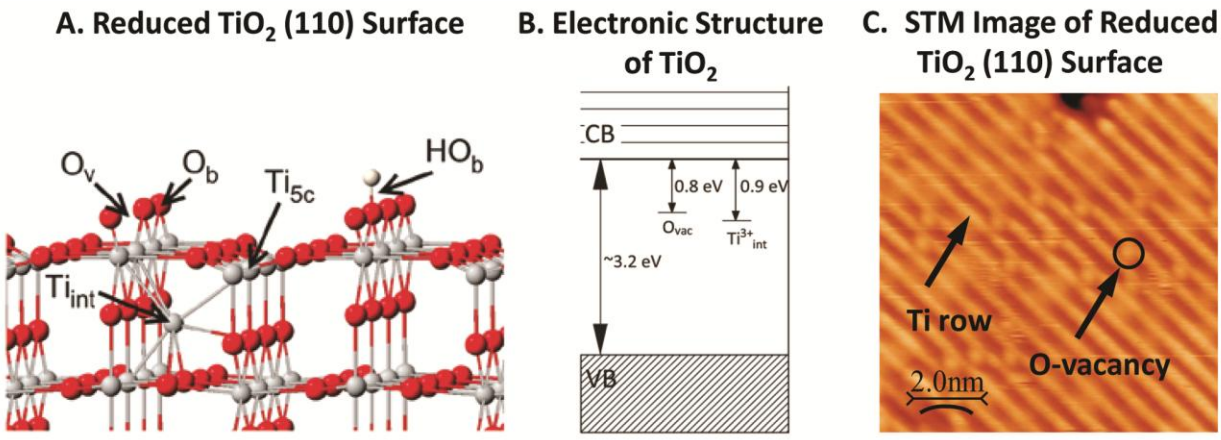

Figure 3 A. Atomic structure of defective TiO_2 (110) surface. Oxygen atoms are depicted in red and titanium atoms are in white. **2 B.** Schematic representation of energy levels of the most common defects O-vacancy and Ti^{3+} interstitials in TiO_2[20]. **3 B.** STM image of a reduced TiO_2 (110) surface shows both Ti atoms (bright rows) and oxygen vacancies (bright spots)[22].

1.3.2 Bend-Banding Model in Nanosized TiO_2 Particles

The TiO_2 used in this thesis is a polycrystalline powder that consists of 75 % anatase and 25 % rutile phases with particles between 30 - 80 nm in size. The band bending phenomenon has been observed in a single crystal as well as on the surface of the nm-sized TiO_2 powder. These nanoparticles also show a lack of stoichiometry which is responsible for the excess negative charge on their surfaces causing the band bending as detected by means of surface photovoltage spectroscopy (SPV)[23, 24] and also, PL spectroscopy[25, 26]. The potential distribution in spherical nanoparticles with radius r_0, was first described by Albery and Bartlett[27] employing the Poisson-Boltzmann equation. The potential difference (the band bending (V_{bb})) at distance r from the center of the particle is given by equation (1):

$$V_{bb}(r) = -\frac{k_B T}{6e}\left[\frac{r-(r_0-D)}{L_D}\right]^2\left[1+\frac{2(r_0-D)}{r}\right] \qquad (1)$$

where D is the depletion length, r_0 is a particle radius, L_D is the Debye length ($L_D = (\varepsilon_0 \varepsilon_r k_B T/e^2 N_d)^{1/2}$, ε_0 is vacuum permittivity, ε_r dielectric constant of the material, N_d is the dopant concentration. For **small particles** with r_0=D, where D is the depletion layer thickness, the above equation reduces to:

$$V_{bb}(r_0) = -\frac{k_B T}{6e}\left(\frac{r_0}{L_D}\right)^2 = \frac{e r_0 N_d}{6\varepsilon_r \varepsilon_0} \qquad (2)$$

For **large particles** with $r_0 > D$, equation (1) can be written as:

$$V_{bb}(r_0) = -\frac{k_B T}{2e}\left(\frac{D}{L_D}\right)^2 = \frac{e N_d D^2}{2\varepsilon_r \varepsilon_0} \qquad (3)$$

Equation (2) and (3) show that the degree of band bending in nanosized particles depends on the size of the particle, dopant concentration and dielectric constant of a solid material. For TiO_2 nanoparticles, the Debye length, L_D, is ~ 4-12 nm, where $\varepsilon_r \approx 31$[28] (anatase) and $\varepsilon_r \approx 100$ (rutile)[29] and $N_d \approx 10^{24}$-10^{25} m^{-3} [30].

This work employs TiO_2 particles with a nominal diameter of ~ 50 nm. To validate the existence of band bending phenomenon in our particles, we employ equation (3) for large particles to estimate the thickness of the deletion layer region. The estimated depletion layer thickness, by assuming a value of 0.1- 0.4 V band bending[31], is D ~ 6-12 nm which is much smaller than the size of one of our TiO_2 particles **(see Appendix 1)** justifying the idea of band bending in the nm-sized particles.

Figure 4 shows that the band bending phenomenon is more prominent in large than in small nanoparticles. For instance, large nanoparticles (d > 10 nm) show a higher degree of band bending, V_{BB} ~ 0.1-0.4 eV[31] while V_{BB} in small nanoparticles (d < 10 nm) is in the order of a several meV[9, 26, 32].

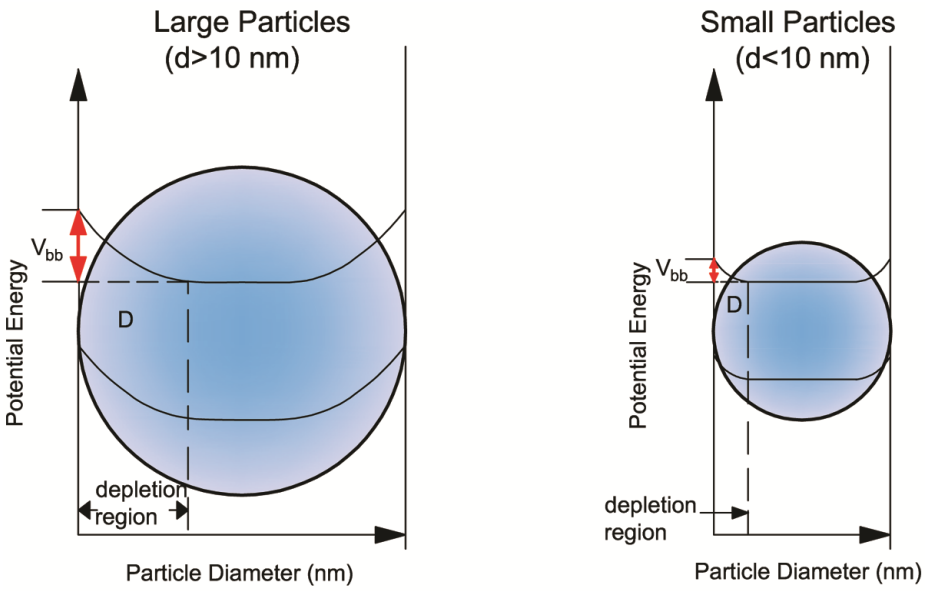

Figure 4. Schematic picture of band bending in large and small nanoparticles.

1.3.3 Light-Induced and Adsorbate-Induced Bend Banding in Semiconductors

Irradiation-induced changes in the electronic structure (band bending) of semiconductors at the surface have first been measured by means of surface photovoltage spectroscopy (SPV). The non-destructive SPV techniques measure the changes in surface potential without direct contact with the surface. One of the SPV techniques that directly measures changes in the work function ($\Delta\phi$) (which is equal to changes in surface band bending (eV_{bb})) is Kelvin probe spectroscopy. Kronik et al.[23, 24] and others[26, 32-35] reported irradiation-induced changes in band bending in TiO_2 particles by means of surface photovoltage measurements. They found that continuous supra-band gap irradiation flattens the originally upward bent bands in n-type TiO_2 particles as shown in Figure 5.

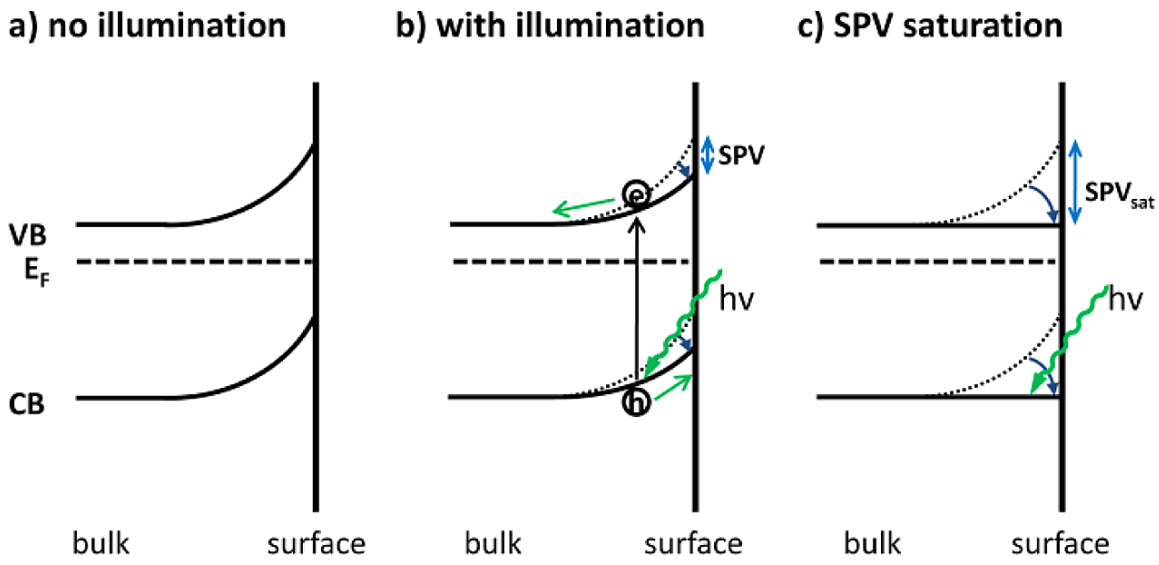

Figure 5. Light-Induced band bending and photovoltage effect. (a) Upward band bending in an n-type semiconductor; (b) Charge carrier separation upon absorption of light causing reduced bend bending due to the favorable hole transport to the surface; (c) Continuous irradiation by light induces a flat-band condition and maximum SPV signal[32, 34] .

On the other hand, modification of a semiconductor surface by adsorption of electron acceptor and electron donor molecules was found also to induce changes in electronic structure of the semiconductor which has been detected by PL spectroscopy. Sites et al.[36] and others[37-39] describe the sensitivity of photoluminescence emission upon adsorption of different molecules. Here, the change in PL emission is explained by the "dead-layer model". In brief, this model recognizes band bending at a surface of a semiconductor where a dead-layer is formed within the region where the bands are bent (Figure 6). Here, photo-excited electrons and holes are swept away from each other as they are driven by the built-in potential and PL emission from the dead-layer region is therefore suppressed. Excitation light is absorbed exponentially with depth in the TiO_2 with an absorption coefficient α which is wavelength-dependent. The photoluminescence

emission originates from the region beyond the depth of the band bending where a fraction of the incident excitation light is deposited.

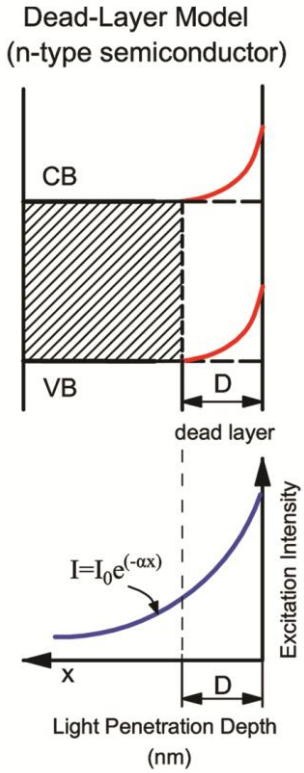

Figure 6. Schematic of the dead-layer model. Band structure of an n-type semiconductor and its corresponding penetration depth profile for excitation irradiation.

Adsorption of electron donor or electron acceptor molecules on a semiconductor surface causes the dead-layer thickness to change and thus causing a change in the intensity of PL emission. Ellis et al. [37-39] studied the change of the dead layer thickness upon adsorption of different amines on n-type CdSe single crystal in a N_2 atmosphere at room temperature (as shown in Figure 7a). They found that the depletion layer thickness reduces by ~ 20-100 nm upon adsorption of different amines as these molecules act as positive charges on a surface due to their electron donor properties. The final result was band flattening of the originally upward bent bands and an increase in PL intensity.

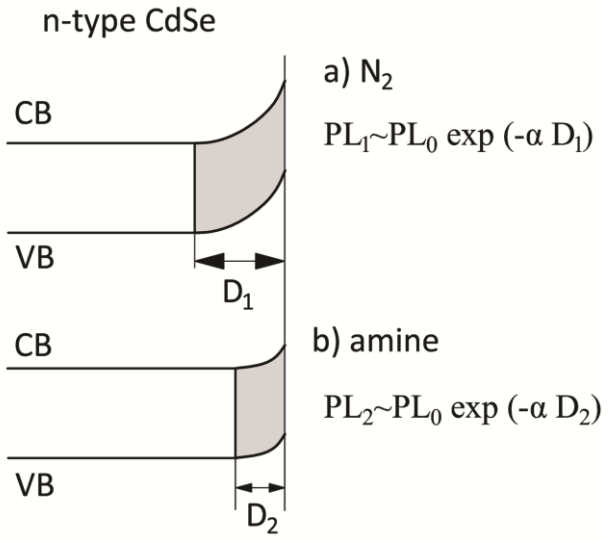

Figure 7. The electronic structure of n-type CdSe single crystal for (a) a high degree of upward band bending in a nitrogen (N_2) atmosphere- reference condition; for (b) a decrease in band bending upon introduction of different adsorbed amines at room temperature. PL_0= photoluminescence intensity for a flat band condition.

There are only a few studies of the electron-hole recombination process in semiconductor nanoparticles or single crystals that are performed under highly controlled conditions in vacuum. Anpo et al.[40-42] studied band bending on both TiO_2 and ZnO nanoparticles under vacuum (P~ 10^{-6} Torr) conditions at liquid nitrogen temperatures. They found that PL intensity decreases irreversibly upon adsorption of oxygen. The adsorbed O_2 acts as electron acceptor forming a negatively charged layer on a surface, which causes upward band bending and suppression of the PL signal. They also found that the formation of positively charged species (unsaturated hydrocarbons, H_2O and H_2) via electron donation to the TiO_2 surface resulted in an enhancement of PL intensity. Idriss et al.[43, 44] studied photoluminescence of ZnO in both powdered and single crystal form under vacuum conditions at room temperature. They reported changes in PL emission of ZnO upon adsorption of O_2, H_2 and CO at high pressures (~ 100 Torr).

1.4 Effect of UV Light and Adsorbates on Photoluminescence of TiO_2

Much of the previous PL literature on semiconductor surfaces were done in poorly-controlled, ambient atmosphere conditions[45-55] in contrast to the work presented in this thesis which is performed using high vacuum techniques under carefully controlled surface conditions. Here, we found that PL spectroscopy is an extremely sensitive tool for studying both: (1) irradiation-induced; and (2) adsorbate-induced changes of electronic structure in powdered TiO_2 under highly controlled conditions at liquid nitrogen temperatures[56] **(as described in Chapter 3)**. In all the experiments presented here, the surface of the TiO_2 is free of hydrocarbons, hydroxyl groups and other impurities as determined by transmission IR spectroscopy. The effect of UV irradiation and adsorbed molecules on the band structure of powdered TiO_2 was studied by directly observing the emission irradiation at 2.34 eV (~ 530 nm) resulting from electron-hole recombination processes under controlled gas adsorption or vacuum conditions. Our approach, combining PL and IR spectroscopy is unique to the field at this time.

We report that the PL effect is enhanced by exposure to UV irradiation which converts n-type TiO_2 (upward band bending) to a flat-band condition as shown in Figure 8, producing a positive surface photovoltage.

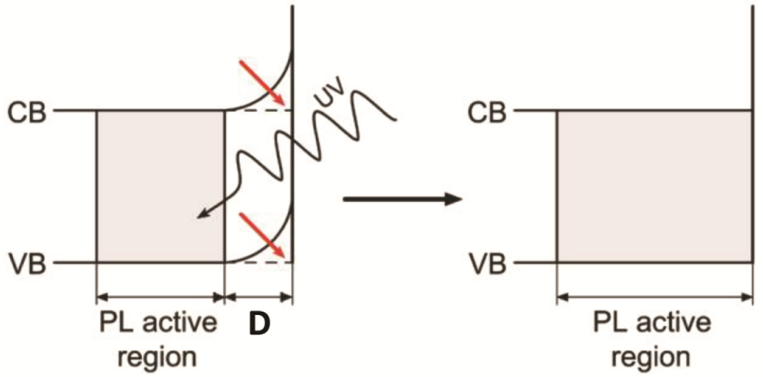

Figure 8. Continuous UV irradiation of n-type TiO_2 induces band flattening as the thickness of the depletion layer region reaches zero, D→0.

In addition, we found that by adding adsorbates (electron-donor or electron-acceptor molecules) in a controlled manner, PL emission is affected as the adsorbed molecules exchange charge with the TiO_2 surface producing a change in the surface band structure **(as described in Chapter 3)**. The development of surface coverage (up to a monolayer) of adsorbates is observed by IR spectroscopy. Adsorption of molecules causes the rearrangement of electronic charge within the surface region adding surface dipoles which induce changes in the work function and band bending of a semiconductor. We found that an electron acceptor molecule such as O_2 induces upward band bending on TiO_2 surface and significantly suppresses the electron-hole recombination in TiO_2. This negative change in PL emission is partially reversible upon O_2 removal. Also, we found that the rate of development of surface photovoltage during exposure to UV irradiation is retarded as the partial pressure of O_2 increased. We also reported that adsorption of CO and NH_3 molecules acting as electron donor molecules and inducing downward band bending causes the PL to respond oppositely to O_2-acceptor adsorption. These molecules adsorb/desorb reversibly at 120 K as observed by the change in PL intensity.

Figure 9A depicts adsorption of an electron acceptor molecule (EA) on the n-type TiO_2 surface. As an electron acceptor molecule such as O_2 approaches the TiO_2 surface, an unfilled

molecular orbital of the EA molecule interacts with the TiO_2 semiconductor and as a result, the energy of the molecular orbital shifts toward the Fermi level of TiO_2. This allows electrons from the TiO_2 surface to transfer to the acceptor O_2 molecule. As a result, an outwardly-negative dipole layer forms on the TiO_2 surface (Figure 9C). This formation of the surface dipole induces an increase in the work function causing upward band bending in TiO_2 as shown in Figure 9B. On the other hand, upon adsorption of an electron donor molecule on the TiO_2 surface, electrons from the donor molecule transfer to the surface forming an outward positive surface dipole which induces downward band bending at the surface of TiO_2.

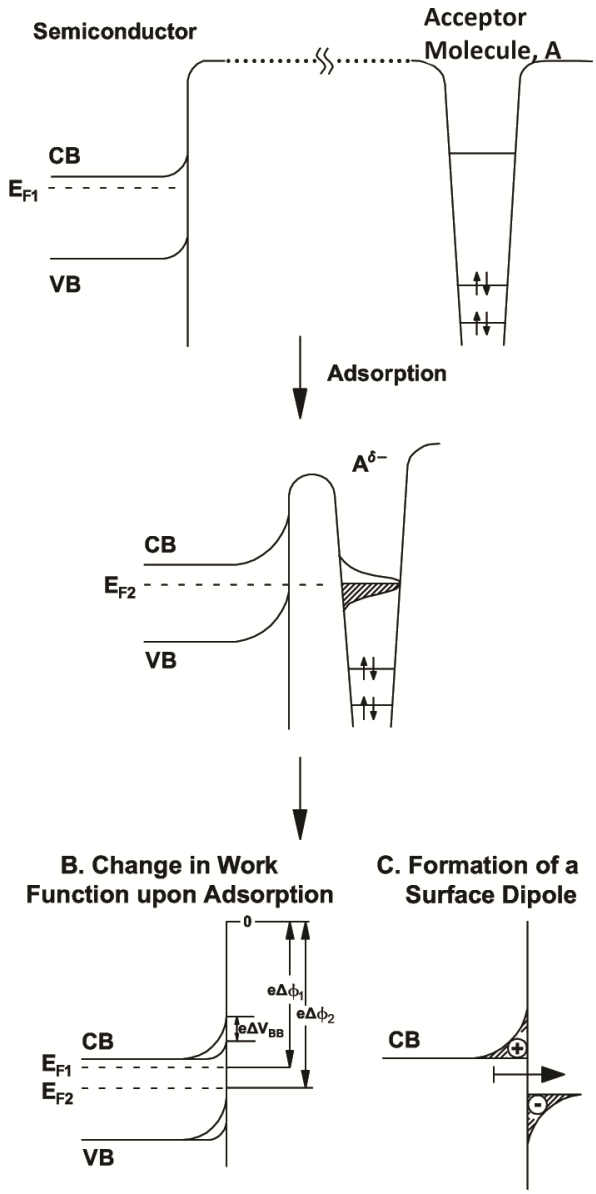

Figure 9. A. Changes in electronic structure upon adsorption of an electron acceptor molecule on a TiO_2 surface; B. Change in the work function, $\Delta\phi$, upon adsorption; and C. Formation of a surface dipole upon adsorption. The acceptor level in EA is broadened by the interaction with the surface.

1.5 Photoluminescence and Infrared Spectroscopy of TiO_2 Powders-Application to the Study of Molecular Diffusion in the Powder.

We found that the combination of the two surface spectroscopies (PL and IR) to be highly informative about molecular diffusion through the depth of the powder as it allows one to observe the kinetics of transport of adsorbate molecules (CO and NH_3) between the outermost surface (~20 nm) region (observed exclusively by PL) and the interior of the TiO_2 powder (observed by deeply penetrating IR irradiation)[57] **(as described in Chapter 4)**. Here, the PL spectroscopy provides information about the adsorbate surface coverage development in the first ~ 20 nm of TiO_2 powder where UV absorption and PL occur, while IR spectroscopy samples through the entire powder thickness (0.0095 cm thick) providing information of the behavior of adsorbates there. The transport into porous TiO_2 powder is governed by the surface mobility of adsorbed molecules. For instance, temperature programmed desorption measurements revealed the activation energies for both NH_3 and CO desorption from TiO_2 to be E_d= 92 kJ mol^{-1} [58-60] and E_d= 49 kJ mol^{-1} [61], respectively. At the isothermal temperature (120 K) of the diffusion measurements, the Boltzmann factor, $e^{-\frac{E_d}{RT}}$, for CO molecule is 1000 times larger than for NH_3 indicating that CO has higher desorption rates (and mobility) than NH_3. For highly mobile molecules such as CO, both spectroscopies show similar development of the adsorbed layer in both the 20 nm region (detected by PL) and throughout the entire powder (detected by IR). In contrast to that, for low mobility species such as NH_3, the PL development shows a monolayer completion in 20 nm region long before the NH_3 diffusion occurs into porous TiO_2 powder as judged by slow IR development. The transport governed by the surface mobility of the adsorbate molecule (CO) showed a hysteresis effect during the adsorption/desorption processes.

1.6 Electron Transport through TiO_2 Particles

This work presents a new method for measuring charge transport between TiO_2 particles using an optical method such as PL spectroscopy[62] **(as described in Chapter 5)**. The main discovery here is that continuous UV irradiation on an n-type TiO_2 electrically charges the TiO_2 powder by the transport of the hole to the surface (the photovoltage effect). In the dark, the powder discharges as negative charge relaxes back to the TiO_2 surface. The relaxation of negative charge back to the surface is found to be a very slow process on a minute time scale in contrast to *in situ* transport processes within single TiO_2 particles which occur on a picosecond time scale in crystalline TiO_2 [63]. The slow migration is assigned to either electron hopping from a TiO_2 surface site to surface site, or from nanocrystallite to nanocrystallite in the TiO_2 matrix. We used the rate of the discharging process to estimate the electron mobility (~ 10^{-10} m^2 V^{-1} s^{-1}) between TiO_2 particles at 300K **(see Appendix 2)**. It was also found that this electron hopping process is temperature-dependent with an activation energy of 15 meV.

Further, we investigated the role of a mixture of semiconducting and metallic single wall carbon nanotubes (SWCNT) and a conjugated linker molecule such as 1, 2- dithiol benzene ($C_6H_6S_2$) on charge transport between TiO_2 particles **(as described in Chapter 6)**. The highly conjugated SWCNTs are believed to be very good electron acceptor molecules and electron conductors due to the electron delocalization in sp^2 hybridized orbitals[64]. We measured the charging and discharging rates for several TiO_2 samples that contained 0%, 1%, 3% and 5% of SWCNTs at a temperature where electrons are mobile (110 K). Our measurements show that TiO_2-containing single wall carbon nanotubes, while acting as electron acceptors by reducing the PL intensity, show the same charging/discharging rates as observed for pure TiO_2 powder (at a constant temperature) with a discharging time constant of t_1= 50 min. This implies that SWCNTs

which connect TiO_2 particles absorb electrons or interfere with electron-hole recombination, but do not enhance electrical conduction between TiO_2 particles. In contrast to this behavior, the gold nanoparticles inhibit the buildup of positive surface photovoltage as they show strong electron accepting properties.

References:

1. Fujishima, A.; Zhang, X.; Tryk, D. A., Tio(2) Photocatalysis and Related Surface Phenomena. *Surf. Sci. Rep.* **2008,** 63, 515-582.
2. Batzill, M.; Katsiev, K.; Diebold, U., Surface Morphologies of Sno2(110). *Surf. Sci.* **2003,** 529, 295-311.
3. Diebold, U., The Surface Science of Titanium Dioxide. *Surf. Sci. Rep.* **2003,** 48, 53-229.
4. Fujishima, A.; Honda, K., Electrochemical Photolysis of Water at a Semiconductor Electrode. *Nature* **1972,** 238, 37-+.
5. Linsebigler, A. L.; Lu, G. Q.; Yates, J. T., Photocatalysis on Tio2 Surfaces - Principles, Mechanisms, and Selected Results. *Chem. Rev.* **1995,** 95, 735-758.
6. Goswami, D. Y., A Review of Engineering Developments of Aqueous Phase Solar Photocatalytic Detoxification and Disinfection Processes. *Journal of Solar Energy Engineering-Transactions of the Asme* **1997,** 119, 101-107.
7. Gratzel, M., Photoelectrochemical Cells. *Nature* **2001,** 414, 338-344.
8. Gratzel, M., Dye-Sensitized Solid-State Heterojunction Solar Cells. *MRS Bull.* **2005,** 30, 23-27.
9. Hagfeldt, A.; Gratzel, M., Light-Induced Redox Reactions in Nanocrystalline Systems. *Chem. Rev.* **1995,** 95, 49-68.
10. Hardin, B. E.; Hoke, E. T.; Armstrong, P. B.; Yum, J. H.; Comte, P.; Torres, T.; Frechet, J. M. J.; Nazeeruddin, M. K.; Gratzel, M.; McGehee, M. D., Increased Light Harvesting in Dye-Sensitized Solar Cells with Energy Relay Dyes. *Nature Photonics* **2009,** 3, 406-411.
11. O'Regan, B.; Gratzel, M., A Low-Cost, High-Efficiency Solar-Cell Based on Dye-Sentisized Collodial Tio_2 Films. *Nature* **1991,** 353, 737-740.
12. Gfroerer, T. H., Photoluminescence in Analysis of Surfaces and Interfaces. In *Encyclopedia of Analytical Chemistry*, John Wiley & Sons: Chichester, 2000; pp 9209-9231.
13. Lüth, H., *Surfaces and Interfaces in Solid Materials*. Springer: 1995.
14. Wendt, S.; Sprunger, P. T.; Lira, E.; Madsen, G. K. H.; Li, Z. S.; Hansen, J. O.; Matthiesen, J.; Blekinge-Rasmussen, A.; Laegsgaard, E.; Hammer, B.; Besenbacher, F., The Role of Interstitial Sites in the Ti3d Defect State in the Band Gap of Titania. *Science* **2008,** 320, 1755-1759.
15. Yim, C. M.; Pang, C. L.; Thornton, G., Oxygen Vacancy Origin of the Surface Band-Gap State of Tio2(110). *Phys. Rev. Lett.* **2010,** 104.
16. Diebold, U.; Lehman, J.; Mahmoud, T.; Kuhn, M.; Leonardelli, G.; Hebenstreit, W.; Schmid, M.; Varga, P., Intrinsic Defects on a Tio2(110)(1x1) Surface and Their Reaction with Oxygen: A Scanning Tunneling Microscopy Study. *Surf. Sci.* **1998,** 411, 137-153.
17. Lu, G. Q.; Linsebigler, A.; Yates, J. T., Ti3+ Defect Sites on Tio2(110) - Production and Chemical-Detection of Active-Sites. *J. Phys. Chem.* **1994,** 98, 11733-11738.
18. Krueger, P.; Jupille, J.; Bourgeois, S.; Domenichini, B.; Verdini, A.; Floreano, L.; Morgante, A., Intrinsic Nature of the Excess Electron Distribution at the Tio2(110) Surface. *Phys. Rev. Lett.* **2012,** 108.
19. Na-Phattalung, S.; Smith, M. F.; Kim, K.; Du, M. H.; Wei, S. H.; Zhang, S. B.; Limpijumnong, S., First-Principles Study of Native Defects in Anatase Tio2. *Phys. Rev. B.* **2006,** 73.
20. Di Valentin, C.; Pacchioni, G.; Selloni, A., Reduced and N-Type Doped Tio2: Nature of Ti3+ Species. *J. Phys. Chem. C* **2009,** 113, 20543-20552.
21. Deskins, N. A.; Rousseau, R.; Dupuis, M., Defining the Role of Excess Electrons in the Surface Chemistry of Tio2. *J. Phys. Chem. C* **2010,** 114, 5891-5897.
22. Mezhenny, S.; Maksymovych, P.; Thompson, T. L.; Diwald, O.; Stahl, D.; Walck, S. D.; Yates, J. T., Stm Studies of Defect Production on the Tio2(110)-(1 X 1) and Tio2(110)-(1 X 2) Surfaces Induced by Uv Irradiation. *Chem. Phys. Lett.* **2003,** 369, 152-158.

23. Kronik, L.; Shapira, Y., Surface Photovoltage Phenomena: Theory, Experiment, and Applications. *Surf. Sci. Rep.* **1999,** 37, 1-206.
24. Kronik, L.; Shapira, Y., Surface Photovoltage Spectroscopy of Semiconductor Structures: At the Crossroads of Physics, Chemistry and Electrical Engineering. *Surf. Interface Anal.* **2001,** 31, 954-965.
25. Jing, L.; Li, S.; Song, S.; Xue, L.; Fu, H., Investigation on the Electron Transfer between Anatase and Rutile in Nano-Sized Tio2 by Means of Surface Photovoltage Technique and Its Effects on the Photocatalytic Activity. *Sol. Energy Mater. Sol. Cells* **2008,** 92, 1030-1036.
26. Jing, L. Q.; Sun, X. J.; Shang, J.; Cai, W. M.; Xu, Z. L.; Du, Y. G.; Fu, H. G., Review of Surface Photovoltage Spectra of Nano-Sized Semiconductor and Its Applications in Heterogeneous Photocatalysis. *Sol. Energy Mater. Sol. Cells* **2003,** 79, 133-151.
27. Albery, W. J.; Bartlett, P. N., The Transport and Kinetics of Photogenerated Carriers in Colloidal Semiconductor Electrode Particles. *J. Electrochem. Soc.* **1984,** 131, 315-325.
28. Tang, H.; Prasad, K.; Sanjines, R.; Schmid, P. E.; Levy, F., Electrical and Optical-Properties of Tio2 Anatase Thin-Films. *J. Appl. Phys.* **1994,** 75, 2042-2047.
29. Diebold, U., Structure and Properties of Tio2 Surfaces: A Brief Review. *Applied Physics a-Materials Science & Processing* **2003,** 76, 681-687.
30. Hendry, E.; Wang, F.; Shan, J.; Heinz, T. F.; Bonn, M., Electron Transport in Tio2 Probed by Thz Time-Domain Spectroscopy. *Phys. Rev. B.* **2004,** 69.
31. Rothschild, A.; Levakov, A.; Shapira, Y.; Ashkenasy, N.; Komem, Y., Surface Photovoltage Spectroscopy Study of Reduced and Oxidized Nanocrystalline Tio2 Films. *Surf. Sci.* **2003,** 532, 456-460.
32. Zhang, Z.; Yates, J. T., Jr., Band Bending in Semiconductors: Chemical and Physical Consequences at Surfaces and Interfaces. *Chem. Rev.* **2012,** 112, 5520-5551.
33. Rothschild, A.; Komem, Y.; Levakov, A.; Ashkenasy, N.; Shapira, Y., Electronic and Transport Properties of Reduced and Oxidized Nanocrystalline Tio2 Films. *Appl. Phys. Lett.* **2003,** 82, 574-576.
34. Sell, K.; Barke, I.; Polei, S.; Schumann, C.; von Oeynhausen, V.; Meiwes-Broer, K.-H., Surface Photovoltage of Ag Nanoparticles and Au Chains on Si(111). *Physica Status Solidi B-Basic Solid State Physics* **2010,** 247, 1087-1094.
35. Williams, R., Surface Photovoltage Measurements on Cadmium Sulfide. *Journal of Physics and Chemistry of Solids* **1962,** 23, 1057-1066.
36. Hollingsworth, R. E.; Sites, J. R., Photo-Luminescence Dead Layer in P-Type Inp. *J. Appl. Phys.* **1982,** 53, 5357-5358.
37. Kepler, K. D.; Lisensky, G. C.; Patel, M.; Sigworth, L. A.; Ellis, A. B., Surface-Bound Carbonyl-Compounds as Lewis-Acids - Photoluminescence as a Probe for the Binding of Ketones and Aldehydes to Cadmium-Sulfide and Cadmium Selenide Surfaces. *J. Phys. Chem.* **1995,** 99, 16011-16017.
38. Meyer, G. J.; Lisensky, G. C.; Ellis, A. B., Evidence for Adduct Formation at the Semiconductor Gas Interface - Photoluminescent Properties of Cadmium Selenide in the Presence of Amines. *J. Am. Chem. Soc.* **1988,** 110, 4914-4918.
39. Winder, E. J.; Moore, D. E.; Neu, D. R.; Ellis, A. B.; Geisz, J. F.; Kuech, T. F., Detection of Ammonia, Phosphine, and Arsine Gases by Reversible Modulation of Cadmium Selenide Photoluminescence Intensity. *J. Cryst. Growth* **1995,** 148, 63-69.
40. Anpo, M.; Chiba, K.; Tomonari, M.; Coluccia, S.; Che, M.; Fox, M. A., Photocatalysis on Native and Platinum-Loaded Tio2 and Zno Catalysts-Origin of Different Reactivities on Wet and Dry Metal-Oxides. *Bull. Chem. Soc. Jpn.* **1991,** 64, 543-551.
41. Anpo, M.; Kubokawa, Y., Photoluminescence of Zinc-Oxide Powder as a Probe of Electron-Hole Surface Processes. *J. Phys. Chem.* **1984,** 88, 5556-5560.
42. Anpo, M.; Tomonari, M.; Fox, M. A., Insitu Photoluminescence of Tio2 as a Probe of Photocatalytic Reactions. *J. Phys. Chem.* **1989,** 93, 7300-7302.
43. Idriss, H.; Barteau, M. A., Photoluminescence from Zinc-Oxide Powder to Probe Adsorption and Reaction of O2, Co, H-2, Hcooh, and Ch3oh. *J. Phys. Chem.* **1992,** 96, 3382-3388.

44. Idriss, H.; Andrews, R. M.; Barteau, M. A., Application of Luminescence Techniques to Probe Surface-Adsorbate Interactions on Oxide Single-Crystals. *Journal of Vacuum Science & Technology a-Vacuum Surfaces and Films* **1993,** 11, 209-218.
45. Knorr, F. J.; Mercado, C. C.; McHale, J. L., Trap-State Distributions and Carrier Transport in Pure and Mixed-Phase Tio2: Influence of Contacting Solvent and Interphasial Electron Transfer. *J. Phys. Chem. C* **2008,** 112, 12786-12794.
46. Zhang, D.; Downing, J. A.; Knorr, F. J.; McHale, J. L., Room-Temperature Preparation of Nanocrystalline Tio2 Films and the Influence of Surface Properties on Dye-Sensitized Solar Energy Conversion. *J. Phys. Chem. B* **2006,** 110, 21890-21898.
47. Vietmeyer, F.; Seger, B.; Kamat, P. V., Anchoring Zno Particles on Functionalized Single Wall Carbon Nanotubes. Excited State Interactions and Charge Collection. *Adv. Mater.* **2007,** 19, 2935-+.
48. Williams, G.; Kamat, P. V., Graphene-Semiconductor Nanocomposites: Excited-State Interactions between Zno Nanoparticles and Graphene Oxide. *Langmuir* **2009,** 25, 13869-13873.
49. Dutta, M.; Jana, S.; Basak, D., Quenching of Photoluminescence in Zno Qds Decorating Multiwalled Carbon Nanotubes. *Chemphyschem* **2010,** 11, 1774-1779.
50. Shi, J.; Chen, J.; Feng, Z.; Chen, T.; Lian, Y.; Wang, X.; Li, C., Photoluminescence Characteristics of Tio2 and Their Relationship to the Photoassisted Reaction of Water/Methanol Mixture. *J. Phys. Chem. C* **2007,** 111, 693-699.
51. Nakajima, H.; Itoh, K.; Murabayashi, M., Influences of C-1-C-3 Alcohols and Purities of Tio2 Powders on Their Photoluminescence Properties at Room Temperature. *Bull. Chem. Soc. Jpn.* **2002,** 75, 601-606.
52. Jasieniak, J.; Pacifico, J.; Signorini, R.; Chiasera, A.; Ferrari, M.; Martucci, A.; Mulvaney, P., Luminescence and Amplified Stimulated Emission in Cdse-Zns-Nanocrystal-Doped Tio2 and Zro2 Waveguides. *Adv. Funct. Mater.* **2007,** 17, 1654-1662.
53. Laferriere, M.; Galian, R. E.; Maurel, V.; Scaiano, J. C., Non-Linear Effects in the Quenching of Fluorescent Quantum Dolts by Nitroxyl Free Radicals. *Chem. Commun.* **2006**, 257-259.
54. Yu, J.; Ma, T.; Liu, G.; Cheng, B., Enhanced Photocatalytic Activity of Bimodal Mesoporous Titania Powders by C-60 Modification. *Dalton Transactions* **2011,** 40, 6635-6644.
55. Anpo, M.; Takeuchi, M., The Design and Development of Highly Reactive Titanium Oxide Photocatalysts Operating under Visible Light Irradiation. *J. Catal.* **2003,** 216, 505-516.
56. Stevanovic, A.; Buttner, M.; Zhang, Z.; Yates, J. T., Jr., Photoluminescence of Tio2: Effect of Uv Light and Adsorbed Molecules on Surface Band Structure. *J. Am. Chem. Soc.* **2012,** 134, 324-32.
57. Stevanovic, A.; Yates, J. T., Jr., Probe of Nh(3) and Co Adsorption on the Very Outermost Surface of a Porous Tio(2) Adsorbent Using Photoluminescence Spectroscopy. *Langmuir : the ACS journal of surfaces and colloids* **2012,** 28, 5652-9.
58. McGill, P. R.; Idriss, H., Ab Initio Study of Surface Acid-Base Reactions. The Case of Molecular and Dissociative Adsorption of Ammonia on the (011) Surface of Rutile Tio2. *Langmuir* **2008,** 24, 97-104.
59. Wilson, J. N.; Idriss, H., Reactions of Ammonia on Stoichiometric and Reduced Tio2(001) Single Crystal Surfaces. *Langmuir* **2004,** 20, 10956-10961.
60. Erdogan, R.; Ozbek, O.; Onal, I., A Periodic Dft Study of Water and Ammonia Adsorption on Anatase Tio2 (001) Slab. *Surf. Sci.* **2010,** 604, 1029–1033.
61. Raupp, G. B.; Dumesic, J. A., Adsorption of Co, Co2, H-2, and H2o on Titania Surfaces with Different Oxidation-States. *J. Phys. Chem.* **1985,** 89, 5240-5246.
62. Stevanovic, A.; Yates, J. T., Jr., Electron Hopping through Tio2 Powder: A Study by Photoluminescence Spectroscopy. *J. Phys. Chem. C* **2013,** 117, 24189-24195.
63. Hendry, E.; Koeberg, M.; O'Regan, B.; Bonn, M., Local Field Effects on Electron Transport in Nanostructured Tio2 Revealed by Terahertz Spectroscopy. *Nano Lett.* **2006,** 6, 755-759.
64. Dresselhaus, M. S.; Dresselhaus, G.; Saito, R., Physics of Carbon Nanotubes. *Carbon* **1995,** 33, 883-891.

Chapter 2

2. Experimental Apparatus and Methods

2.1 General Description.

The experiments to be reported here involve the use of a newly constructed high vacuum apparatus and spectroscopic cell in which both photoluminescence (PL) and transmission infrared (FTIR) spectroscopy can be applied to a powdered sample. Figure 11 shows the arrangement of the setup used in these experiments. The base pressure of the high vacuum system is achieved by continuous pumping with a turbomolecular pump. The base pressure of the system measured by a cold cathode gauge is ~1.5×10^{-9} after bake out at 120 °C for 30 hours. The apparatus for both IR and PL measurements consists of a sample mounted on a liquid nitrogen cooled XYZ translational stage in the high vacuum cell and a calibrated gas handling system equipped with the various pressure gauges, a turbomolecular pump and a quadrupole mass spectrometer for residual gas analysis in the vacuum system. The measurements employ two spectrometers: (1) Transmission Infrared Spectrometer (Perkin-Elmer, Spectrum 100 FTIR); and (2) Photoluminescence Spectrometer (Perkin-Elmer, LS-55).

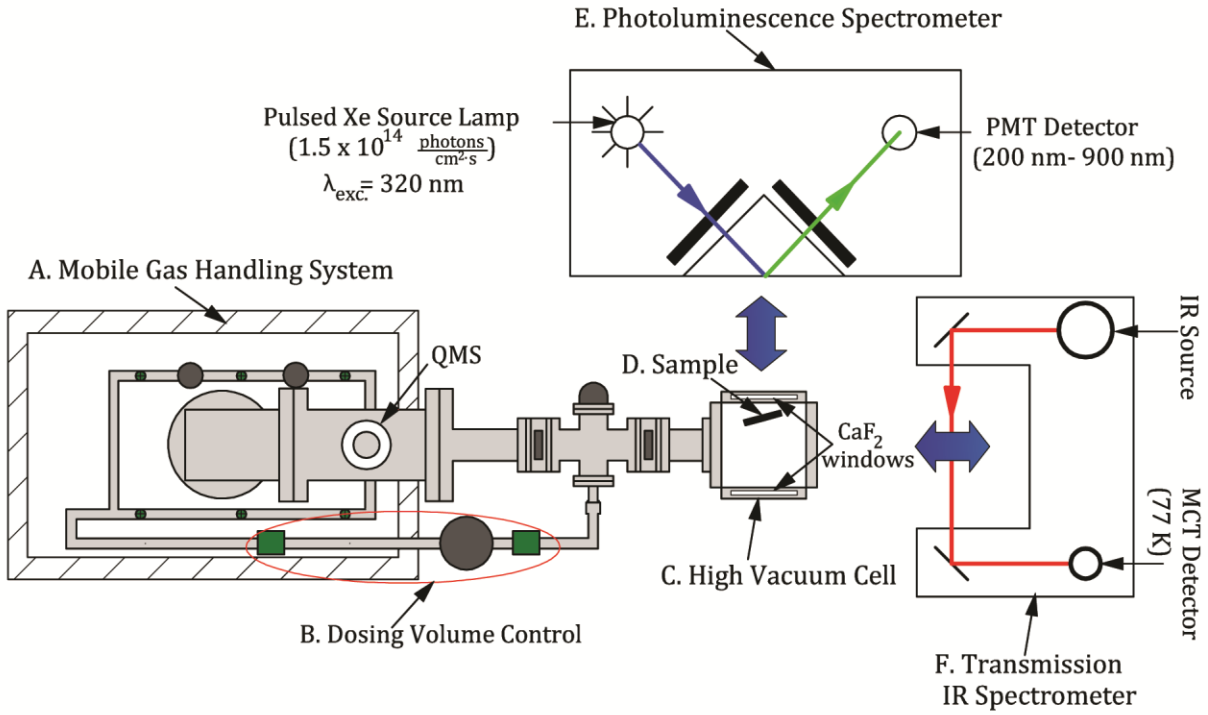

Figure 11. Top view-schematic diagram of the experimental set up. A. Mobile gas handling system B. Dosing Volume (V_0=50 cm^3); C. High vacuum cell; D. Sample; E. PL spectrometer and F. IR spectrometer. See Figure 16 for more details on the PL spectrometer.

2.2 Parts of the Experimental Set up

2.2.1 High Vacuum Cell.

The high vacuum cell is a stainless steel cube with six 4.5 inch ports, connected to a small portable high vacuum pumping system on wheels that can be moved from a purged-IR spectrometer to a nearby photoluminescence spectrometer, and could be accurately repositioned in each spectrometer as shown in Figure 11. Positioning of the cell and vacuum system is done with small laser pointers projecting onto an external scale, and with the screw-driven mechanism to slightly swing the apparatus in the horizontal direction **(see Appendix C1)**. The picture of the stainless steel vacuum cell, shown in Figure 12, contains two CaF_2 windows of 23 and 48 mm

diameters which are used either for IR or PL measurements respectively. The sample can be moved and precisely positioned (to an accuracy of 0.001 inches in the x- and y-directions and to 0.04 inches accuracy in the z-direction) by an XYZ-stage manipulator. The stainless steel re-entrant Dewar attached to the XYZ-stage is design to provide ℓ-N_2 for sample cooling, as shown in Figure 13. The cell sits on FTIR or PL base plates which are designed to maintain the constant position of the cell for both IR/PL measurements. The cell is pumped with a Leybold 150 turbopump (150 L/s) and achieves a limiting pressure of 1.5 x 10^{-9} Torr. Pressure is measured with a cold cathode ionization gauge or with a quadrupole mass spectrometer (SRS Model RGA 200).

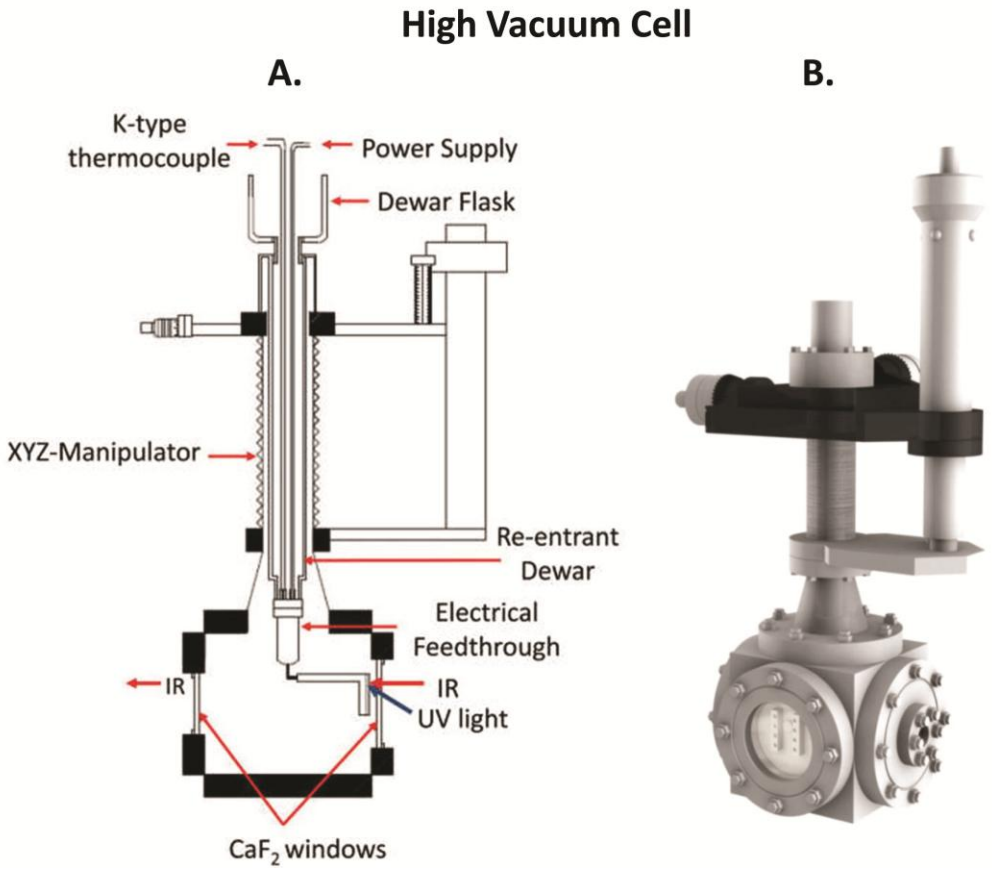

Figure 12. A. Schematic of the high vacuum cell employed in PL and IR measurements; and B. 3D representation of the high vacuum cell with the sample holder closely coupled to the CaF_2 window.

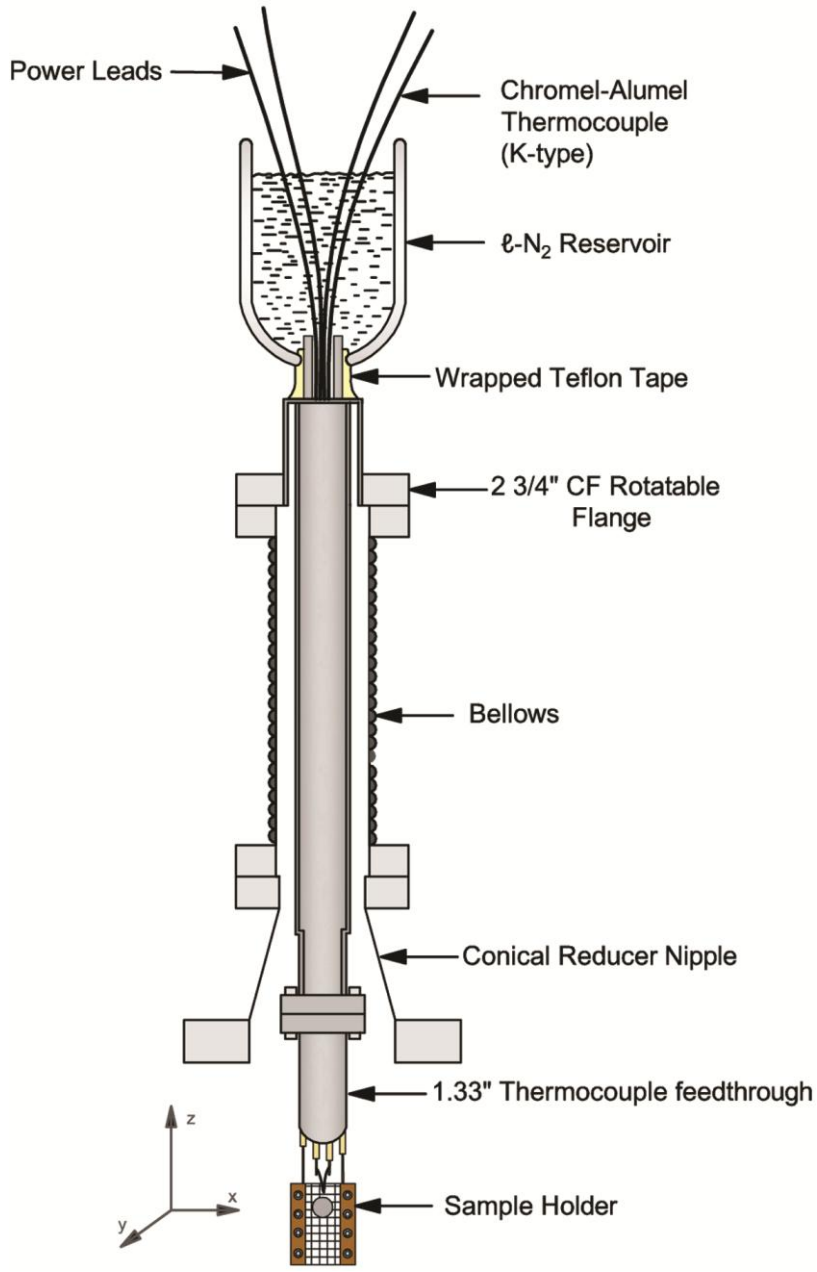

Figure 13. Schematic of a re-entrant Dewar for ℓ-N_2 storage that connects to a sample holder. The sample holder is made of oxygen-free high conductivity Cu to provide maximum thermal conductivity between the sample and the re-entrant Dewar at 77 K. The minimum achieved temperature is 84 K.

2.2.2 Sample Holder

The TiO_2 powdered sample is pressed at 6000 psi as a 7 mm diameter disk of thickness 0.0095 cm into a tungsten grid containing 0.22 mm x 0.22 mm square grid openings as shown in Figure 13. The optical transparency of the empty grid is about 70%. In some experiments, two powdered samples are pressed into the grid mesh. The grid assembly is stretched between two heavy oxygen-free high thermal conductivity copper (OFHC) clamps which are attached to a re-entrant ℓ-N_2 Dewar at the end of an electrical feedthrough. The L- shaped Cu clamp bars enable the sample to be brought to the focal point, positioned very close (~0.6 mm) to the front CaF_2 window, in order to detect more efficiently the emitted light from the sample. The PL emission signal strongly depends on a distance (Δy) from the focal point as shown in **Appendix C1**.

The temperature of the powdered samples is measured with a type-K thermocouple, welded to the top center of the grid, and the grid may be programmed upwards and downwards in temperature using a PID controller (Eurotherm 2404) or a data acquisition card (National Instrument, DAC) and feedback from the thermocouple to control the heating current. The temperature range is from 84 K to 1000 K (± 0.1 K precision) and the closely-spaced grid wire immersed in the powdered sample allows uniform temperatures to be achieved across the grid[1].

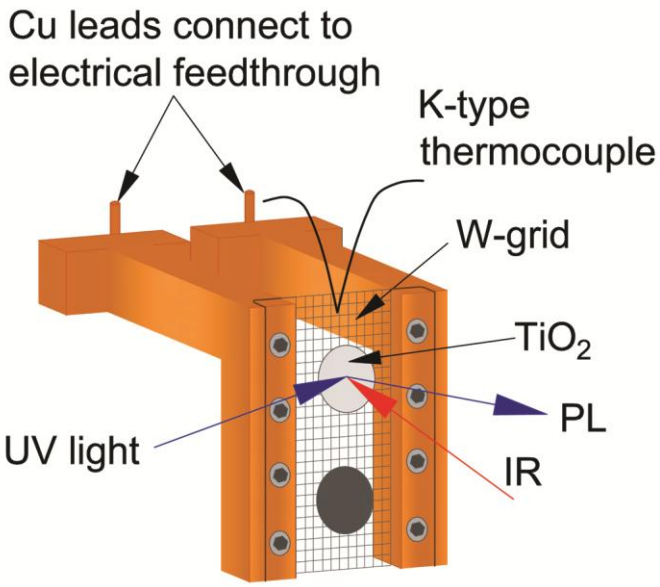

Figure 14. Sample holder with clamped tungsten grid and the TiO_2 pressed powder samples which are studied independently.

2.2.3 Calibrated Gas Handling System.

The calibrated system consists of a large diameter tubing (6in O.D and 2 3/4in O.D) that provided high pumping speed as continually pumped by the Leybold 150 turbopump. It is also equipped with the manifold for gas handling that accommodates five different gas dosing cylinders or gas-filled glass bulbs. The background pressure in the manifold is measured either by a cold cathode gauge (pressure range 10^{-11}-10^{-2} Torr) and is ~1.0 x 10^{-7} Torr or by a Baratron gauge (pressure range 0.01-100.00 Torr) when the manifold is filled with a gas. Both the gas handling system and the manifold volume were calibrated by using a method that involves expansion of N_2 gas from a reference volume to different volumes of interest in the manifold **(see Appendix C2)**. There is a calibrated volume (V_0= 50 cm^3) that served for precise gas dosing into the cell. The gas pressure from the volume, V_0, is measured by a second Baratron gauge that works in the pressure range 0.001-10.000 Torr.

2.3 Stages of a Typical Experiment.

The powdered TiO_2 (Evonic Industries- formerly Degussa P-25 material) was used in all of this work. We measured the N_2-BET surface area of P-25 TiO_2 to be 60 m^2 g^{-1} with a nominal pore size diameter of ~12 nm **(see Appendix C3)**. The TiO_2 is ~ 75% anatase and ~ 25 % rutile with average particle size ~30 nm and ~80 nm, respectively. Each experiment involves sample cleaning in the high vacuum cell. The typical cleaning procedure is performed by heating the sample in vacuum to ~700 K when O_2 is introduced to remove surface impurities such are hydrocarbons as measured by IR spectroscopy. The sample is then evacuated at ~700 K and cooled back down to ℓ-N_2 temperatures for PL and IR measurements. The sample is linearly heated and cooled with a 1 K/s rate using a LabVIEW program.

In all experiments the PL measurements are conducted by employing 320 nm (3.88 eV) irradiation. The surface charging, achieving a near-flat band condition, is obtained by continuously irradiating the surface for ~ 200 min in vacuum. To study the effect of different adsorbates on a surface, the gas line is filled by a certain gas to the required pressure measured by the Baratron gauge. From a dosing volume of V_0 = 50 cm^3 and knowing the pressure of the gas in the volume, we are able to calculate the number of molecules that are introduced into the cell by employing the ideal gas law. To obtain a monolayer of adsorbed gas on the powdered TiO_2 surface, it is necessary to adsorb ~ 10^{18} molecules **(see Appendix C4)**. As the re-entrant Dewar is at ~ 77 K, the dosed gas often extensively adsorbs there and we assume that only ~10 % of the dosed gas adsorbs on the TiO_2 surface. Thus, one dose from the volume V_0 introduces about 0.1 of a monolayer on the TiO_2 surface and the dose is proportional to the number of adsorbed molecules on the TiO_2 surface.

During gas delivery into the cell and its adsorption on the sample, UV light is blocked by a shutter. Single scan PL measurements were made using 68 s exposures from the Xe source and involved a total exposure to 9.8 x 10^{15} photons cm^{-2}. Experiments show that a 68 s single scan measurement of the PL only slightly modifies the TiO_2 sample as judged by the constancy of the PL signal. However, continuous irradiation by 320 nm light produces a continuous increase in PL intensity due to the surface photovoltage effect. The PL peak shape and position is invariant during the experiments shown here. Small changes in the sample position in the PL spectrometer cause some variation in PL intensity and this effect is minimized by geometrical adjustments.

The IR transmission measurements are obtained by passing the IR beam through the sample and collecting the signal by a ℓ-N_2 cooled MCT detector that covers the range 4000 cm^{-1} to 1000 cm^{-1}. FTIR spectra are obtained by averaging 128-1024 interferograms with 2 cm^{-1} spectral resolution. Each IR measurement is a ratio of IR spectra of the sample and an empty portion of the tungsten grid, obtained under identical conditions. The sample positioning in the IR spectrometer is discussed in **Appendix C5**.

2.4 Photoluminescence Spectroscopy of Semiconductors

The photoluminescence (PL) intensity is a direct measure of the rate of the recombination process of electrons and holes in a photoexcited semiconductor. Figure 15 depicts a typical PL process where electrons in a semiconductor are excited by absorption of photons with energy greater than the bandgap of the semiconductor. Upon excitation of an electron into the conduction band, it quickly relaxes to the bottom of the band by giving up energy to phonons, and then finds a defect site where it recombines with a hole. This recombination process is usually accompanied by emission of photons ($h\nu_{emiss.}$) of lower energy than that of the excitation photons ($h\nu_{exc.}$) and is known as photoluminescence (PL) emission.

Photoluminescence measurements are usually performed at low temperatures as phonon vibrations are significantly reduced and the probability for an electron to be scattered by a phonon is therefore minimized. As a result, the recombination of charge carriers is enhanced, resulting in a strong PL signal. On the other hand at higher temperatures, phonons are thermally activated resulting in enhanced electron-phonon interaction and a decrease in the PL emission. We found that the electron-hole recombination process is temperature-dependent process with an activation energy of 72 ± 2 meV **(see Appendix C6)**.

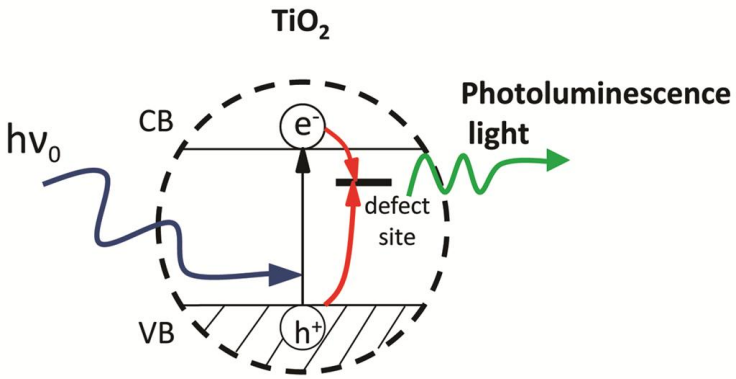

Figure 15. Schematic of photoluminescence process. Recombination of photo-excited charge carriers at a defect site result in emission of photoluminescence light.

2.4.1 Photoluminescence Measurements.

In this thesis, photoluminescence measurements were made using the pulsed Xe source operating at 60 Hz with a pulse width of <10 µs. During measurements, continuous exposure to the pulsed incident radiation takes place unless a shutter is used to block the radiation. The measured power at the sample, averaged over time, is 9.1×10^{-5} J s^{-1} cm^{-2} [1.5×10^{14} photons cm^{-2} s^{-1}] at the incident wavelength of 320 ± 10 nm (3.88 eV), using a grating and a band pass filter on the source side **(see Appendix C7)**. There are two Monk-Gillieson type monochromators on both the excitation and emission side that cover the wavelength ranges 200-800 nm and 200-900

nm for the excitation and emission, respectively. Both monochromators have slit widths that can be varied to yield a spectral range of 2.5- 20 nm. The schematic of the PL instrumentation used for photoluminescence measurements in this work is depicted in Figure 16. The UV radiation falls across the center of the sample in a rectangular region 2 mm in width by 7 mm in height (0.14 cm^2). The spectra were obtained using 20 nm slit width on the source and the detector side and a scan speed of 500 nm min^{-1}. The instrument ratios the PL signal to the pulsed source signal. The PL signal is detected by an R928 photomultiplier tube that covers the 200 – 900 nm range. In our experiments, the incident light strikes the sample at an angle of ~ 60° with respect to the normal as the sample in the IR/PL cell is tilted by ~ 15° away from the incident light. This geometry enables excitation light to be absorbed by the sample to produce photoluminescence but it also minimizes the detection of reflected excitation light. The PL signals were measured 15° off the specular direction in order to minimize reflection of the source light from the sample surface and CaF_2 window **(see Appendix C8)**. A cutoff filter at 390 nm was used on the detector side to further minimize the influence of reflected source light.

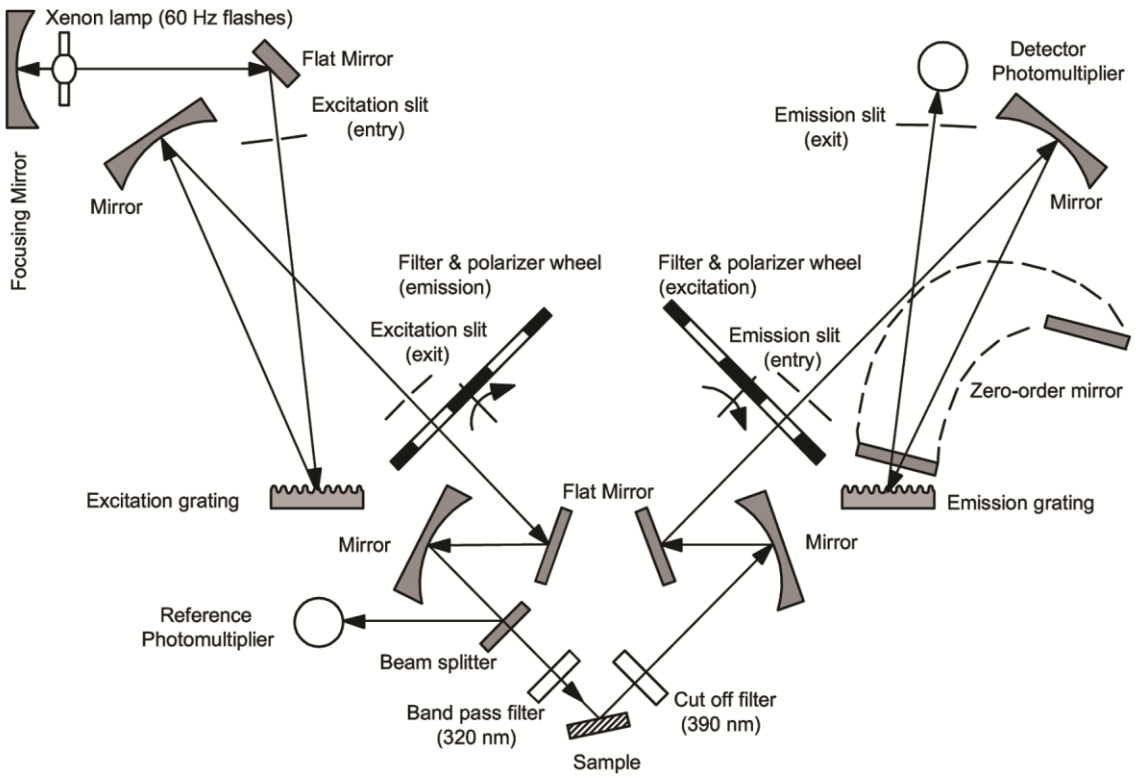

Figure 16. Schematic representation of a standard photoluminescence instrument that employs right-angle detection geometry. The standard instrument is modified by a 320 nm band pass filter and a 390 nm cut off filter.

2.5 Transmission Infrared Measurements.

In this work, we employ Transmission Fourier Transform Infrared (Transmission-FTIR) spectroscopy to study the adsorption of gases on the powdered TiO_2 surface. The IR beam path in the infrared spectrometer must be free of infrared absorbing atmospheric gases such as CO_2 and H_2O. Both gases are eliminated by continuous purging of the beam path with dried-air that is itself free of H_2O and CO_2. The dried-air is obtained from a gas generator unit (Parker) **(see Appendix C9)**. Here, the IR beam path in the sample compartment is separately purged from the IR source and detector by sealing the IR pathway volume with a specially designed rubber

sleeves **(see Appendix C9)**. The small volume within the rubber sleeves is rapidly purged by dried-air and purging is 30 times faster than purging the entire IR compartment. In our measurements, it was important to develop quick purging of the IR beam as the cell and its connecting tubing is frequently transferred in and out of the spectrometer.

The infrared instrument employed here is a commercially available Perkin-Elmer (Spectrum 100, FTIR) spectrometer that consists of an infrared source emitting continuous IR irradiation. The IR beam is reflected by a mirror and directed to a beam splitter (KBr) inside the Michelson interferometer. The beam splitter assists in passing 50 % of the IR beam onto a moving mirror that travels back and forth through a distance (Δx) with a constant velocity, as well as in passing the other 50 % of the beam onto a fixed mirror. The velocity of the moving mirror is monitored by a HeNe laser installed in the spectrometer. Upon the light reflection from both mirrors, two IR beams recombine at the beam splitter. Further, the beam is focused by mirrors and passed through the sample ultimately reaching a Mercury-Cadmium-Telluride (MCT) detector that operates at 77 K. The MCT detector measures the photocurrent induced by incoming IR irradiation. Here, the IR light excites electrons into the conduction band of the HgCdTe alloy which band gap energy can be tunable in the range between 0-1.5 eV depending on the Cd content. The recorded signal contains information about all IR excited vibrations in the system and as a function of time, S (t). The recorded function S (t), known as interferogram, is easily converted into a signal in frequency domain, S (ν), by employing a mathematical method called Fourier Transformation.

2.6 Photoluminescence and Infrared Surface Sensitivity.

The penetration depth of monochromatic excitation light depends on the absorption coefficient of TiO_2 and it is wavelength-dependent[2-4]. In other words, by selecting a desired

excitation wavelength, it is possible to select the penetration (sampling) depth of the material. In the study here, the PL measurements employ 320 nm (3.88 eV) excitation light which penetrates only ~ 20 nm providing information only about the very outer surface of the powdered TiO_2 as shown in Figure 17. It is calculated **(see Appendix C10)** that the total number of sites exposed to UV irradiation in a 20 nm depth is ~ 8.0 x 10^{14} sites while the entire depth of 0.0095 cm (95,000nm) of the powder contains ~5.0 x10^{18} sites. Thus, the number of sites probed by PL spectroscopy is only ~ 10^{-4} of the total number of sites in the powdered sample. On the other hand, transmission infrared spectroscopy employed here, provides information about adsorption of molecules throughout the entire depth of TiO_2 powder[5].

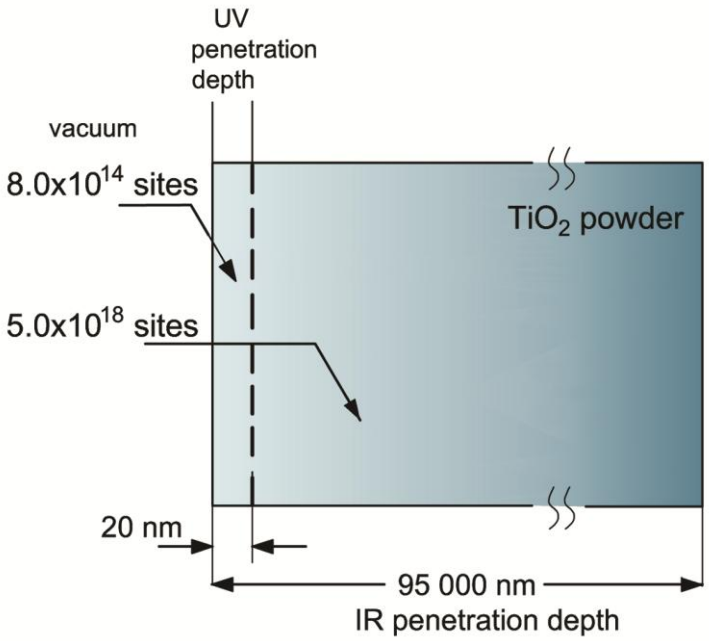

Figure 17. PL spectroscopy penetrates ~ 20 nm into a TiO_2 surface and samples 8.0 x 10^{14} sites while IR spectroscopy penetrates 95,000 nm into TiO_2, sampling 3.0 x 10^{18} sites.

References:

1. Muha, R. J.; Gates, S. M.; Yates, J. T.; Basu, P., Digital Temperature Programmer for Isothermal and Thermal-Desorption Measurements. *Rev. Sci. Instrum.* **1985,** 56, 613-616.
2. Ghosh, G., *Handbook of Optical Constants of Solids*. Academic Press: 1985.
3. Eagles, D. M., *J. Phys. Chem. Solids* **1964,** 25, 1243.
4. Cardona, M. H., G., Optical Properties and Band Structure of Wurtzite-Type Crystals and Rutile. *Phys. Rev. B.* **1964,** 137, A1467.
5. Stevanovic, A.; Yates, J. T., Jr., Probe of Nh(3) and Co Adsorption on the Very Outermost Surface of a Porous Tio(2) Adsorbent Using Photoluminescence Spectroscopy. *Langmuir : the ACS journal of surfaces and colloids* **2012,** 28, 5652-9.

Chapter 3.

Photoluminescence of TiO_2- Effect of UV Light and Adsorbed Molecules on Surface Band Structure

Published worked: **Stevanovic, A.;** Buttner, M.; Zhang, Z.; Yates, J. T., Jr., ***J. Am. Chem. Soc.*** **2012,** 134, 324-32.

Abstract

The photoluminescence (PL) of TiO_2 at 529.5 nm (2.34 eV) has been found to be a sensitive indicator of the modification of the band structure by surface charging due to UV- induced positive surface potential changes which shift the depth of the depletion layer. In addition, reversible band bending due to the adsorption of the electron donor NH_3 and CO molecules has been observed in measurements which combine photoluminescence with FTIR surface spectroscopy. It has been found that the O_2 molecule acts in two ways- as a reversibly adsorbed electron acceptor molecule and as an irreversibly adsorbed molecule which heals natural oxygen vacancy defects in the near surface region.

1. Introduction

Titanium dioxide is vital for solar-driven technologies such as sunlight-activated environmental remediation for photodegradation of toxic materials [1, 2]. Also, photovoltaic cells based on TiO_2 are widely used [3, 4]. Titanium dioxide has a band gap of 3.0 - 3.2 eV that permits activation by the UV component of sunlight. An electron-hole (e^--h^+) pair is produced. The hot electron quickly relaxes to the bottom of the conduction band where its mobility can carry it to a defect site or elsewhere. The presence of defects or impurities perturbs the local band structure of TiO_2 and breaks the periodicity of the lattice. Defects generate a local charge anomaly and thus act as traps of photogenerated electrons and holes [5]. At low temperatures, as employed in

this work, the interactions between photoexcited charge carriers and lattice phonons are significantly reduced and as a result, charge carriers become trapped at defect sites where they recombine emitting photoluminescence light (PL) or heat.[6-8] The energy of the emitted photon depends on the band structure and defect site energies in the material.

Ellis, et al.[9, 10] first suggested that the variation in PL intensity by the adsorption of charge - donating molecules on an n-type semiconductor could alter the surface band structure of the semiconductor by reduction in the depletion width as donor molecules are adsorbed. This concept builds on earlier investigations[11], where effects of band bending on changing the depth of the depletion layer in semiconductors were observed to affect the intensity of PL since the depletion layer is a dead layer for electron-hole pair recombination processes leading to PL. The idea that donor or acceptor molecules could influence PL in TiO_2 as a result of changes in the thickness of the dead layer due to band bending was developed by Anpo and coworkers[12, 13]. In addition, Solomon et al.[14] and Dunstan[15] suggested that UV light irradiation alters the band bending in amorphous silicon, flattening the band due to the recombination of photoexcited electrons and naturally present positive charge at or near the surface. In contrast to recombination in the bulk, work by McHale et al.[16] has identified a photoluminescence band at ~ 530 nm in TiO_2 in agreement with our measurements, and has ascribed this PL emission to recombination of a mobile electron with a trapped hole on the TiO_2 surface, where the TiO_2 is in contact with solvents.

This paper considers the effect of UV light on the surface band structure of TiO_2 particles in high vacuum or following controlled gas adsorption. It is found that the PL effect is enhanced by exposure to UV which ultimately converts n-type TiO_2 to a flat-band condition, as a result of changes in the surface photovoltage. In addition, the intensity of PL can be modified by

adsorbates which exchange charge with TiO_2, producing a change of the surface band bending structure. We also find that O_2 adsorption irreversibly reduces the concentration of natural defects in the surface region of TiO_2 particles, reducing PL intensity. It is likely that these defects are oxygen vacancies or Ti^{3+} sites at very low concentration.

2. Experimental

TiO_2 powder (Evonic Industries- formerly Degussa P-25 material) was used in all of this work. The mass of the sample is 6.3×10^{-3} g. Thus, in 1 cm^2 geometrical area exposed to UV, about 4×10^{18} surface sites within the depth (0.005 cm) of the sample are exposed to gas during adsorption. Since UV irradiation at 320 nm has an absorption depth of ~12-25 nm in bulk rutile[17-21] and ~ 17 nm in anatase[19], approximately approximately 8×10^{14} surface sites cm^{-2} in the nominal penetration depth are involved in adsorption within the depth of PL emission. Thus, within the approximations used here, about 0.1 photon (surface TiO_2 site·s)$^{-1}$ is incident during the PL measurements.

For cleaning the TiO_2 was heated in vacuum to 700 K and 0.12 Torr of O_2 was introduced for 30 min. to remove surface impurities and to partially oxidize the sample. The sample was then evacuated for 30 min. at 700 K. Research grade O_2 (99.99 %), NH_3 (99.99 %) and CO (99.99 %) were used for adsorption in the experiments presented here.

3. Experimental Results

A. Infrared Spectrum of TiO_2

Figure 1 shows the IR spectrum of the as-received TiO_2 material and the material after the O_2 treatment for 1h at 700 K and cooling to 87 K in vacuum. Both spectra were acquired at 87 K. Originally, TiO_2 powder (as-received) contains adsorbed isolated Ti-OH groups on the surface.

The O-H stretching modes show several different sharp absorption bands in the range 3750-3400 cm^{-1} which indicate the presence of different types of isolated Ti-OH groups on the surface[22, 23]. Hydrogen bonding between OH groups at high surface coverages produces a broad low frequency band which is not observed here. In addition, saturated hydrocarbons are present on the surface as indicated by C-H stretching modes at 2956 cm^{-1}, 2925 cm^{-1}, and 2854 cm^{-1}. After the cleaning procedure in O_2, the TiO_2 surface contains a very small fraction of Ti-OH- and C-H-bearing species as estimated by the low absorbances in Figure 2. Adsorbed carbonate (CO_3^{2-}) on the surface, yielding modes in the 1300-1800 cm^{-1} region, originates from CO_2 adsorption on the TiO_2 surface. The IR spectrum of the prepared sample remains unchanged throughout the experiments shown here.

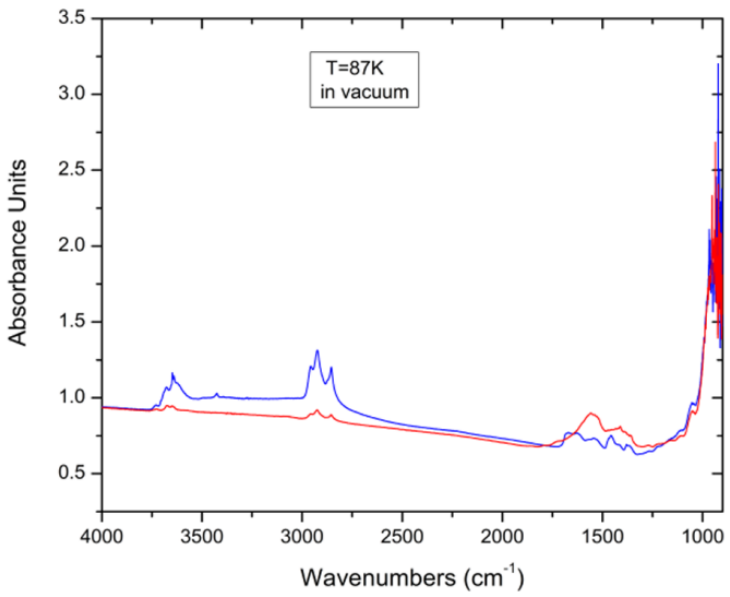

Figure 1. Infrared spectra of "as received" (blue) and clean (red) TiO_2 powder at 87K in vacuum. The clean surface was obtained by treating the sample at 700K in an oxygen atmosphere. The IR spectrum is invariant over the experiments reported here.

B. **Photoluminescence Development During UV Irradiation**

Figure 2A shows the PL development during continuous UV irradiation in vacuum at 87 K. The sample was irradiated at λ=320 nm (3.88eV). The PL intensity maximum occurs at λ=529.5 nm (2.34 eV) and it increases as UV radiation is continuously absorbed. Two spurious peaks are observed at 390 nm and 780 nm, respectively. The peak at λ=390 nm is due to a small amount of reflected source radiation and its intensity remains constant during irradiation as PL develops. The peak at 780 nm is a second-order feature of the 390 nm reflected light and also remains constant during irradiation. It is also weakly seen in the reference spectrum measured for the clean grid support (blue line). Figure 2B shows a plot of the increasing PL peak maximum intensity from the data in Figure 2A as a function of UV irradiation time. After the sample was irradiated for ~ 160 min, the UV light was blocked for ~ 60 min and then the sample was irradiated again for ~ 90 min. The PL peak intensity produced by UV irradiation remains essentially unchanged (region b in Figure 2B) when the TiO_2 is stored ~ 60 min. in the dark in vacuum. The storage of charge on the irradiated TiO_2 surface has previously been observed[24, 25]. Under the vacuum conditions employed here, any trace of adsorbed background gas, not measured by IR, does not change the efficiency of PL. The enhancement of PL continues when the sample is irradiated again in vacuum, after storage in the dark at 87 K, as shown beyond 220 min. in region (c) in Figure 2B. This experiment shows that the increasing PL intensity produced by UV irradiation corresponds to the production of a stable surface condition at 87 K in vacuum. In addition, the absorption spectrum of TiO_2 (not shown) indicated no evidence for an absorption band in the frequency range of the PL light emission.

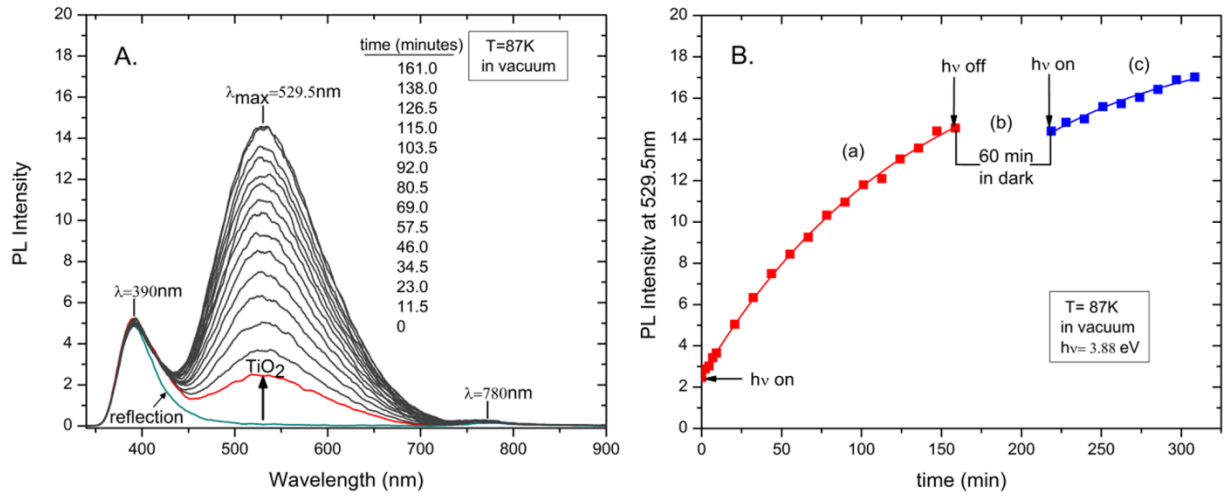

Figure 2. A. Photoluminescence development of TiO_2 during irradiation in vacuum. Reference spectrum, a clean W-grid at the sample position, is shown by the blue line. B. The photoluminescence intensity of TiO_2 increases as a function of UV exposure at 87 K in vacuum: (a) The sample was irradiated by λ= 3.88 eV for 160 min (red curve). The photoluminescence intensity increases with irradiation as the number of photon-accessible defects increases; (b) The sample was stored in the dark in vacuum for 60 min; (c) The sample was irradiated again by λ= 3.88 eV for 90 min. (blue curve). Photoluminescence remains constant when the UV light is off (~60 min) and continues to increase when the UV light is on.

C. Photoluminescence Enhancement

Figure 3A indicates the change in PL intensity during UV irradiation at different photon fluxes. Three identical experiments were performed with 100 %, 70 % and 40 % of the full photon flux, respectively, using neutral density grids to reduce the incident photon intensity. The TiO_2 powder was irradiated for ~ 216 min in vacuum at 87 K. In all three experiments, the PL intensity increases with time and approaches a saturation level. Two important observations may be made: (1) The increase in PL intensity is a result of exposure of the material to incident UV light (process k_1); and (2) A saturation condition is achieved after long irradiation. In addition in

Figure 3A, when the incident UV photon flux is reduced, the PL generation rate decreases, achieving the saturation point more slowly.

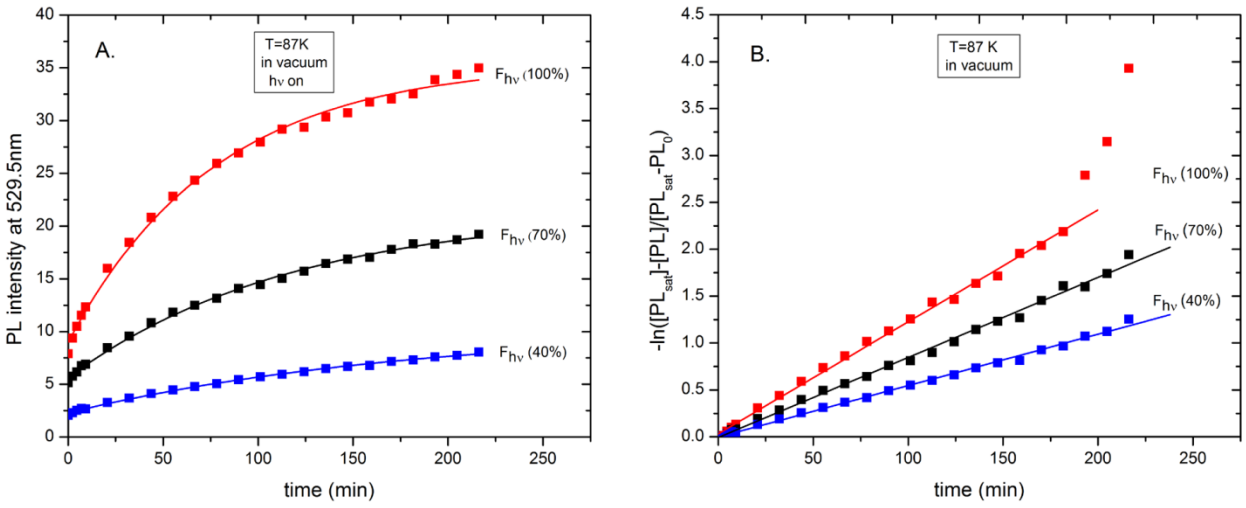

Figure 3. A. Photoluminescence intensity of TiO_2 as a function of time at different photon fluxes: 100%; 70%; and 40%. The rate of production of photon-accessible defect concentration decreases as the light intensity decreases. **B.** Functional fit of PL intensity development during irradiation for different photon fluxes: F_{hv} = 100%; F_{hv} = 70%; and F_{hv} = 40%. Solid squares represent experimental data. All data are fitted by equations (3) and (5) and fits are shown by solid lines.

Charging the surface by exposure to UV photons will alter the surface potential (photovoltage) and the degree of band bending and hence will produce changes in the depth of the depletion region. Accumulation of a positive charge on an n-type semiconductor surface (decrease in work function) will decrease upward band bending leading to a flat-band structure, resulting in the saturation of PL intensity as the length of the depletion region decreases to zero.

Based on these observations, the effect can be described by a model where 1 cm^2 of surface area is considered: UV irradiation induces a reduction in surface charge which enhances PL due to a reduction in upward band bending on the n-type semiconductor; the PL intensity is

proportional to the active defect concentration [D] (cm^{-3}) averaged over the entire depth of light penetration in an individual TiO_2 particle. A natural saturation will be achieved at long UV exposure times when the band bending is reduced to zero. Therefore, the change in photon-accessible defect concentration during UV exposure can be described by the following equations:

$$\frac{d[D]}{dt} = k_1 F_{h\nu} ([D_{sat}] - [D]) \quad (1)$$

$$ln \frac{[D_{sat}]-[D]}{[D_{sat}]-[D_0]} = -k_1 F_{h\nu} t \quad (2)$$

where [D] = the PL active defect concentration expressed as an average concentration of the photon-accessible defects over the active PL region and the dead region considered together; k_1 = the rate constant for photon-accessible defect production; $F_{h\nu}$= the photon flux at 3.88 eV; and $[D_{sat}]$ = upper limit of photon-accessible defect concentration available for PL. At any time, the quantity ($[D_{sat}]$-[D]) = the photon-accessible defect concentration which may be developed by irradiation until saturation.

We may write for the photoluminescence rate,

$$[PL] = k_2 F_{h\nu} [D] \quad (3)$$

Since,

$$[D] = \frac{[PL]}{k_2 F_{h\nu}} \quad (4)$$

where k_2 = proportionality constant for PL; [PL]= intensity of 2.34 eV photoluminescence light.

Using the expressions (2) and (4) the photoluminescence intensity development during UV irradiation is obtained:

$$[PL] = PL_{sat} - (PL_{sat} - PL_0) e^{-k_1 F_{h\nu} t} \quad (5)$$

or,

$$\ln\left(\frac{PL_{sat}-PL}{PL_{sat}-PL_0}\right) = -k_1 F_{h\nu} t \quad (6)$$

Equation (5) accurately fits the experimental data in Figure 4, including scaling with $F_{h\nu}$ as shown by the line fits to the points in Figure 4A and 4B. Figure 4B shows the PL intensity dependence on the photon flux as the logarithmic function derived in equation (6). The slopes of the curves are directly proportional to the $F_{h\nu}$ of incident light. Deviation of a few points on the upper plot from the linear dependence at 100% $F_{h\nu}$ is probably due to some small experimental error.

D. Annealing Effect

Figure 4 shows that the PL intensity decreases as the annealing temperature (T_a) is increased in vacuum following near saturation of the photon-available defect concentration by UV irradiation. After each annealing process, the PL increases again for increasing exposure to UV radiation. The sample was annealed from 87 K to T_a, and then cooled back down to 87 K. All PL measurements were obtained at 87 K. This observation is consistent with an irreversible thermal effect which removes the flat band condition previously established by irradiation. The heating may cause redistribution of negative charge on the surface that induced band bending and hence decrease in the PL intensity.

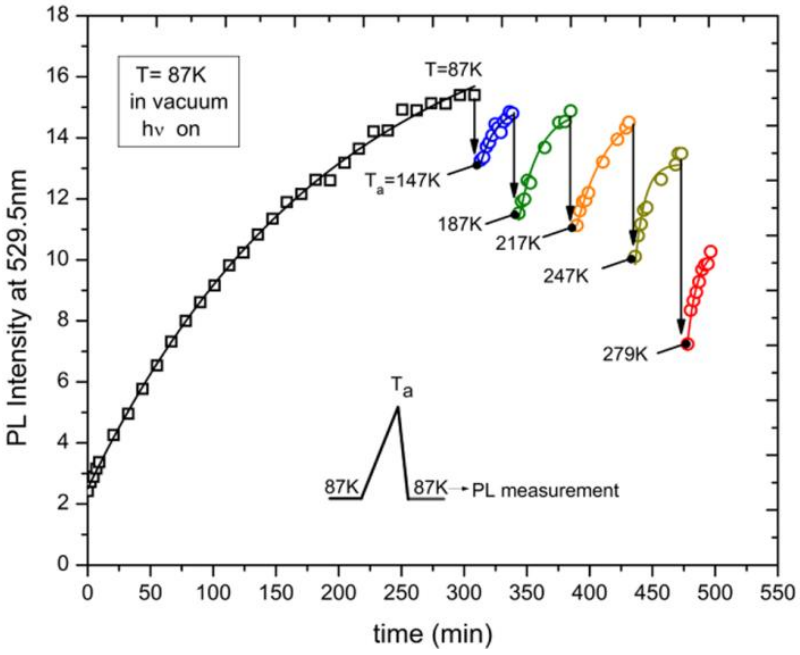

Figure 4. The PL intensity decrease as the annealing temperature increases in vacuum. The sample was annealed from 87 K to T_a and then cooled back down to 87 K. All PL measurements were obtained at 87 K. After annealing in vacuum, continuous irradiation causes PL enhancement.

E. Effect of the Adsorption of NH_3

Following the photo-production of a near-saturated level of photon-accessible defects able to cause e^--h^+ recombination (flat-band condition), donor NH_3 molecules were adsorbed on the TiO_2 at 200 K. In Figure 5, the first dose of NH_3 decreased the intensity of photoluminescence immediately, and subsequent NH_3 doses had no additional effect (region (b)). Upon evacuation, the PL intensity returned to near its initial value immediately (region (c)). This is evidence for the reversible adsorption/desorption of NH_3 on the outer TiO_2 surface regions being probed by photoluminescence. The adsorption of NH_3 is observed by IR spectroscopy for the exposures used here at 200 K (not shown). All PL measurements, following NH_3 adsorption at 200 K in Figure 5, are made after adsorption at 200 K and then cooling to 120 K. It may be seen that a perfectly ***reversible*** behavior is observed as the PL responds to adsorbed NH_3. This is in

accordance with the development of a surface potential moving in the negative direction for NH_3 adsorption on a flat band condition achieved by prior irradiation. Adsorption results in downward band bending, consistent with the known behavior of NH_3 as a donor molecule.

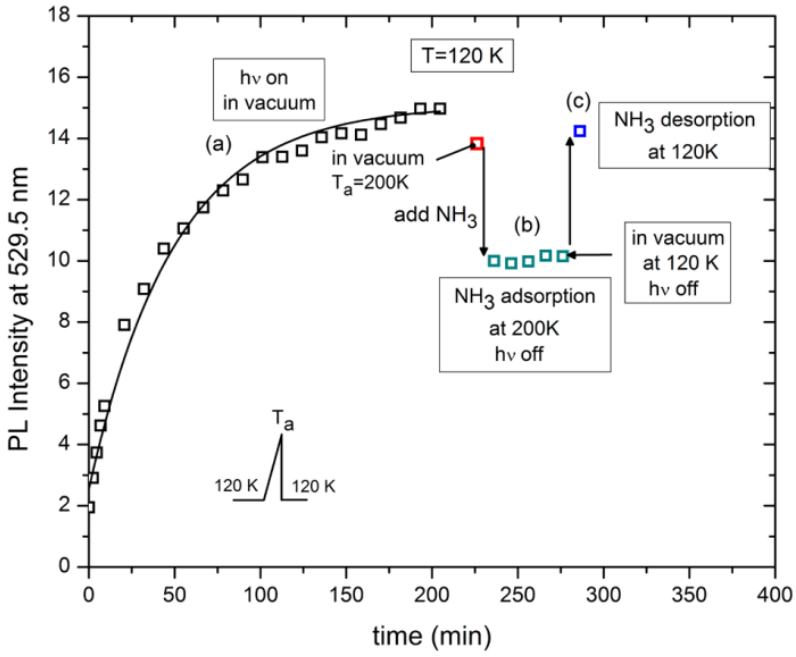

Figure 5. Effect of NH_3 adsorption and desorption on PL intensity following production of positive surface charge by irradiation. Adsorption and desorption at 200 K occurs rapidly in the near-surface region of the powdered layer when excited by UV irradiation.

F. Effect of Adsorption of CO

As shown in Figure 6, carbon monoxide was adsorbed at 120 K on an irradiated sample (region (a)) showing initially a near maximum photoluminescence intensity. CO adsorption was carried out in region (b). An absorption band at ν(CO) ~ 2180 cm^{-1}, accompanied by a small IR feature at ν(CO) ~ 2165 cm^{-1}, was observed to develop (not shown). Since the frequencies are above the gas phase ν ($CO_{(g)}$) ~ 2143cm^{-1}, the CO molecule is behaving as a weak donor

molecule. The PL intensity decreased as CO was adsorbed, region (b). As desorption of the CO occurs after the cell evacuation back to high vacuum at ~120 K, the PL is restored and the intensity of PL returns to the value originally achieved by irradiation. These results indicate that the CO also acts as a donor molecule resulting in downward band bending from the initial flat-band condition. The PL responds ***reversibly*** to the adsorption/desorption of CO. This observation is consistent with the development of a surface potential moving in the negative direction upon CO adsorption.

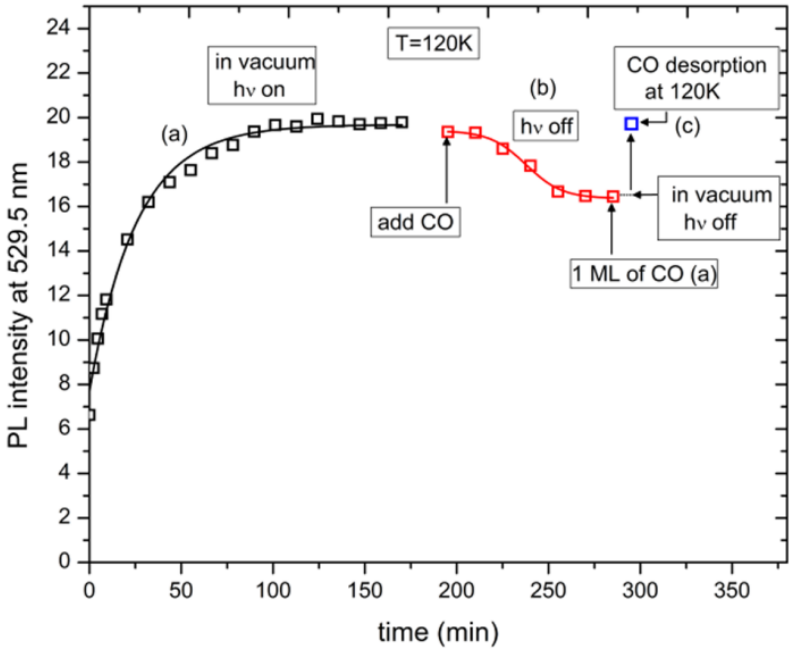

Figure 6. (a) Black curve represents PL evolution during continuous UV exposure in vacuum; (b) Red curve shows the change in PL intensity during CO adsorption until saturation coverage was attained (as judged by IR) in the dark at 120 K; (c) The PL intensity recovers reversibly after the system was evacuated in the dark at 120K.

G. Effect of O_2

Figure 7 shows the change in PL intensity during UV irradiation when O_2(g) is present. It shows a suppression of the photoluminescence enhancement rate in increasing O_2 pressures at 120 K for continuous exposure to UV light. In other words, the UV-light induced PL intensity enhancement is inhibited by O_2 at 120 K. No change in PL intensity is observed in region (b) after the system is evacuated back to high vacuum and stored in the dark for ~15 min, implying that the surface condition (produced by UV irradiation in low O_2(g) pressures at 120 K) is stable in vacuum in the dark. This is in agreement with a similar observation at 87 K as shown in Figure 2B (region (b)). In addition, in region (c) when the sample is continuously UV irradiated again in vacuum, the PL intensity increases again due to the continued formation of a negative surface potential by UV irradiation in the absence of O_2.

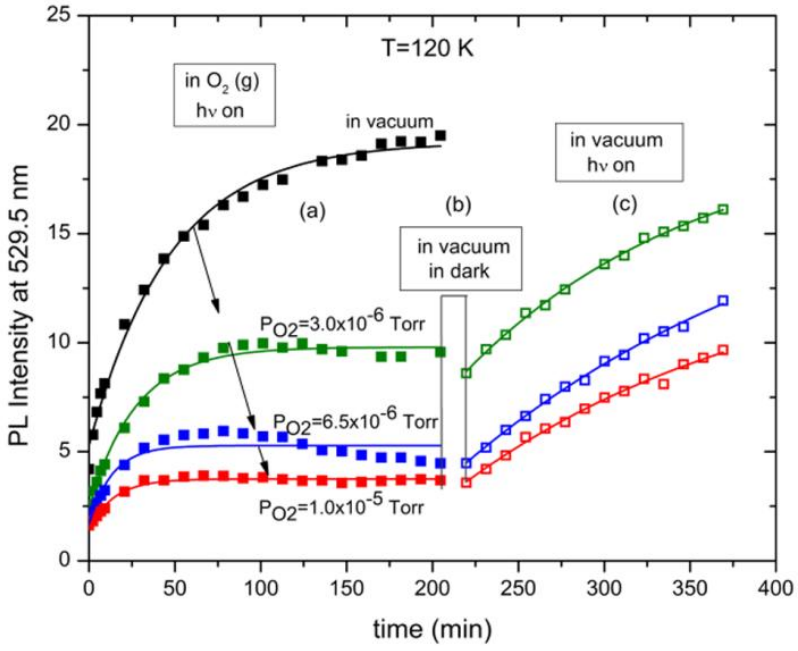

Figure 7. The PL intensity development during irradiation when low pressures of O_2 (g) are present: (a) PL development in: vacuum (black) and in O_2 atmosphere (green - 3.0×10^{-6} Torr; blue - 6.5×10^{-6} Torr and

red -1.0x10^{-5} Torr); (b) No change in PL intensity occurs in dark in vacuum for 15 min; (c) PL intensity increases again in vacuum when exposed to UV irradiation.

Figure 8A (region (b)) shows the change in PL intensity caused by O_2 adsorption in the dark at 120 K after first achieving the maximum PL intensity by irradiation. The PL intensity smoothly decreases (inset e) after introducing increasing O_2 pressures, P_{O_2}. The initial and final O_2 pressures are 1.5x10^{-2} Torr and 3 Torr, respectively. The UV light is blocked between O_2 doses in the region (b). These results indicate that the PL intensity at 120 K is extremely sensitive to the presence of O_2 molecules which cause a decrease in PL. This effect is related to the production of weakly-adsorbed O_2 in equilibrium with gas phase O_2[26] which is a precursor to the chemisorption of O_2. The PL intensity decreases quickly when the TiO_2 is exposed to small pressures of O_2 (1.5x10^{-2} Torr – 4.0x10^{-1} Torr) and reaches a minimum at ~3 Torr at 120 K. After O_2(g) is pumped away (region (c)) the PL intensity rises immediately as weakly-bound O_2 desorbs. Following abrupt O_2 desorption in region (c), the PL shows the previously observed effect (an increase in PL intensity) when the sample is further irradiated by UV light in vacuum. Figure 8B shows (in region (a)) the change in PL intensity achieved by UV exposure in vacuum. Region (b) shows the PL behavior after O_2 adsorption at 113 K in the dark. After each O_2 dose (0.1 Torr, 0.5 Torr, 5.0 Torr, 9 Torr), the PL is recorded as a function of time. The UV light is always maintained on between the measurements in contrast to the experiments shown in Figure 8A. The PL intensity decreases dramatically when the first O_2 dose (0.1 Torr) is in contact with the surface. The PL intensity remains almost unchanged in the presence of O_2 at various high values of P_{O_2} during UV irradiation. This shows that at sufficiently high P_{O_2}, UV irradiation cannot cause enhancement in PL. The small decrease in PL intensity for increasing P_{O_2} is

probably due to the slight TiO_2 sample warming as higher O_2(g) pressures were used, caused by heat transfer to the sample from the cell walls at 300 K.

Comparing these results to those obtained in the adsorption of NH_3 and CO, one sees that while O_2 behaves as an acceptor molecule as expected, causing PL to decrease, as it bends the flattened surface band upward, ***it does not behave completely reversibly*** as do NH_3 and CO**.** The same oxygen behavior was observed by Anpo et al.[27] in ZnO powder. It is likely that O_2 also irreversibly heals TiO_2 defect sites (oxygen vacancies or Ti^{3+} interstitials) naturally present in the sample. The healing of these defects causes a reduction in PL intensity because of the linear dependence of PL on the defect concentration.

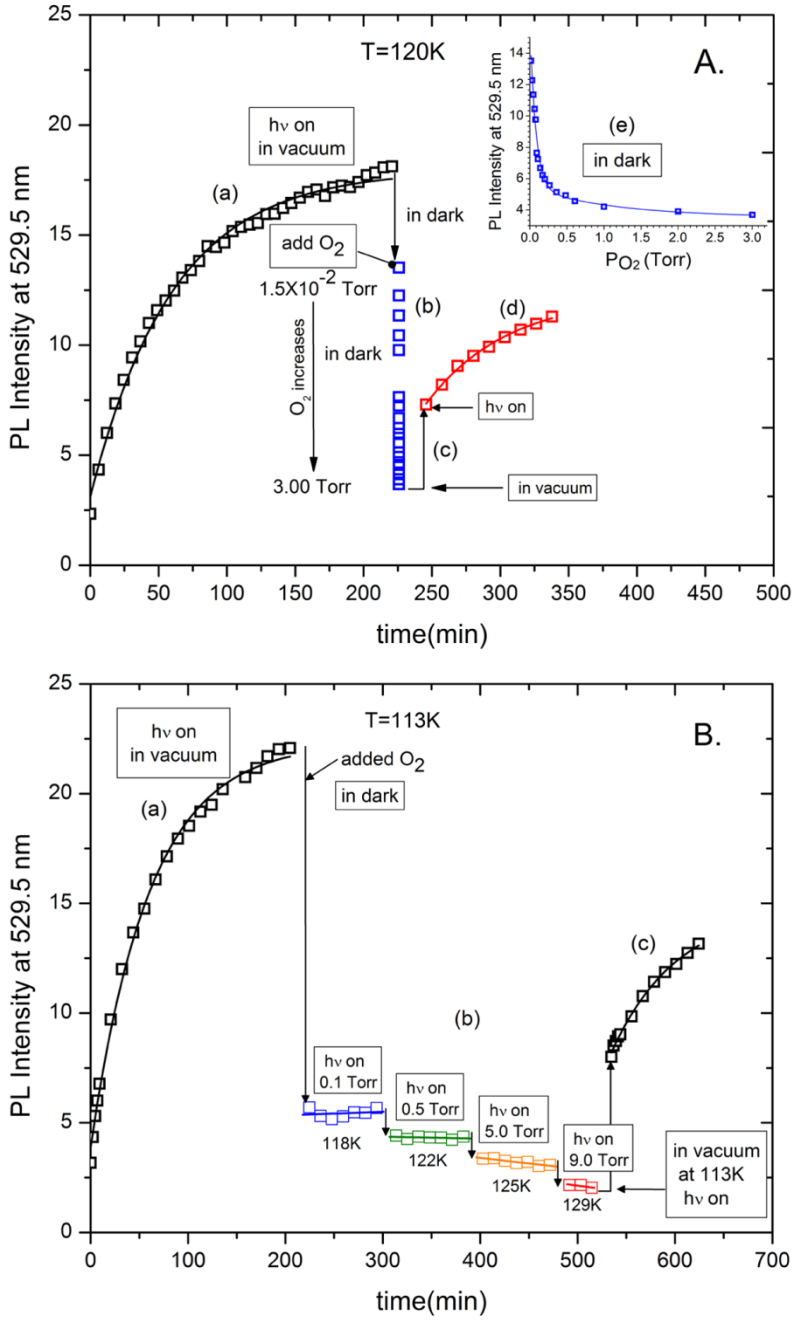

Figure 8. A. (a) Black squares show PL development in vacuum during continuous radiation; (b) Blue squares represent PL intensity after introducing different amounts of O_2 in the dark, plotted at the same time. The inset (e) depicts the PL intensity decrease in the dark as a function of O_2 pressure, P_{O2}; (c) O_2 was evacuated in the dark; the PL intensity increases due to O_2 desorption; (d) Increase of PL with continuous irradiation in vacuum (red squares); **B.** (a) Black squares represent PL development during

exposure to UV irradiation at 113 K in vacuum; (b) Different partial pressures of O_2 were introduced (0.1 Torr- blue, 0.5 Torr green, 5.0 Torr- orange, 9.0 Torr- red). After each oxygen dose, PL was recorded at the shown P_{O_2} as a function of time. Continuous UV irradiation occurred between the measurements; (c) PL increases with evacuation due to O_2 desorption and during continuous irradiation in vacuum (black squares).

4. Discussion

A. Surface Potential Changes during UV Irradiation of TiO_2

The fundamental premise of this work is that the enhancement of photoluminescence during exposure of TiO_2 to a flux of UV radiation (3.88 eV) produces a change in the concentration [D] of photon-accessible defects which then serve to mediate e^- - h^+ pair recombination to produce photoluminescence light as originally suggested by Solomon[14] and Dunstan[15]. A model involving band bending due to surface photovoltage changes provides a conceptual framework, where the length of the depletion layer, in the region of the bent band profile, changes as UV irradiation occurs, causing the number of photon-available defect sites for recombination in the flat band region to vary. Changes due to the surface photovoltage effect cause changes in the concentration of photon-accessible defect sites, [D], expressed as an average over the depth of the surface of individual TiO_2 particles which is penetrated by UV radiation. PL can only occur deeper in the semiconductor beneath the dead layer depletion region since carriers will be swept away from each other in the depletion region. The depth of penetration of UV irradiation with photon energies above the bandgap energy is reported, for bulk TiO_2, in the range 12-25 nm[17-21], and the number of defect sites within the flat band region in the 12-25 nm photon penetration depth will therefore govern the intensity of PL. To qualitatively support the band bending model in the nanosized particles we estimated, by using the approach outlined in reference[28], that the

depth of the depletion layer in the powdered TiO_2 is ~ 6 nm. The estimated depletion layer thickness is an order of magnitude smaller than the average TiO_2 particle size (30 nm- 80 nm) used in this work implying validity of the band bending model for our TiO_2 nanoparticles.

The generation of new photoactive sites by UV irradiation may be envisioned as in Figure 9. As photons enter the n-type TiO_2 sample, the average concentration of photoactive sites increases as the surface photovoltage decreases and the active PL region expands toward the surface, as the upward bent band flattens, as shown in Figure 9A. The rate of generation of photon-accessible defect sites, $\frac{d[D]}{dt}$, decreases as the active PL region expands as shown by equation (1), until the rate reaches zero as $[D_{sat}]$ is achieved. As shown in Figure 9B, the normal positive surface potential of n-type TiO_2 decreases as the degree of upward band bending diminishes during irradiation.

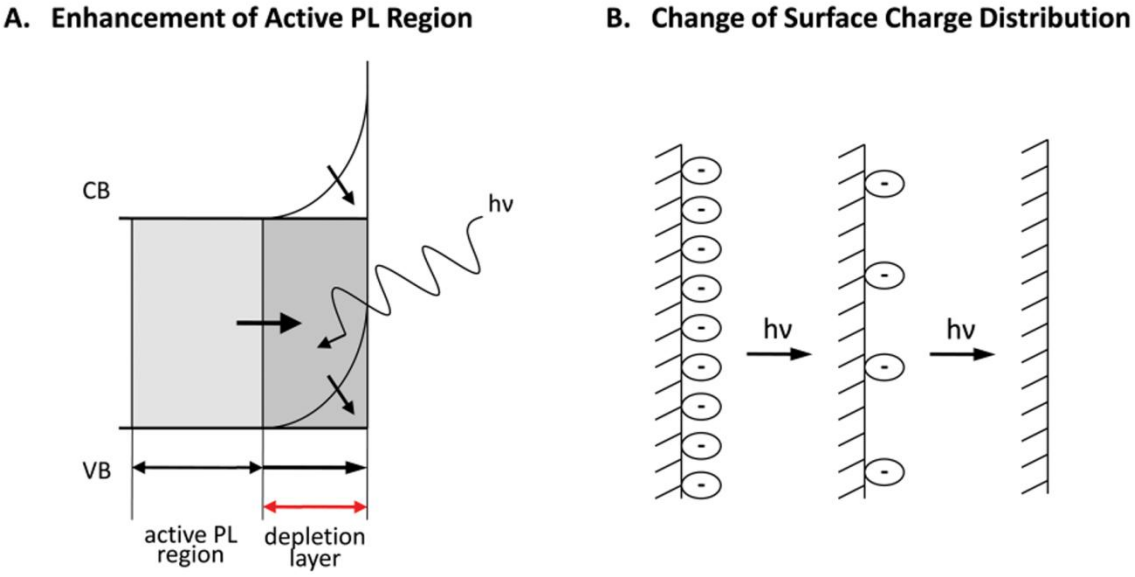

Figure 10. Schematic of effect of UV irradiation on n-type TiO_2. The flattening of the band is associated with a reduction of surface charge during irradiation. The process culminates when a flat-band condition is achieved.

B. Effect of Donor or Acceptor Molecule Adsorption

As shown in Figure 10, when the flat-band condition (achieved by long UV irradiation in vacuum) is modified by either donor or acceptor adsorbed molecules, the depletion region is expanded, and the number of photon-accessible defects able to facilitate e^-- h^+ recombination decreases, as the surface band is bent upwards or downwards.

The reversible response of the PL intensity caused by NH_3 and CO donor adsorbate surface modifiers is consistent with this picture of surface potential changes.

C. Irreversible Effect of Oxygen

The irreversible effect of O_2 adsorption on TiO_2 is likely superimposed on a reversible effect due to the acceptor nature of the adsorbed O_2 molecule. It is well known that TiO_2 surfaces, prepared as in this work, are oxygen deficient and therefore n-type and possess oxygen vacancies, as observed by STM [29], by ESR[30] and theoretically[31]. Treatment with O_2, even under the mild conditions of this experiment, can alter the natural oxygen vacancy concentration in the surface, and possibly in the near-surface region. Thus, on TiO_2(110), oxygen vacancy sites are observed by STM to be present at the 8% ML surface coverage. These surface vacancies are known to adsorb O_2 molecules [32], and to serve as dissociation sites for the production of O atoms which heal the vacancy site as well as attaching to Ti_{5c} sites nearby [33-36].Thus, the irreversible adsorption of O_2 and its dissociation on natural defects present in TiO_2 should be expected to result in an irreversible decrease in PL due to defect healing, as observed.

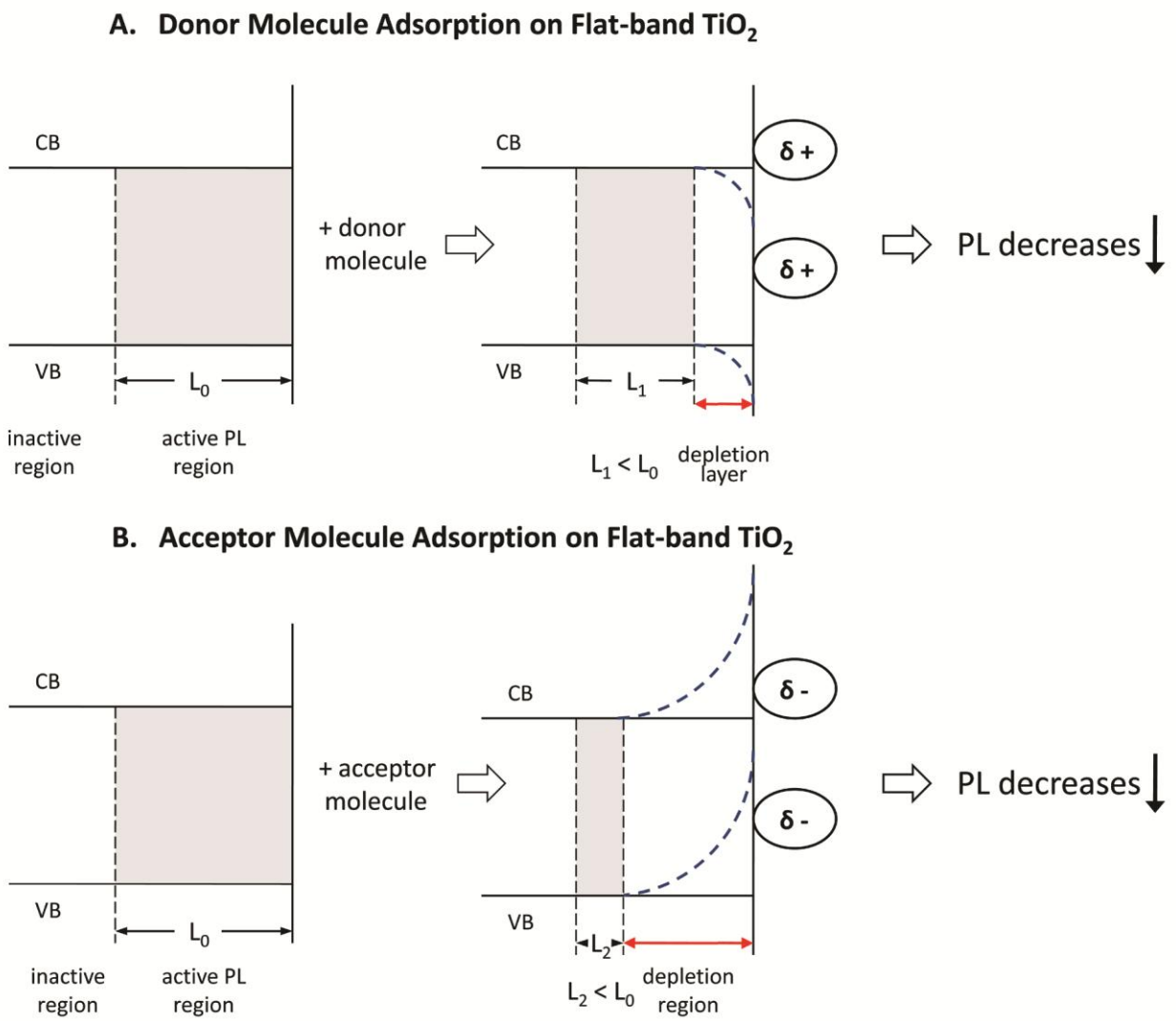

Figure 11. Schematic effect of donor and acceptor molecules on the thickness of the active PL region. A. TiO_2 with flat-band condition achieved by maximum UV exposure in vacuum. The active PL region length = L_0. Upon adsorption of an electron donor molecule the active PL region decreases to L_1 where $L_1 < L_0$ resulting in the PL intensity decrease; B. After adsorption of an electron acceptor molecule the length of the active PL region narrows ($L_2<L_0$) leading to PL intensity decrease.

D. **Possible Oxygen Vacancy Formation by Ultraviolet Light Irradiation.**

The STM has been used to study the possible formation of surface defects on TiO_2 (110) by UV irradiation[37] . In the photon energy range 1.6 – 5.6 eV, no production of defects was found

for intense UV irradiation. An upper limit of the damage cross section ($Q = 10^{-23.5\pm0.2}$ cm^2 $photon^{-1}$) was measured for surface defect formation. At the low UV fluxes (F_{hv}) used here in the photoluminescence measurements, the measured upper limit of the TiO_2 damage cross section, Q, suggest that the maximum number of defects produced in 200 minutes of continuous irradiation will be less than ~$5x10^{-6}$ fraction of available TiO_2 units in a 10 nm depth of UV penetration (**see Appendix C10**). This suggests that permanent UV-induced defect production is not involved in the PL effects reported here. Instead the effect of band bending due to increasing surface photovoltage in governing the depth of the active PL region determines the intensity of the PL observed in these experiments.

5. Summary

It was found that altering the surface potential in TiO_2 by UV light or by adsorbed electron acceptor/donor molecules results in a change in depth of the active PL region and in the intensity of the observed PL due to the band-bending effect. It was shown that:

1. UV light induces a negative surface potential which diminishes upward band bending in n-type TiO_2 and causes the PL active region to expand toward the surface providing an additional number of photon-accessible defects for e^--h^+ recombination. The increase in photon-accessible defects, due to an increase in the flat-band active region, results in an increase in PL intensity. It is likely that the maximum PL intensity produced by UV irradiation results in the production of a flat band condition at the surface.
2. Adsorption of NH_3 and CO (donor adsorbates) on the photoirradiated surface (flat band) results in downward band bending and expansion of the depletion region, providing a lower concentration of photon-accessible defect recombination centers. As a result, the PL intensity decreases reversibly upon the adsorption of these molecules.

3. Adsorption of O_2 (acceptor adsorbate) on the photoirradiated surface (flat band) produces upward band bending which also increases the depletion region and reduces the concentration of photon-accessible defect recombination centers. Thus, PL intensity decreases reversibly upon the adsorption of O_2.
4. The PL intensity responds reversibly to NH_3 and CO adsorption/desorption. On the other hand, the PL intensity does not respond completely reversibly to O_2 desorption. This is due to the fact that O_2, in addition to being a reversibly-adsorbed electron acceptor molecule, also dissociates causing the healing of defect sites that are naturally present in the sample.
5. The ability of PL to measure the rate of the e^--h^+ recombination process during UV irradiation presents an opportunity to understand more deeply the exchange of charge experienced by various surface modifier molecules upon adsorption on TiO_2. Such knowledge could be valuable in controlling processes driven by light on TiO_2 surfaces.

ACKNOWLEDGMENT

We acknowledge with thanks the full support of this work by the Army Research Office under grant number 55748CH.

References:

1. Thompson, T. L.; Yates, J. T., Surface Science Studies of the Photoactivation of Tio2-New Photochemical Processes. *Chem. Rev.* **2006,** 106, 4428-4453.
2. Linsebigler, A. L.; Lu, G. Q.; Yates, J. T., Photocatalysis on Tio2 Surfaces - Principles, Mechanisms, and Selected Results. *Chem. Rev.* **1995,** 95, 735-758.
3. Gratzel, M., Photoelectrochemical Cells. *Nature* **2001,** 414, 338-344.
4. Hardin, B. E.; Hoke, E. T.; Armstrong, P. B.; Yum, J. H.; Comte, P.; Torres, T.; Frechet, J. M. J.; Nazeeruddin, M. K.; Gratzel, M.; McGehee, M. D., Increased Light Harvesting in Dye-Sensitized Solar Cells with Energy Relay Dyes. *Nature Photonics* **2009,** 3, 406-411.
5. Gfroerer, T. H., Photoluminescence in Analysis of Surfaces and Interfaces. In *Encyclopedia of Analytical Chemistry*, John Wiley & Sons: Chichester, 2000; pp 9209-9231.
6. Amtout, A.; Leonelli, R., Time-Resolved Photoluminescence from Excitons in Tio2. *Solid State Commun.* **1992,** 84, 349-352.
7. Najafov, H.; Tokita, S.; Ohshio, S.; Kato, A.; Saitoh, H., Green and Ultraviolet Emissions from Anatase Tio2 Films Fabricated by Chemical Vapor Deposition. *Japanese Journal of Applied Physics Part 1-Regular Papers Short Notes & Review Papers* **2005,** 44, 245-253.
8. Tang, H.; Prasad, K.; Sanjines, R.; Schmid, P. E.; Levy, F., Electrical and Optical-Properties of Tio2 Anatase Thin-Films. *J. Appl. Phys.* **1994,** 75, 2042-2047.
9. Meyer, G. J.; Lisensky, G. C.; Ellis, A. B., Evidence for Adduct Formation at the Semiconductor Gas Interface - Photoluminescent Properties of Cadmium Selenide in the Presence of Amines. *J. Am. Chem. Soc.* **1988,** 110, 4914-4918.
10. Winder, E. J.; Moore, D. E.; Neu, D. R.; Ellis, A. B.; Geisz, J. F.; Kuech, T. F., Detection of Ammonia, Phosphine, and Arsine Gases by Reversible Modulation of Cadmium Selenide Photoluminescence Intensity. *J. Cryst. Growth* **1995,** 148, 63-69.
11. Hollingsworth, R. E.; Sites, J. R., Photo-Luminescence Dead Layer in P-Type Inp. *J. Appl. Phys.* **1982,** 53, 5357-5358.
12. Anpo, M.; Tomonari, M.; Fox, M. A., Insitu Photoluminescence of Tio2 as a Probe of Photocatalytic Reactions. *J. Phys. Chem.* **1989,** 93, 7300-7302.
13. Anpo, M.; Chiba, K.; Tomonari, M.; Coluccia, S.; Che, M.; Fox, M. A., Photocatalysis on Native and Platinum-Loaded Tio2 and Zno Catalysts-Origin of Different Reactivities on Wet and Dry Metal-Oxides. *Bull. Chem. Soc. Jpn.* **1991,** 64, 543-551.
14. Solomon I. , P. J., Bourdon B. In Proc. 14th Int. Conf. Phys. Semiconductors, Edinburgh, Sept. 1978, 1978; Inst. Phys. Conf. Ser. : Edinburgh, 1978; pp 689-692.
15. Dunstan, D. J., Photoluminescence Studies of Band-Bending in Hydrogenated Amorphous Silicon Thin Films. *J. Phys. C: Solid State Phys.* **1981** 14, 1363-1371.
16. Knorr, F. J.; Mercado, C. C.; McHale, J. L., Trap-State Distributions and Carrier Transport in Pure and Mixed-Phase Tio2: Influence of Contacting Solvent and Interphasial Electron Transfer. *J. Phys. Chem. C* **2008,** 112, 12786-12794.
17. Ghosh, A. K.; Maruska, H. P., Photoelectrolysis of Water in Sunlight with Sensitized Semiconductor Electrodes. *Journal of the Electrochemical Society* **1977,** 124, 1516-1522.
18. Eagles, D. M., *J. Phys. Chem. Solids* **1964,** 25, 1243.
19. Mo, S. D.; Ching, W. Y., Electronic and Optical-Properties of 3 Phases of Titanium-Dioxide - Rutile, Anatase, and Brookite. *Phys. Rev. B.* **1995,** 51, 13023-13032.
20. Cardona, M. H., G., Optical Properties and Band Structure of Wurtzite-Type Crystals and Rutile. *Phys. Rev. B.* **1964,** 137, A1467.
21. Ghosh, G., *Handbook of Optical Constants of Solids*. Academic Press: 1985.
22. Deiana, C.; Fois, E.; Coluccia, S.; Martra, G., Surface Structure of Tio2 P25 Nanoparticles: Infrared Study of Hydroxy Groups on Coordinative Defect Sites. *J. Phys. Chem. C* **2010,** 114, 21531-21538.

23. Panayotov, D. A.; Yates, J. T., Depletion of Conduction Band Electrons in Tio2 by Water, Chemisorption - Ir Spectroscopic Studies of the Independence of Ti-Oh Frequencies on Electron Concentration. *Chem. Phys. Lett.* **2005,** 410, 11-17.
24. Berger, T.; Diwald, O.; Knozinger, E.; Sterrer, M.; Yates, J. T., Uv Induced Local Heating Effects in Tio(2) Nanocrystals. *PCCP* **2006,** 8, 1822-1826.
25. Berger, T.; Sterrer, M.; Diwald, O.; Knozinger, E.; Panayotov, D.; Thompson, T. L.; Yates, J. T., Light-Induced Charge Separation in Anatase Tio2 Particles. *J. Phys. Chem. B* **2005,** 109, 6061-6068.
26. Green, I. X.; Yates, J. T., Vibrational Spectroscopic Observation of Weakly Bound Adsorbed Molecular Oxygen on Powdered Titanium Dioxide. *J. Phys. Chem. C* **2010,** 114, 11924-11930.
27. Anpo, M.; Kubokawa, Y., Photoluminescence of Zinc-Oxide Powder as a Probe of Electron-Hole Surface Processes. *J. Phys. Chem.* **1984,** 88, 5556-5560.
28. Hagfeldt, A.; Gratzel, M., Light-Induced Redox Reactions in Nanocrystalline Systems. *Chem. Rev.* **1995,** 95, 49-68.
29. Diebold, U.; Lehman, J.; Mahmoud, T.; Kuhn, M.; Leonardelli, G.; Hebenstreit, W.; Schmid, M.; Varga, P., Intrinsic Defects on a Tio2(110)(1x1) Surface and Their Reaction with Oxygen: A Scanning Tunneling Microscopy Study. *Surf. Sci.* **1998,** 411, 137-153.
30. Brandao, F. D.; Pinheiro, M. V. B.; Ribeiro, G. M.; Medeiros-Ribeiro, G.; Krambrock, K., Identification of Two Light-Induced Charge States of the Oxygen Vacancy in Single-Crystalline Rutile Tio2. *Phys. Rev. B.* **2009,** 80.
31. Na-Phattalung, S.; Smith, M. F.; Kim, K.; Du, M. H.; Wei, S. H.; Zhang, S. B.; Limpijumnong, S., First-Principles Study of Native Defects in Anatase Tio2. *Phys. Rev. B.* **2006,** 73.
32. Diebold, U., The Surface Science of Titanium Dioxide. *Surface Science Reports* **2003,** 48, 53-229.
33. Lira, E.; Hansen, J. O.; Huo, P.; Bechstein, R.; Galliker, P.; Laegsgaard, E.; Hammer, B.; Wendt, S.; Besenbacher, F., Dissociative and Molecular Oxygen Chemisorption Channels on Reduced Rutile Tio2(110): An Stm and Tpd Study. *Surf. Sci.* **2010,** 604, 1945-1960.
34. Petrik, N. G.; Kimmel, G. A., Photoinduced Dissociation of O-2 on Rutile Tio2(110). *Journal of Physical Chemistry Letters* **2010,** 1, 1758-1762.
35. Scheiber, P.; Riss, A.; Schmid, M.; Varga, P.; Diebold, U., Observation and Destruction of an Elusive Adsorbate with Stm: O(2)/Tio(2)(110). *Phys. Rev. Lett.* **2010,** 105.
36. Wang, Z. T.; Du, Y. G.; Dohnalek, Z.; Lyubinetsky, I., Direct Observation of Site-Specific Molecular Chemisorption of O(2) on Tio(2)(110). *Journal of Physical Chemistry Letters* **2010,** 1, 3524-3529.
37. Mezhenny, S.; Maksymovych, P.; Thompson, T. L.; Diwald, O.; Stahl, D.; Walck, S. D.; Yates, J. T., Stm Studies of Defect Production on the Tio2(110)-(1 X 1) and Tio2(110)-(1 X 2) Surfaces Induced by Uv Irradiation. *Chem. Phys. Lett.* **2003,** 369, 152-158.

Chapter 4.

Probe of NH_3 and CO Adsorption on The Very Outermost Surface of a Porous TiO_2 Adsorbent using Photoluminescence Spectroscopy

Published worked: **Stevanovic, A.**; Yates, J. T., Jr., ***Langmuir*** **2012,** 28, 5652-9.

Abstract

We report the first measurements of the kinetics of adsorption on the very outermost surface sites of a porous material, compared to measurements made of adsorption on the interior sites. NH_3 and CO were employed in this study as representative of slow diffusion and fast diffusion, respectively, through porous TiO_2. Adsorption of NH_3 at 200 K occurs at the very near-surface (~20 nm) region as observed by photoluminescence (PL) spectroscopy and its distribution by surface diffusion through the powder is highly retarded as judged by transmission IR spectroscopy. In contrast, adsorption of CO in the near-surface region is followed by fast distribution of CO by surface diffusion into TiO_2 powder, causing the near-surface CO coverage to lag behind the coverage in the bulk. In the desorption process, the near-surface region delivers adsorbed CO molecules into the gas phase, accompanied with the supply of diffusing CO molecules from the interior. As a result, the adsorption/desorption processes for CO in the near-surface region of porous TiO_2 show a pronounced hysteresis effect. As surface diffusion is retarded at lower temperatures, the hysteresis effect gradually disappears.

1. Introduction

This paper concerns adsorption onto a porous TiO_2 surface, using the useful property of the semiconducting TiO_2 to exhibit photoluminescence (PL) when excited by UV irradiation. The PL process occurs only from the extreme outer regions of the TiO_2 geometrical surface, providing insight into the behavior of adsorbate molecules there. This is the first study to employ

photoluminescence spectroscopy combined with quantitatively controlled gas adsorption in high vacuum to monitor monolayer quantities of gas adsorbing on the outer exposed sites. In addition, this capability allows one to monitor adsorbate diffusion into the interior of the porous powder. The use of PL spectroscopy supplies an unusual capability to monitor adsorption on the very outermost layers of a powdered solid. TiO_2 has found vast applications as a support in heterogeneous catalysis[1], as an active material in photocatalysis[2-4], as a white pigment[5-7], as a basis for photocells to capture solar energy[8, 9] , and as a gas sensor[10, 11]. Using PL we probe the adsorption of gases and their surface diffusion into and out of the interior of the meso-porous TiO_2. The mesoporosity is related to transport by diffusion of molecules across the TiO_2 grain surfaces and from particle to particle. Surface diffusion is known to be controlled by the meso-pore geometry and the properties of the meso-pore walls[12].

A study by Monson and co-workers[13] theoretically investigated hysteresis under equilibrium condition in adsorption/desorption processes on porous surfaces by using molecular dynamics and Monte-Carlo simulations, considering four types of pore geometries. Models for each pore geometry suggest that extreme differences in equilibrium coverages, measured deep in a pore compared to coverages at the mouth of a pore, will exist during all stages of both adsorption and desorption processes. Classical ideas about the equilibrium coverages found in the internal and external regions of an inkwell pore have been shown to be incorrect.

There have been no reported experimental studies of the diffusion of adsorbed molecules through a porous substrate, where nanometer-depth spatial resolution has been employed in the measurement of local surface coverage. Yet it is in this nanometer depth range near the surface where different models of diffusion through meso-pores may be critically tested. In this study we employ photoluminescence (PL) spectroscopy to probe the development of adsorbed layers on

the very outermost surface sites of a porous solid adsorbent (TiO_2) in regions where the meso-pores, separating 30-80 nm particles, join the gas phase. In parallel, we also employ transmission infrared (IR) spectroscopy to gain insight into the extent of adsorption averaged over the entire depth of the diffusion process.

Photoluminescence spectroscopy on semiconductor surfaces is highly sensitive to adsorbate molecules by virtue of the adsorbate-induced modification of the electronic structure of the semiconductor surface in regions within 10's of nm of the surface[14-17]. The reason for the high surface sensitivity of this spectroscopic technique is the short penetration length of the exciting UV radiation within individual semiconductor particles when the photon energy is well above the bandgap energy. Hence, our studies on powdered TiO_2 involve 3.88 eV photon excitation energy where the semiconductor bandgap is in the range of 3.0 – 3.2 eV. This results in a sampling depth of 12-25 nm[17-19]. UV irradiation of 3.88 eV produces a hot electron which relaxes to the bottom of conduction band where its mobility can carry it to a defect site or elsewhere. Trapped charge carriers recombine at this defect site that lies within the band gap, emitting 530 nm light.

Continuous irradiation of TiO_2 in vacuum by 3.88 eV light induces a continuous PL intensity increase due to the accumulation of positive charge on the surface (positive surface photovoltage)[20-23] and thus, a change of the degree of band-bending. In other words, long UV irradiation times decrease the degree of upward band bending in the n-type TiO_2 as the thickness of the depletion layer (Δd) decreases. This provides an additional number of defects near the surface which are active for electron-hole (e^--h^+) pair recombination yielding photoluminescence, and finally results in a flat-band condition accompanied by the formation of zero depletion layer thickness, and maximized PL intensity. Adsorbed electron donor or acceptor molecules on the

flat-band TiO_2 surface exchange charge with the surface, altering the band-bending structure from the flat-band condition by bending the bands downward or upward, respectively, and expanding the depletion layer thickness[17, 24-26]. This band bending due to donor or acceptor adsorbent molecules causes the intensity of PL to decrease from the intensity measured for the flat-band semiconductor. The PL spectrum of adsorbed molecules can also be used to monitor the surface coverage of these molecules with great sensitivity, where single molecule detection is often achieved[27].

2. Experimental

The base pressure in the cell after bake out, measured with a cold cathode gauge or a quadrupole mass spectrometer (SRS Model RGA 200), is ~3.0 x 10^{-9} Torr. The apparatus used in this study was previously described in Chapter 2.

FTIR transmission measurements are obtained by averaging 64 interferograms with 2 cm^{-1} spectral resolution employing a ℓ-N_2 cooled MCT detector. Each IR measurement is a ratio of IR spectra of the sample and an empty portion of the tungsten grid, obtained under identical conditions.

In all experiments here, long continuous light exposures are used initially to develop the PL signal as a positive surface photovoltage develops in vacuum. In contrast, during gas adsorption/desorption and annealing, the light was blocked by a shutter to avoid any change in PL by UV light. After modifying the surface by adsorption, the PL was recorded employing small UV exposures of 67 s from the Xe pulsed lamp. Such small exposures to UV light do not appreciably alter the intensity of PL from the surface.

The mass of the TiO_2 sample pressed into a W-grid is 6.3 x 10^{-3} g. For adsorption studies, research-grade purity gases CO (99.99 %) and NH_3 (99.99 %) were employed. For the cleaning procedure, research-grade O_2 (99.99 %) was used.

To remove impurities from the surface, the sample was cleaned by performing an identical cleaning cycle before each experiment. The TiO_2 was heated in vacuum to 700 K and then treated with 0.125 Torr O_2 at the same temperature for 20 min to oxidize any impurities adsorbed on the sample. To remove the chemisorbed molecular O_2 and other volatile oxidized impurities from the surface, the cell was evacuated to high vacuum and held at 700 K for another 45 min. This cleaning procedure provided a partially-dehydroxylated TiO_2 surface which also probably contains oxygen-vacancy defects[28-30]. For both PL and IR measurements the sample was cooled down to 86 K. The very small concentration of surface hydroxyl groups present on the TiO_2 remain constant upon UV irradiation as judged by the IR spectrum.

The change in the PL intensity as a function of the depletion layer thickness after adsorbing gas on the surface is given by Lambert-Beer Law (equation 1), as previously described by Ellis and co-workers [25, 26].

$$[PL]_\theta = [PL]_0 \cdot e^{-\gamma \cdot \Delta d} \quad (1)$$

or,

$$ln \frac{[PL]_0}{[PL]_\theta} = \gamma \cdot \Delta d \quad (2)$$

where $[PL]_\theta$ is the PL intensity at certain adsorbate coverage (θ); $[PL]_0$ is the saturation PL intensity after long UV irradiation at θ=0; γ is the sum of absorptivities for absorbed and emitted light in TiO_2; Δd is the difference in the depletion layer thickness before and after gas adsorption.

To model the correlation between the change in the PL intensity and the surface coverage (θ) of adsorbates, we first developed the relationship between the depletion layer thickness and surface coverage by using Poisson's equation for the near surface region, eq. (3)[31], and the well-known relationship between the change in work function, (ΔΦ), and the surface coverage, (θ), eq. (4), assuming that adsorbate-adsorbate intermolecular depolarization effects are not significant. It should be noted that the change in the work function due to adsorption on a semiconductor is equivalent to the change in the electrostatic potential at the surface, or in other words, the degree of band bending at the surface.

$$\Delta\Phi = \frac{2\pi e N_d}{\varepsilon} \cdot \Delta d^2 \qquad (3)$$

$$\Delta\Phi = \frac{\mu}{\varepsilon_0} \cdot \theta \qquad (4)$$

where ΔΦ is the change in work function in the surface region (eV); e is electron charge (C) ; N_d is the dopant concentration (m^{-3}); ε is dielectric constant for TiO_2 ($F \cdot m^{-1}$); ε_0= vacuum permittivity ($F \cdot m^{-1}$); μ is the dipole moment of an adsorbed molecule (C·m).

Combining equations (3) and (4) we obtained the relationship between the surface coverage of adsorbate and the depletion layer thickness:

$$\theta = \frac{2\pi e \varepsilon_0 N_d}{\mu\varepsilon} \cdot \Delta d^2 \qquad (5)$$

Finally by using expressions (5) and (2), equation (6) shows the relationship between the change in PL intensity and the surface coverage of adsorbed molecules:

$$\theta = \frac{2\pi e \varepsilon_0 N_d}{\mu\varepsilon\gamma^2} \cdot \left[\ln \frac{[PL]_0}{[PL]_\theta}\right]^2 \qquad (6)$$

In this work, equation (6) was used to relate the surface coverage of adsorbed molecules to the PL intensity. This treatment assumes that adsorption does not change the PL intensity for any reason other than the change in depletion length.

3. Experimental Results

A. Photoluminescence Development Under UV Irradiation at Different Temperatures- Preparation of TiO_2 in the Flat-Band Condition

Figure 1 shows the PL development under long UV irradiation in vacuum at three different temperatures: 100 K, 110 K and 120 K. The sample is irradiated by 320 nm (3.88 eV) light for 218 minutes. In all three experiments the PL intensity increases with UV irradiation and approaches a saturation level. The PL saturation intensity is higher at lower temperatures. Insert (a) shows one example of the evolution of the PL emission band at 529.5 nm for increasing exposure to UV irradiation. Two features at 390 nm and 780 nm originate from the reflected source light. The peak at 780 nm is a half-harmonic feature of the 390 nm peak. These two background features were also present when a portion of the W-grid, that does not contain TiO_2, was irradiated (not shown here).

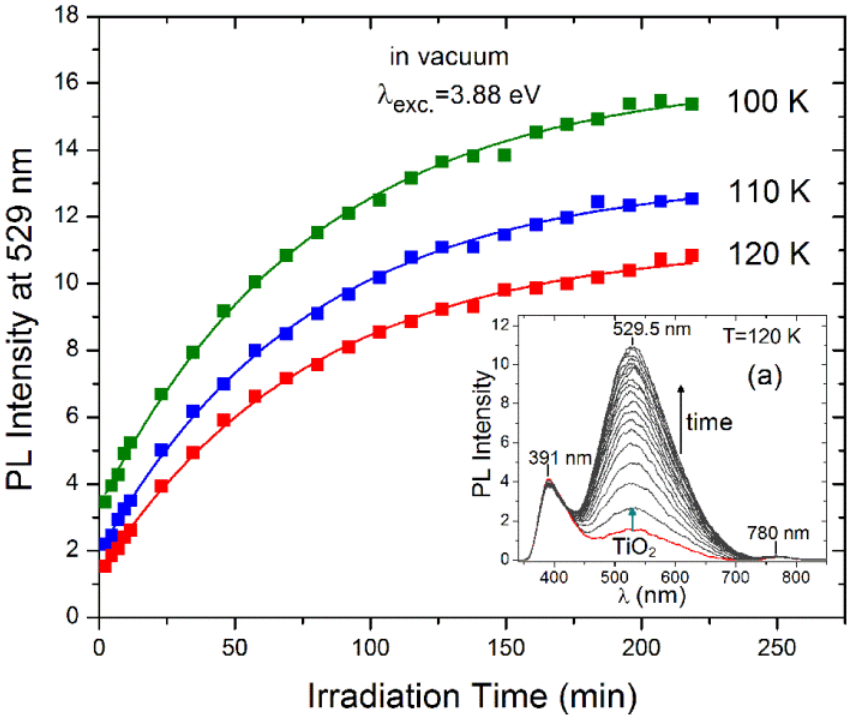

Figure 1. Photoluminescence Development under UV Irradiation- Building of Positive Surface Charge. Photoluminescence intensity development as a function of UV irradiation in vacuum at different temperatures: 100 K; 110 K and 120 K. The sample was irradiated by 320 nm (3.88 eV) for 218 min. Inset (a) shows the PL spectral development for TiO_2 in vacuum. The PL peak maximum at 529.5 nm (2.34 eV) increases as the sample continuously absorbs UV irradiation. Two peaks at 390 nm and 780 nm originate from the reflected source light. The peak at 780 nm is a half-harmonic feature of the 390 nm peak.

Under UV irradiation the depletion region (Δd) in n-type TiO_2 gradually narrows due to the accumulation of positive charge on the surface, providing additional UV-light accessible PL-active defects that facilitate the e^--h^+ recombination process and result in the PL intensity increase[17]. Ultimately, the depletion layer thickness is reduced to zero and a flat band condition is achieved leading to saturation of the PL intensity as shown schematically in Figure 2. The saturation PL intensity decreases as the temperature is increased from 100 K to 120 K. This is

due to the scattering of charge carriers by phonons, reducing the efficiency of the radiative charge recombination and increasing non-radiative recombination decay as the temperature is increased under constant light flux[32, 33].

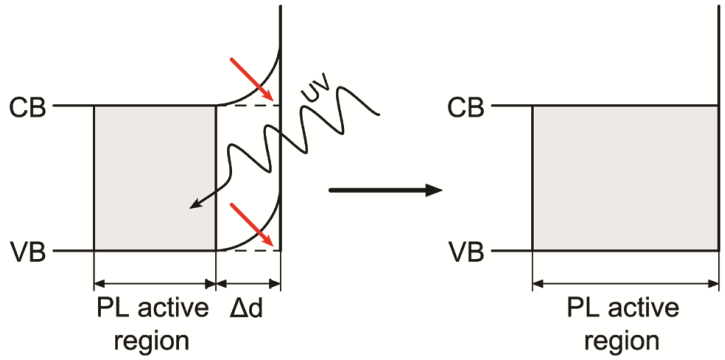

Figure 2. Enhancement of PL-Active Region by UV irradiation. The enhancement of PL-active region under long UV irradiation provides additional number of defects that facilitate the e^-- h^+ recombination process leading to a gradual PL intensity increase. The PL only occurs in the PL-active region since electrons and holes are swept away from each other in the depletion region (Δd). Upon long UV irradiation, the PL-active region expands to its maximum where the depletion layer is zero in thickness, producing a flat-band condition.

B. Adsorption of NH_3 on TiO_2 Powder

Figure 3A shows the change in PL intensity as a function of increasing adsorption of ammonia on TiO_2, previously prepared to the flat band condition by continuous exposure to UV light. At this condition, NH_3 is adsorbed on the surface in the dark at 200 K. Adsorbed NH_3 causes downward band bending, expanding the depletion region and leading to a decrease in PL intensity. Figure 3B shows the evolution of the IR spectra of adsorbed NH_3 on the TiO_2 surface at 200 K with increasing numbers of admitted NH_3 gas molecules. The transmission IR measurements sample the entire depth of the porous TiO_2. Several absorption bands due to

adsorption of NH_3 appear at ~ 3355 cm^{-1}, 3252 cm^{-1}, 3161 cm^{-1}, 3068 cm^{-1}, 1597 cm^{-1}, 1292 cm^{-1} and 1153 cm^{-1}.

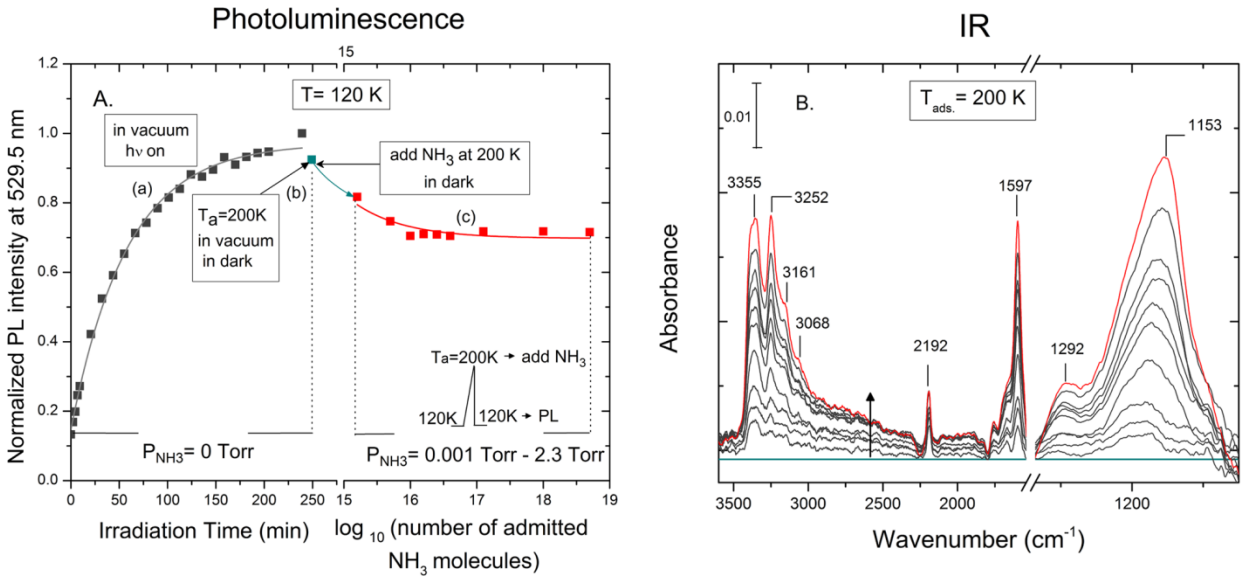

Figure 3. Adsorption of NH_3 on TiO_2 Powder. 3A. (a) Black squares represent PL development in vacuum at 120 K during continuous irradiation (~ 218 min); (b) Blue point shows the PL change after the sample was heated in the dark from 120 K to 200 K and then cooled back to 120 K; (c) Red squares show the PL intensity decrease as a function of the admitted number of NH_3 molecules at 200 K. After introducing ~ 1 x 10^{16} NH_3 molecules the PL intensity reaches the saturation level. All PL measurements were recorded at 120 K. Figure 3B shows the IR development when different amounts (2.28 x 10^{20} – 8.85 x 10^{21} molecules (red spectrum)) of NH_3 at a TiO_2 temperature of 200 K are introduced into the system. The limiting IR absorbance of 1 ML of chemisorbed NH_3 was obtained by warming the TiO_2 to 215 K under P_{NH3}= 12 Torr, and then cooling back to 200 K.

C. Changes During NH_3 Adsorption-Comparison of PL and IR

Figure 4 shows the surface coverage development plotted together as a logarithmic function of the number of admitted NH_3 molecules. A large fraction of the admitted NH_3 molecules condenses on the re-entrant Dewar at 77 K. In the PL measurements the sample is heated to 200

K in the dark to adsorb NH_3 gas, and then the sample is cooled down to 120 K to acquire PL spectra. A small exposure of 67 s of UV radiation is used to measure the PL after adsorption and does not appreciably affect the PL intensity. Also, in the IR measurements, NH_3 gas is adsorbed at 200 K. The NH_3 distribution through the powder at 200 K is strongly retarded due to its slow surface diffusion into the interior region of the TiO_2 powder, as indicated by slow development of IR spectra for adsorbed NH_3, whereas the PL signal changes rapidly and saturates at low NH_3 exposures due to the ability of PL to sample only the outermost surface of the porous TiO_2.

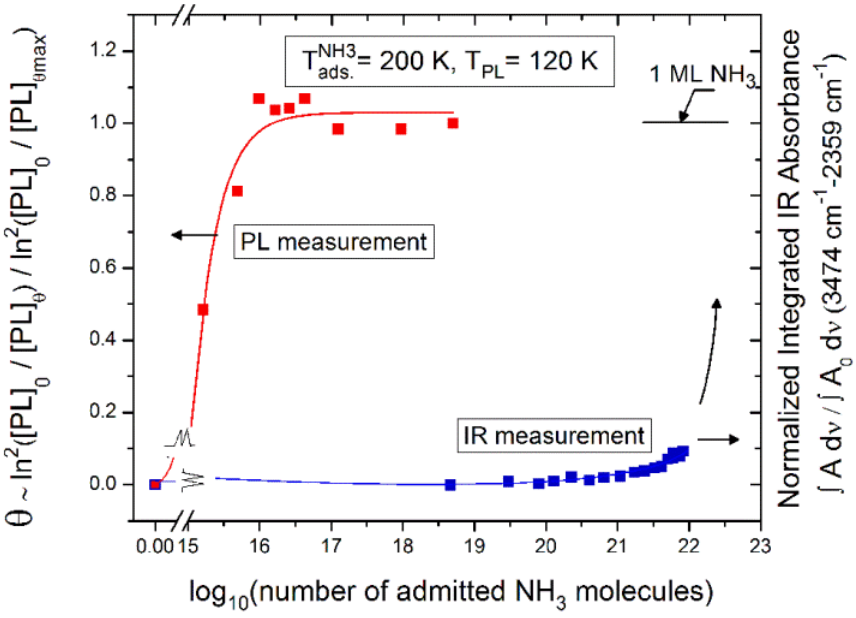

Figure 4. Probe of NH_3 Adsorption by PL and IR. The PL and IR spectral development when NH_3 gas is adsorbed on TiO_2 powder at 200 K. (a) Red squares represent the fraction of NH_3 coverage in the near-surface region as sampled by PL as a function of the number of admitted NH_3 molecules. (b) Blue squares show the integrated IR absorbance of NH_3 modes in the 3474 cm^{-1}-2359 cm^{-1} region and reflect the average NH_3 coverage in the depth of the TiO_2 powder. Infrared spectra are recorded at 200 K.

D. Adsorption of CO on TiO_2 Powder

Figure 5A shows the PL development during ~218 min. of UV irradiation in high vacuum at 120 K (region (a)) achieving the flat-band condition and an upper limit of PL intensity. Adsorption of CO gas occurs in the dark at 120 K at the flat-band condition as shown in region (b). During adsorption, 67 s of UV exposure is used to acquire the PL spectral points. During adsorption it is observed that the PL intensity decreases gradually as the number of admitted CO molecules increases. Idriss et al.[34] observed the same effect on ZnO powder. Adsorption of CO on TiO_2 alters the surface potential by bending the flat bands downward and expanding the depletion region, resulting in a decrease of PL intensity.

Figure 5B shows the IR absorbance development for adsorbed CO at 120 K. When CO gas is adsorbed on the partially-dehydroxylated TiO_2 surface, several IR bands due to the CO stretching mode develop with absorbance maxima at 2180 cm^{-1}, 2175 cm^{-1}, 2165 cm^{-1} and 2138 cm^{-1}. The strong and narrow band at 2180 cm^{-1} is assigned to Ti^{4+}- CO species formed, as reported by others[35]. After increasing the coverage of CO, a small absorption band develops at 2165 cm^{-1}. This feature is attributed to formation of adsorbed CO on a separate site, as reported in the literature[36]. Also, the feature at 2138 cm^{-1} is attributed to a weakly-bound physisorbed species. The 2138 cm^{-1} band immediately disappears after evacuation for 30 sec at 120 K.

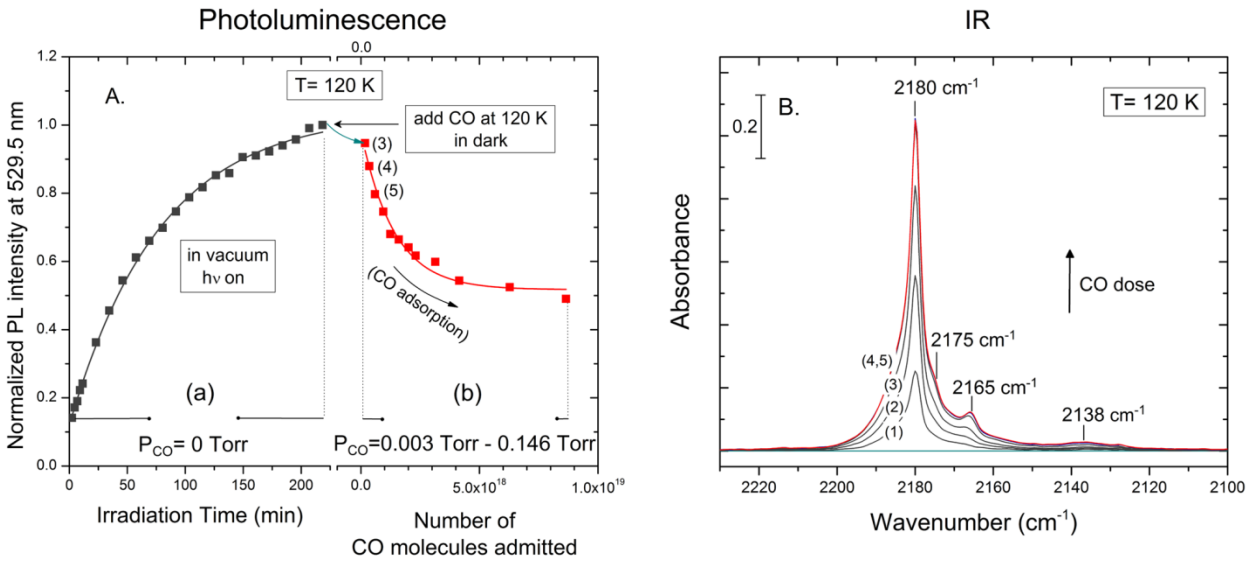

Figure 5. Adsorption of CO on TiO_2 Powder. 5A (a) Black squares show PL development in vacuum at 120 K during continuous UV irradiation for 218 min. ; (b) Red squares represent the PL decrease during adsorption as a function of CO partial pressure, $P_{CO,}$ at 120 K. The first change in PL intensity occurs after introducing 0.003 Torr (1.58 x 10^{17} molecules) of CO; the PL intensity reaches a near saturation point at 0.146 Torr (7.71 x 10^{18} molecules) of admitted CO; 5B. The IR absorbance development for CO at 120 K. ((1)- 5.3 x 10^{15} molecules admitted; (2)-1.0 x 10^{17} molecules admitted; (3)-1.6 x 10^{17} molecules admitted; (4)- 3.2 x 10^{17} molecules admitted; (5)- 5.3 x10^{17} molecules admitted). The numbered spectra (1)-(5) correspond to each other for PL and IR measurements.

E. Adsorption/Desorption of CO: Hysteresis Effect

Figure 6 shows the surface coverage change in the near surface region as measured by PL when CO gas is adsorbed/desorbed at three different temperatures: A. 120 K, B. 110 K and C. 100 K. All data are normalized to the PL saturation (flat-band) values obtained after large UV exposures in vacuum at each temperature. In all three PL experiments, the CO surface coverage, θ_{CO}, increases when the CO partial pressure, P_{CO}, is increased. At 110 K and 100 K complete saturation of the near-surface region is not achieved at the highest pressure plotted due to the loss

of temperature control as higher gas pressures caused slight warming of the TiO_2 sample. Upon evacuation to lower pressures, the CO surface coverage in the near-surface region, θ_{CO}, decreases when CO desorption takes place at all three temperatures and an adsorption/desorption hysteresis is observed.

In these experiments it is observed that for adsorption, the CO surface coverage in the near surface region measured by PL, increases more rapidly as the adsorption temperature is decreased from 120 K to 100 K. This result suggests that the surface diffusion of CO through the TiO_2 powder is more retarded at lower temperatures and thus, the CO coverage in the near surface region rises faster during adsorption under the same CO(g) supply conditions, causing a more rapid change in PL intensity. For the desorption process achieved as P_{CO} is lowered, it is seen in the desorption that CO surface coverage in the near-surface region is observed to begin its decrease at lower P_{CO} for lower temperatures. The separation between the adsorption-desorption processes (the hysteresis) is reduced at lower temperatures as the rate of the CO surface diffusion process diminishes in importance. At all temperatures, the PL intensity eventually returns to its initial value when all CO has desorbed.

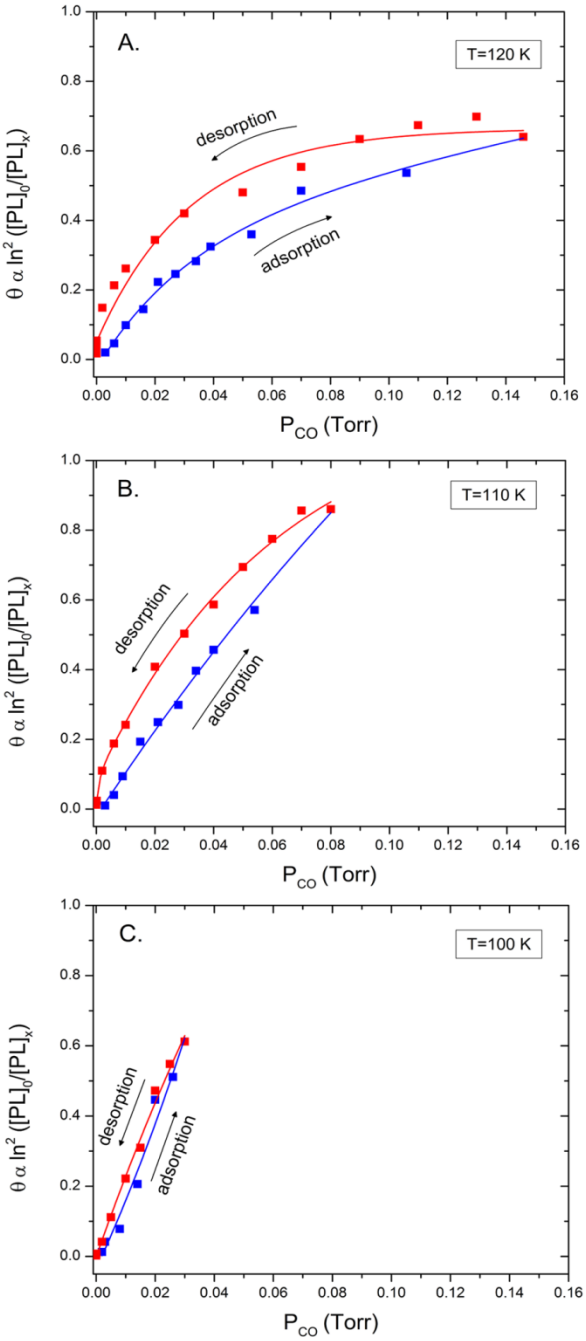

Figure 6. CO Adsorption/Desorption-Hysteresis Effect using Photoluminescence. PL measurements of the change in the surface CO coverage upon CO adsorption (blue squares) and desorption (red circles) at different temperatures: A. 120 K, B.110 K and C. 100 K. PL data are normalized to their vacuum value.

F. Changes During CO Adsorption-Comparison of PL and IR

Figure 7 shows the change in PL intensity and IR absorbance as CO adsorption is increased at 120 K, 110 K and 100 K. We observed that the PL intensity responds more slowly to CO adsorption compared to the development of IR absorbance. This is just opposite to observations for NH_3 adsorption, shown previously in Figure 4. This indicates that during CO adsorption, the surface coverage of CO in the near-surface region lags behind the average CO coverage in the interior of the powdered TiO_2. During adsorption, depletion processes from the near-surface region to the bulk region occur by CO surface diffusion, and kinetically produce lower CO coverage in the near surface region than deep in the pore structure. Reducing the adsorption temperature, the rate of CO coverage growth in the ~ 20 nm near-surface region increases due to kinetically retarded CO diffusion into the bulk, as shown previously in Figure 6.

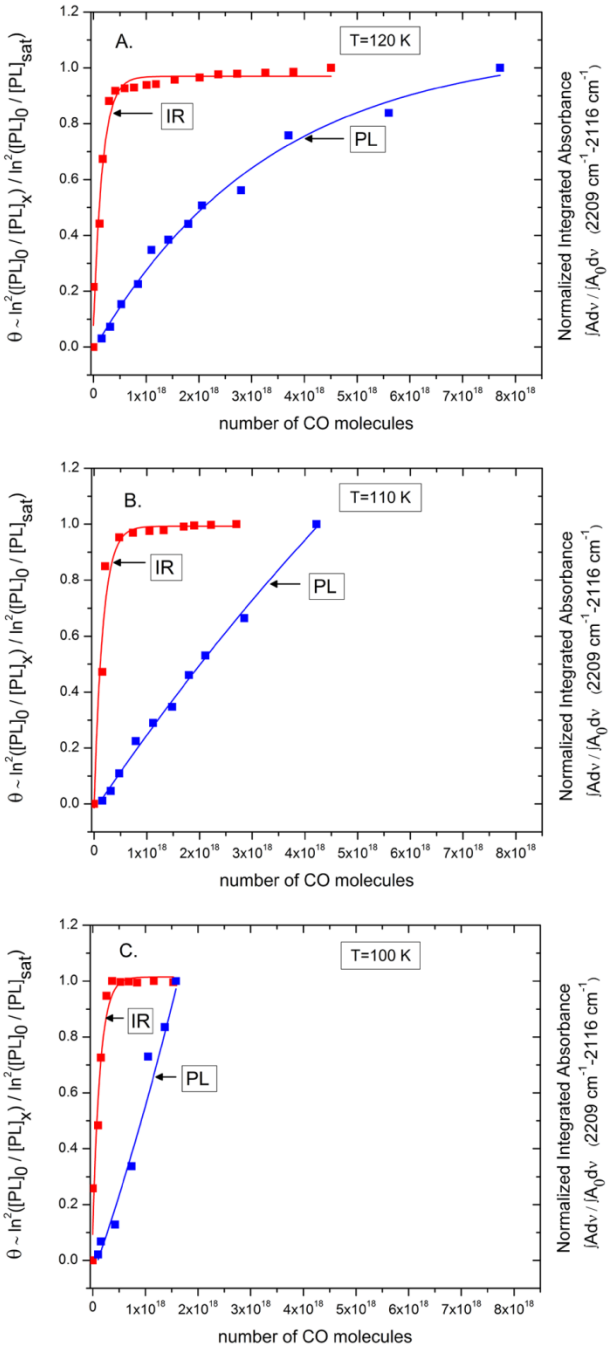

Figure 7. Probe of CO Adsorption by PL and IR. PL (blue squares) and IR (red squares) development upon CO adsorption at: A. 120 K B. 110 K and C. 100 K. (a) Blue squares represent the change of surface CO coverage in the surface region measured by PL as the number of admitted CO molecules increases. (b) Red squares show the change of integrated CO IR absorbance in the 2209 cm^{-1} -2116 cm^{-1} region, a measurement of the average coverage throughout the TiO_2 powder thickness. For the 110 K and

100 K cases, CO adsorption was discontinued below the saturation condition, and the saturation condition was estimated.

4. Discussion

A. Geometrical Consideration

The penetration depth of UV light into semiconductors is wavelength dependent which implies that by selecting the desired excitation wavelength a certain depth of the material can be probed by PL spectroscopy. In this study, the PL measurements employ 320 nm (3.88 eV) excitation irradiation which penetrates only ~20 nm [14-19] deep into the powdered TiO_2, providing information only about the very outermost surface region of the porous TiO_2, as shown schematically in Figure 8. In this ~ 20 nm region, the approximate number of available active sites for gas adsorption, in 1 cm^2 geometrical area, is ~ 1 x 10^{15} sites cm^{-2} based on the BET surface area of the TiO_2 [37] and assuming a saturation adsorbate density of ~ 5 x 10^{14} sites cm^{-2}. The IR spectroscopy samples throughout the entire depth (0.0076 cm) of the TiO_2 powder observing on 1 cm^2 of geometrical area, ~ 5 x 10^{18} surface active sites. Combining two sensitive spectroscopies allows one to compare adsorption/desorption processes in the very outer surface of porous materials to adsorption in the bulk. A cross section through the porous TiO_2 surface which includes particles at the surface and deeper in the material can be pictured as containing pores with mouths opening to vacuum and a long tortuous tube extending deep in the material, as shown in Figure 8 for a single pore. Considering the average TiO_2 particle size, the PL spectroscopy primarily detects molecules adsorbed on the outer-entry walls of the pore openings which join to the vacuum or gas phase.

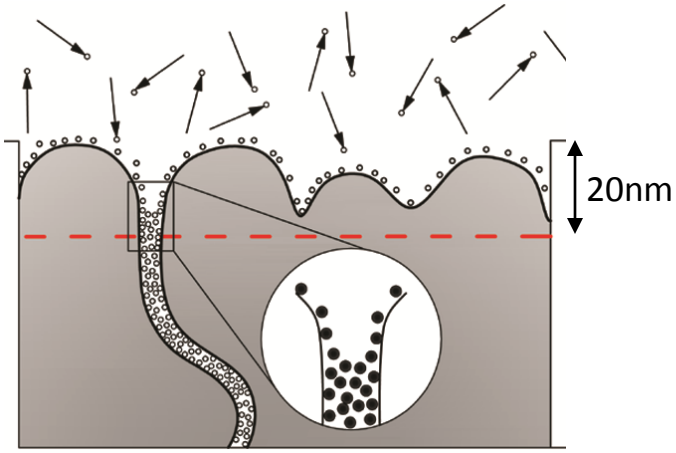

Figure 8. PL and IR Sampling of Adsorbed Gas in Porous TiO_2. Schematic representation of PL and IR sampling depth for adsorbed gas in porous TiO_2. Note that the adsorbate concentration increases as one moves into the pore structure due to the higher adsorption energy in the confined region.

B. Adsorption of NH_3 on TiO_2 at 200 K.

The fast PL response to adsorbed NH_3 at 200 K indicates that the development of NH_3 coverage in the near surface region occurs quickly at low exposures, and that NH_3 gas primarily adsorbs on the pore walls at the very near surface. The retarded IR development during NH_3 adsorption (Figure 4) indicates extremely retarded NH_3 diffusion deeper into the powdered TiO_2, implying a kinetically-controlled condition involving adsorbed NH_3 in the pore walls in the near-surface region with little NH_3 adsorbed on the pore walls deeper in the bulk. Temperature-programmed desorption (TPD) measurements revealed activation energies for desorption of NH_3 (near zero surface coverage) to be E_d=92 kJ mol^{-1} from reduced TiO_2(011) [38-40]. At the isothermal temperature of the NH_3 diffusion measurements (200 K), $e^{-\frac{E_d}{RT}} \sim 10^{-24}$.

C. Adsorption of CO on TiO_2 at 120 K.

During CO adsorption, diffusion of adsorbed CO molecules from the pore walls in the very near surface region into the bulk of the TiO_2 takes place by multiple rapid kinetic diffusion steps, and ultimately adsorbed CO gas becomes trapped by chemisorption deep in the pores. The CO molecules adsorbed deep in a pore are not able to desorb in one kinetic step due to CO re-adsorption on the adjacent pore wall. We observe that the growth rate of CO coverage in the 20 nm near-surface region lags behind the development of surface coverage deeper in the material as rapid CO diffusion takes place from the near surface sites to the more stable adsorption sites in the bulk during adsorption (Figure 7). By lowering the adsorption temperature, diffusion of CO molecules from the ~ 20 nm region to the bulk is slowed as judged by the slower relative rate of near-surface CO coverage in Figure 7 compared to the IR development rate. The desorption activation energy for CO from polycrystalline TiO_2 is 49 kJ mol^{-1} [41]. At the isothermal temperature of the CO diffusion measurements (120 K), $e^{-\frac{E_d}{RT}} \sim 10^{-21}$ which is 1000 times larger than for adsorbed NH_3 at 200 K, leading to kinetic behavior for CO which is more characteristic of a mobile species.

D. Hysteresis Effect- Adsorption/Desorption of CO on TiO_2.

The external surface coverage of CO as measured by PL during the desorption process is enhanced in comparison with that of the adsorption process at the same P_{CO} as shown in Figure 6. In the adsorption process, a pore entry in the near-surface region delivers mobile CO molecules to the interior. Surface CO coverage at the pore entry is being replaced with arriving molecules from gas as depletion to the interior takes place. In the desorption process, the CO molecules from the pore walls in the near-surface region desorb from the surface while constantly being resupplied by CO molecules which diffuse from the bulk, leading to the

adsorption/desorption hysteresis observed in Figure 6. The hysteresis observed at the near-surface regions disappears at lower temperatures as surface transport processes between the inner and outer regions of the porous solid becomes less important. For NH_3 in our experiments no hysteresis effect would be expected because of the immobility of the adsorbed NH_3 at 200 K.

E. Connection to Equilibrium Measurements

During adsorption, the measurements shown here reflect kinetic effects involving the rate of gas transport to the surface of a porous solid coupled with surface diffusion into the interior. During desorption, the desorption processes from the outer surface region occur in parallel with outward diffusion of adsorbed molecules to the outer surface region. In none of the measurements does true equilibrium exist. In spite of the kinetic nature of the measurements, for the most mobile species, CO, equilibrium behavior is probably approached during adsorption and desorption. The lower surface coverage of CO in the outer regions of the porous solid observed during adsorption (compared to the coverage in the interior), as shown in Figure 7, is reminiscent of the calculated equilibrium distributions of adsorbed molecules in pores as presented by Monson et al.[13] Here molecular dynamics and GCMC calculations show that **at equilibrium**, the surface coverage at the pore mouth of a uniform pore should be smaller than the coverage in the interior, simply because of the lower attractive potential experienced by a molecule near the pore mouth. However we believe that it is most appropriate in our measurements to attribute the observed partitioning of adsorbed CO molecules between the pore mouth and the interior to kinetic effects. Figure 7 shows that as temperature is raised, causing surface mobility to increase, the CO pressure needed to saturate the near-surface region increases, as adsorbed CO distributes into the bulk more rapidly during adsorption.

5. Conclusions and Summary of Results

The following results were obtained through a comparison of surface coverage measurements for NH_3 and CO adsorption on high surface area TiO_2 powder, using photoluminescence of the TiO_2 sorbent to observe adsorbate surface coverage in the near surface region (~ 20 nm), and infrared transmission spectroscopy to measure the average surface coverage throughout the porous TiO_2 adsorbent depth.

1. Adsorption of NH_3 occurs at the very outer region (~ 20 nm) of porous TiO_2 without penetrating deep into tortuous pores of the material as judged by rapid PL development and retarded IR development. This is due to the relatively high adsorption (and surface diffusion) energy for NH_3, leading to immobility at 200 K.
2. Adsorption of CO at the near surface region (~ 20 nm) of porous TiO_2 is followed by surface diffusion of CO molecules deeper into the material at 120 K, resulting in the development of a surface concentration gradient corresponding to CO depletion at the pore entrance, as judged by comparison of the CO coverage development in the near-surface (~ 20 nm) region measured by PL spectroscopy compared to the CO average surface coverage in the entire depth of the powder (0.0076 cm) as measured by IR.
3. Adsorption/desorption of CO on TiO_2 results in hysteresis behavior. During the CO desorption, the near-surface CO coverage (θ_{CO}) is enhanced relative to the observed near-surface CO coverage (θ_{CO}) during adsorption at the same P_{CO}. The enhancement of CO coverage in the near-surface region during the desorption process compared to the adsorption process occurs due to a more rapid rate of CO diffusion from the bulk, compared to the rate of CO desorption.

4. The hysteresis behavior of CO gradually disappears at lower temperatures (from 120 K to 100 K) due to the retarded surface transport kinetics involving the molecules at the entry of the pores and in the depth of the powdered TiO_2.

ACKNOWLEDGMENT

We acknowledge with thanks the full support of this work by the Army Research Office under grant number 55748CH. We also acknowledge helpful discussion with Professor Peter A. Monson of University of Massachusetts, Amherst and Dr. Matthias Thommes of the Quantachrome Corporation.

References:

1. Linsebigler, A. L.; Lu, G. Q.; Yates, J. T., Photocatalysis on Tio2 Surfaces - Principles, Mechanisms, and Selected Results. *Chem. Rev.* **1995,** 95, 735-758.
2. Diebold, U., The Surface Science of Titanium Dioxide. *Surf. Sci. Rep.* **2003,** 48, 53-229.
3. Hoffmann, M. R.; Martin, S. T.; Choi, W. Y.; Bahnemann, D. W., Environmental Applications of Semiconductor Photocatalysis. *Chem. Rev.* **1995,** 95, 69-96.
4. Thompson, T. L.; Yates, J. T., Surface Science Studies of the Photoactivation of Tio2-New Photochemical Processes. *Chem. Rev.* **2006,** 106, 4428-4453.
5. Fujishima, A.; Zhang, X.; Tryk, D. A., Tio(2) Photocatalysis and Related Surface Phenomena. *Surf. Sci. Rep.* **2008,** 63, 515-582.
6. McNeil, L. E.; French, R. H., Multiple Scattering from Rutile Tio2 Particles. *Acta Mater.* **2000,** 48, 4571-4576.
7. Chen, J.; Poon, C.-s., Photocatalytic Construction and Building Materials: From Fundamentals to Applications. *Building and Environment* **2009,** 44, 1899-1906.
8. Gratzel, M., Photoelectrochemical Cells. *Nature* **2001,** 414, 338-344.
9. Hardin, B. E.; Hoke, E. T.; Armstrong, P. B.; Yum, J. H.; Comte, P.; Torres, T.; Frechet, J. M. J.; Nazeeruddin, M. K.; Gratzel, M.; McGehee, M. D., Increased Light Harvesting in Dye-Sensitized Solar Cells with Energy Relay Dyes. *Nature Photonics* **2009,** 3, 406-411.
10. Schierbaum, K. D.; Kirner, U. K.; Geiger, J. F.; Gopel, W., Schottky-Barrier and Conductivity Gas Sensors Based Upon Pd/Sno2 and Pt/Tio2. *Sensors and Actuators B-Chemical* **1991,** 4, 87-94.
11. Savage, N.; Chwieroth, B.; Ginwalla, A.; Patton, B. R.; Akbar, S. A.; Dutta, P. K., Composite N-P Semiconducting Titanium Oxides as Gas Sensors. *Sensors and Actuators B-Chemical* **2001,** 79, 17-27.
12. Turro, N. J., Photochemistry of Ketones Adsorbed on Porous Silica. *Tetrahedron* **1987,** 43, 1589-1616.
13. Sarkisov, L.; Monson, P. A., Modeling of Adsorption and Desorption in Pores of Simple Geometry Using Molecular Dynamics. *Langmuir* **2001,** 17, 7600-7604.
14. Ghosh, G., *Handbook of Optical Constants of Solids*. Academic Press: 1985.
15. Mo, S. D.; Ching, W. Y., Electronic and Optical-Properties of 3 Phases of Titanium-Dioxide - Rutile, Anatase, and Brookite. *Phys. Rev. B.* **1995,** 51, 13023-13032.
16. Eagles, D. M., *J. Phys. Chem. Solids* **1964,** 25, 1243.
17. Stevanovic, A.; Buttner, M.; Zhang, Z.; Yates, J. T., Jr., Photoluminescence of Tio2: Effect of Uv Light and Adsorbed Molecules on Surface Band Structure. *J. Am. Chem. Soc.* **2012,** 134, 324-32.
18. Ghosh, A. K.; Maruska, H. P., Photoelectrolysis of Water in Sunlight with Sensitized Semiconductor Electrodes. *Journal of the Electrochemical Society* **1977,** 124, 1516-1522.
19. Cardona, M. H., G., Optical Properties and Band Structure of Wurtzite-Type Crystals and Rutile. *Phys. Rev. B.* **1964,** 137, A1467.
20. Kronik, L.; Shapira, Y., Surface Photovoltage Spectroscopy of Semiconductor Structures: At the Crossroads of Physics, Chemistry and Electrical Engineering. *Surf. Interface Anal.* **2001,** 31, 954-965.
21. Kronik, L.; Shapira, Y., Surface Photovoltage Phenomena: Theory, Experiment, and Applications. *Surf. Sci. Rep.* **1999,** 37, 1-206.
22. Schroder, D. K., Surface Voltage and Surface Photovoltage: History, Theory and Applications. *Meas. Sci. Technol.* **2001,** 12, R16-R31.
23. Rothschild, A.; Levakov, A.; Shapira, Y.; Ashkenasy, N.; Komem, Y., Surface Photovoltage Spectroscopy Study of Reduced and Oxidized Nanocrystalline Tio2 Films. *Surf. Sci.* **2003,** 532, 456-460.
24. Zhang, Z.; Yates, J. T., Effect of Adsorbed Donor and Acceptor Molecules on Electron Stimulated Desorption: O(2)/Tio(2)(110). *Journal of Physical Chemistry Letters* **2010,** 1, 2185-2188.
25. Kepler, K. D.; Lisensky, G. C.; Patel, M.; Sigworth, L. A.; Ellis, A. B., Surface-Bound Carbonyl-Compounds as Lewis-Acids - Photoluminescence as a Probe for the Binding of Ketones and Aldehydes to Cadmium-Sulfide and Cadmium Selenide Surfaces. *J. Phys. Chem.* **1995,** 99, 16011-16017.

26. Meyer, G. J.; Lisensky, G. C.; Ellis, A. B., Evidence for Adduct Formation at the Semiconductor Gas Interface - Photoluminescent Properties of Cadmium Selenide in the Presence of Amines. *J. Am. Chem. Soc.* **1988,** 110, 4914-4918.
27. Lakowicz, J. R., *Principles of Fluorescence Spectroscopy*. Springer: 2006.
28. Pan, J. M.; Maschhoff, B. L.; Diebold, U.; Madey, T. E., Interaction of Water, Oxygen, and Hydrogen with Tio2(110) Surfaces Having Different Defect Densities. *Journal of Vacuum Science & Technology a-Vacuum Surfaces and Films* **1992,** 10, 2470-2476.
29. Lu, G. Q.; Linsebigler, A.; Yates, J. T., Ti3+ Defect Sites on Tio2(110) - Production and Chemical-Detection of Active-Sites. *J. Phys. Chem.* **1994,** 98, 11733-11738.
30. Göpel, W.; Rocker, G.; Feierabend, R., Intrinsic Defects of Tio_{2}(110): Interaction with Chemisorbed O_{2}, H_{2}, Co, and Co_{2}. *Phys. Rev. B.* **1983,** 28, 3427-3438.
31. Zangwill, A., *Physics at Surfaces*. Cambridge University Press: 1988.
32. Najafov, H.; Tokita, S.; Ohshio, S.; Kato, A.; Saitoh, H., Green and Ultraviolet Emissions from Anatase Tio2 Films Fabricated by Chemical Vapor Deposition. *Japanese Journal of Applied Physics Part 1-Regular Papers Short Notes & Review Papers* **2005,** 44, 245-253.
33. Amtout, A.; Leonelli, R., Time-Resolved Photoluminescence from Excitons in Tio2. *Solid State Commun.* **1992,** 84, 349-352.
34. Idriss, H.; Barteau, M. A., Photoluminescence from Zinc-Oxide Powder to Probe Adsorption and Reaction of O2, Co, H-2, Hcooh, and Ch3oh. *J. Phys. Chem.* **1992,** 96, 3382-3388.
35. Hadjiivanov, K., Ftir Study of Co and Nh3 Co-Adsorption on Tio2 (Rutile). *Appl. Surf. Sci.* **1998,** 135, 331-338.
36. Hadjiivanov, K.; Lamotte, J.; Lavalley, J. C., Ftir Study of Low-Temperature Co Adsorption on Pure and Ammonia-Precovered Tio2 (Anatase). *Langmuir* **1997,** 13, 3374-3381.
37. Ohno, T.; Sarukawa, K.; Tokieda, K.; Matsumura, M., Morphology of a Tio2 Photocatalyst (Degussa, P-25) Consisting of Anatase and Rutile Crystalline Phases. *J. Catal.* **2001,** 203, 82-86.
38. Wilson, J. N.; Idriss, H., Reactions of Ammonia on Stoichiometric and Reduced Tio2(001) Single Crystal Surfaces. *Langmuir* **2004,** 20, 10956-10961.
39. McGill, P. R.; Idriss, H., Ab Initio Study of Surface Acid-Base Reactions. The Case of Molecular and Dissociative Adsorption of Ammonia on the (011) Surface of Rutile Tio2. *Langmuir* **2008,** 24, 97-104.
40. Erdogan, R.; Ozbek, O.; Onal, I., A Periodic Dft Study of Water and Ammonia Adsorption on Anatase Tio2 (001) Slab. *Surf. Sci.* **2010,** 604, 1029–1033.
41. Raupp, G. B.; Dumesic, J. A., Adsorption of Co, Co2, H-2, and H2o on Titania Surfaces with Different Oxidation-States. *J. Phys. Chem.* **1985,** 89, 5240-5246.

Chapter 5.

Electron Hopping Through TiO_2 Powder- A Study by Photoluminescence Spectroscopy

Published work: **Stevanovic, A.**; Yates, J. T., **Jr.,** ***J. Phys. Chem. C*** **2013,** 117, 24189-24195.

Abstract

Photoluminescence spectroscopy was employed to observe electron transport between TiO_2 particles. Ultraviolet (UV) irradiation (3.88 eV) was shown to positively enhance the photovoltage of TiO_2 particles at the powder surface causing an enhancement of their photoluminescence (PL) at 530 nm. The charging of the TiO_2 particles on the powder surface by UV irradiation is observed to partially discharge in the dark where the displaced bulk negative charge diffuses back toward the TiO_2 surface. This charge flow partially restores upward band bending causing the PL intensity to decrease. The rate of the discharging process was used to estimate the electron migration mobility (~ 10^{-10} m^2Vs^{-1} at 300 K) between TiO_2 particles in the TiO_2 matrix. Electron migration between TiO_2 particles is temperature dependent with an activation energy of 0.015 ± 0.008 eV. In addition, it was found that the adsorption of an immobile electron-donor molecule (NH_3), which forms a positively charged species on the TiO_2 surface, does not show charge mobility behavior in contrast to mobile electrons. These measurements were carried out in high vacuum in the absence of oxygen and surface impurities detectable by IR spectroscopy.

I. Introduction

Metal oxide nanostructures such as TiO_2, ZnO, SnO_2 and Nb_2O_5 have attracted great attention in photovoltaic applications due to their ability to capture and convert sunlight into electrical

energy[1-4]. Among these metal oxides, the most intensively studied material is the n-type TiO_2 semiconductor due to its superior properties which are heavily utilized for photovoltaic purposes[5, 6] and in photocatalysis[7-10]. In TiO_2–based photovoltaic devices, the semiconductor particles are sensitized with a light-harvesting dye molecule which serves to deliver photo-generated electrons into a network of interconnected TiO_2 particles. The electrons percolate amongst interconnected TiO_2 particles and are collected by an electrode. In mesoporous TiO_2, electrons in single crystallites travel by crossing several particle-particle interfaces. In TiO_2 involving, 20-nm sized particles, electrons may cross as many as 50 interfaces in a typical photovoltaic cell[11-13]. It was shown that the photoconductivity of the mesoporous TiO_2 single crystal material is two orders of magnitude higher than the photoconductivity in a nanometer TiO_2 particle network due to the lower number of particle-particle interfaces. An understanding of charge transport in networks of semiconductor particles is essential for improving the efficiency of photovoltaic devices involving porous semiconducting material.

Charge transport has been intensively studied by optical and electrical methods such as photovoltage measurements[14, 15], impedance spectroscopy[16], Hall effect measurements[17, 18], photoluminescence[19] and also modeling[20-22]. Electron transport in porous TiO_2 occurs under UV exposure as shown by Dittrich et al.[14] and others[23, 24] as photo-generated electrons in the conduction band move either freely or by trapping-detrapping processes from particle to particle across the TiO_2 network. It has been found by employing tetrahertz time domain spectroscopy that the average charge mobility ***within*** a TiO_2 nanoparticle is four orders of magnitude larger[25] than the charge mobility ***between*** TiO_2 particles in the TiO_2 matrix that does not contain electrolyte [26, 27]. In an electrolyte-filled TiO_2 matrix, electron mobility between TiO_2 particles is about an order of magnitude faster than in a porous TiO_2 network[28, 29].

The surface and electronic properties of porous TiO_2 depend strongly on the presence of adsorbed molecules on the surface as adsorbates perturb the distribution of electron trap sites, thus affecting electron conductivity. The vast majority of reports on charge carrier transport in porous materials present measurements performed in air or in different solutions where the surface electronic properties of TiO_2 are altered from that found in vacuum. It was found for example that in porous nanocrystalline TiO_2, the conductivity of charge carriers in TiO_2 particles increases by six orders of magnitude under vacuum conditions due to the removal of adsorbed oxygen[23]. It is postulated that lattice oxygen removal by annealing leads to excess electrons in the surface-oxygen vacancy defect sites. The excess electrons contribute to increased conductivity[30] and to upward band bending[31]. Compared to measurements in air, the experiments presented in this paper involve a high level of control of the surface as the TiO_2 preparation and measurements are conducted under high vacuum conditions and adsorbed species on to the surface are monitored by IR spectroscopy.

In the TiO_2 powder, in the case of n-type material, the production of electron-hole pairs occurs only in the very outer surface region of the powder due to the short penetration depth (~20 nm) of the exciting UV irradiation[32-35]. This causes the development of a positive surface photovoltage which is confined to the outermost TiO_2 particles in the powder where the particle size is of the same order of magnitude as the light penetration depth. The TiO_2 surface is oxygen deficient and therefore n-type due to the excess electrons in the lattice-oxygen vacancies on the surface which increase the electronic potential energy near the surface causing the bands to bend upward. Here, under UV irradiation, energetically preferred electron transport occurs into the bulk from the surface of the particles where the bands are initially bent upward[36-38]. In this region e^--h^+ recombination is retarded as charges are swept away from each other due to the electric

field in the first 10-20 nm of the TiO_2 surface. UV irradiation therefore decreases the depletion layer thickness. The positive charge accumulation at the TiO_2 surface during UV irradiation lowers the surface electrostatic potential causing initially upward-bent bands to flatten. As a result, UV irradiation causes the photoluminescence intensity to be enhanced[31, 32, 39-41] as more semiconductor volume within the UV light penetration depth becomes available for e^-- h^+ recombination.

In this investigation, using photoluminescence spectroscopy (PL), we have observed under high vacuum conditions the change in surface photovoltage upon UV irradiation of interconnected TiO_2 particles. Here, surface negative charge is distributed into the bulk by absorption of energetic photons (3.88 eV) (Figure 1A). Our key finding is that upon discontinuation of UV irradiation, some of the negative charge originally distributed in the TiO_2 network returns back to the surface of the outermost TiO_2 particle (Figure 1B), partially restoring upward band bending and reducing the PL intensity. Here the production of a charged powdered TiO_2 surface by UV irradiation, followed by its discharge in the dark by migration of displaced electrons back to the surface, may be viewed as the behavior of a planar capacitor. The rate of discharge may be used to estimate the charge mobility as electrons hop from particle to particle if the electric field inducing electron mobility can be estimated. In addition, it was found that this process is temperature dependent as electron hopping between particles is enhanced at higher temperatures. Further, we have employed a chemical species, an electron donor (NH_3) molecule, to produce immobilized positively charged species on the TiO_2 surface analogous to the surface charging during irradiation. As expected, upon discontinuation of UV irradiation when adsorbed NH_3 is present, electrons in TiO_2 do not transport in the same manner as observed for electrons when the surface is positively charged by UV photons.

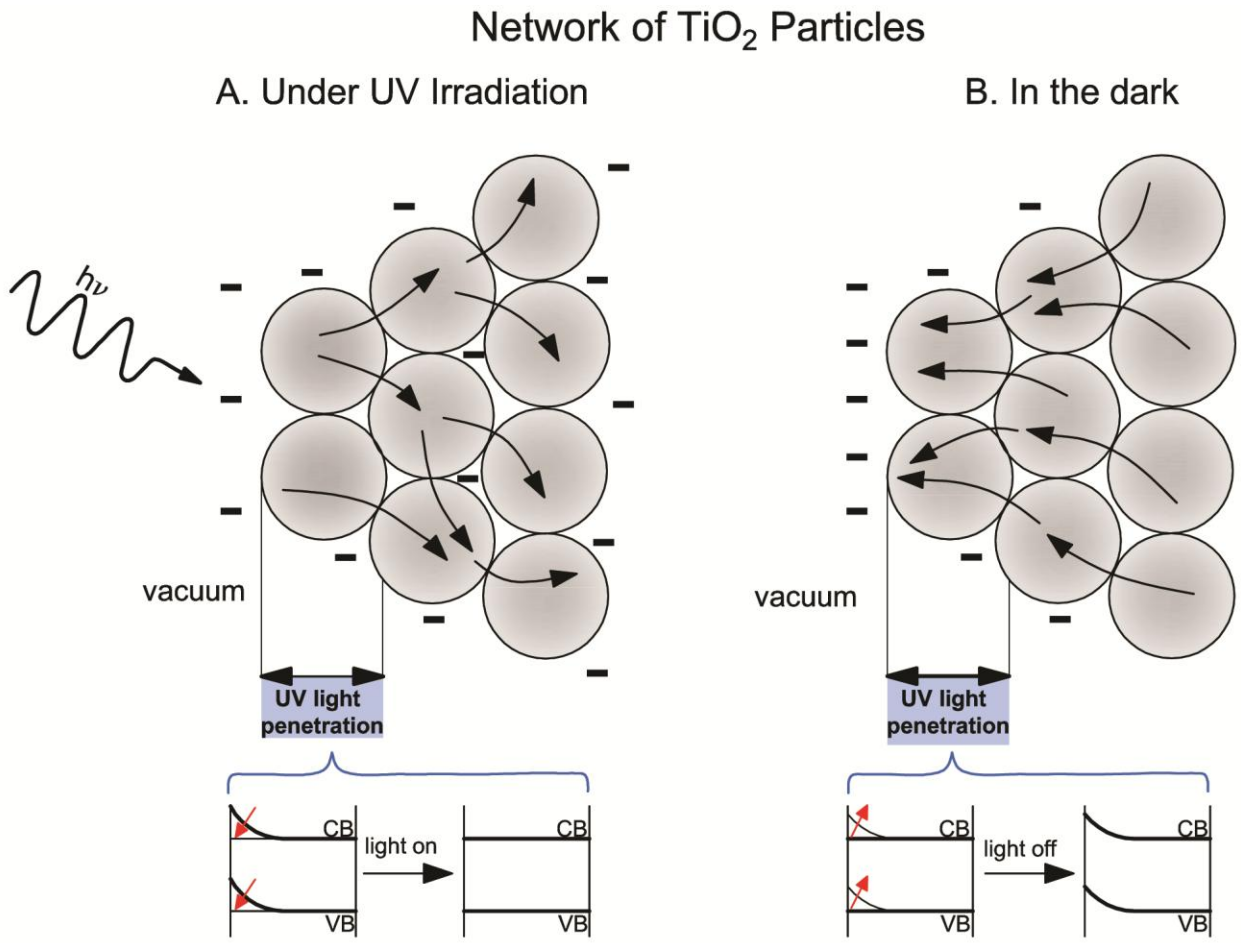

Figure 1. A. Distribution of surface negative charge into the TiO_2 powder caused by absorption of UV photons and inducing a more positive surface photovoltage on the outer TiO_2 particles causing band flattening; B. Diffusion of the bulk negative charge back to the TiO_2 surface in the dark partially restores upward band bending.

II. Experimental Section

The experimental apparatus was described previously.[32] In brief, a stainless steel optical cell with CaF_2 windows was employed allowing both PL and transmission IR measurements to be made on powdered TiO_2. The base pressure in the high vacuum stainless steel cell after bake out is ~ 3.0 x 10^{-9} Torr as measured by a cold cathode gauge or a quadrupole mass spectrometer

(SRS model RGA 200). The TiO_2 powder sample is fabricated as a pressed disk held in a temperature-controlled tungsten grid. The high vacuum cell is rigidly attached to a small portable high vacuum system which allows it to be moved from an infrared spectrometer (Perkin-Elmer Spectrum 100) to an adjacent photoluminescence spectrometer (Perkin-Elmer LS-55), maintaining the cell position accurately constant in both spectrometers. The TiO_2 powder is pressed with 6000 psi into a 0.0095 cm thick tungsten grid filling hundreds of window openings (0.022 x 0.022 cm) by the creation of a 7 mm diameter circular spot which can be accurately positioned in the UV or IR optical beam. The mass of the TiO_2 sample is 5.9×10^{-3} g. The sample is held on the tungsten grid which is clamped to a Cu (OFHC) sample holder that is connected to electrical feedthroughs and mounted on the end of a re-entrant Dewar. The temperature of the sample is measured by a 0.0095 cm diameter K-type thermocouple, spot welded on the center top of the grid. Temperature control is achieved to 0.1 K using ℓ-N_2 cooling and electrical heating. The temperature of the grid can be linearly programmed between 84 K and 1000 K by using a data acquisition card (National Instrument, DAC) and feedback from the thermocouple to control the heating current. This allows for precise isothermal measurements.

The photoluminescence measurements employ 320 ± 10 nm (3.88 eV) incident light from a pulsed Xe source (60 Hz with a pulse width of <10 μs). The continuous power measured at the sample position is 9.1×10^{-5} J s^{-1} cm^{-2} [1.5×10^{14} photons cm^{-2} s^{-1}]. A grating and a 320 nm band pass filter are employed on the source side. The spectra are obtained using 15 nm slit width at the excitation side and 20 nm slit width at the emission side with a scan speed of 500 nm min^{-1}. The PL spectra are detected by an R928 photomultiplier tube that covers the 200-900 nm range. For the PL measurements, the sample is positioned 15^0 off the specular reflection direction of the

source light to minimize detection of the reflected incident light from the sample surface and from the CaF_2 window.

The TiO_2 powdered samples employed in this work were provided by Evonik Industries (P-25, formerly Degussa). The TiO_2 P-25 consists of 75 % of anatase and 25 % rutile phase with particle sizes between 30-80 nm and a surface area[2] of 50 $m^2 g^{-1}$. A water slurry of TiO_2 particles was dried in air at 353 K. Additional adsorbed water was removed by treatment of the pressed sample in vacuum at 650 K for 30 minutes. Further thermal treatment at 650 K in vacuum followed by treatment in O_2(g) at 0.5 Torr for 30 min at 650 K was carried out. The sample was finally treated in vacuum at 650 K for 10 min, and then cooled to liquid nitrogen temperatures in vacuum for the experiments. Following this treatment the IR spectrum of the sample indicated that no OH and C-H containing adsorbed species were present at the detection limit of about 1% of a monolayer. The oxygen treatment was shown to effectively remove traces of adsorbed organic impurities which display C-H stretching modes in the 3000 cm^{-1} region.

III. Experimental Results

A. Charging and Discharging of the TiO_2 Surface.

In Figure 2a the gray spectra with maximum at 530 nm show that the PL intensity from TiO_2 particles increases during long UV exposures using the light in the PL spectrometer to activate long term changes in the TiO_2. The peak at 395 nm is an optical artifact and is disregarded[32]. In Figure 2b gray points show the development of the 530 nm peak over time. The PL intensity ultimately approaches a near-saturation plateau indicating a near-flat band condition. Here, the concentration of negative surface charge diminishes as electrons are distributed into the network of TiO_2 particles (charging process) as shown in Figure 1. In Figure 2b the red curve shows that

the PL intensity decreases upon discontinuation of UV irradiation for 192 min in vacuum (discharging process). The PL intensity reaches its minimum value when only a fraction of distributed electrons diffuse from the depth of the powder back to the surface thereby causing only partial restoration of upward band bending of the outermost particles. These measurements in the dark involve short UV exposures of 45 s each yielding a measurement of the discharging rate as seen by the drop in the PL intensity, where the long term influence of the UV light can be disregarded as it is only 2.5 % of that used to produce the inital charging curve.

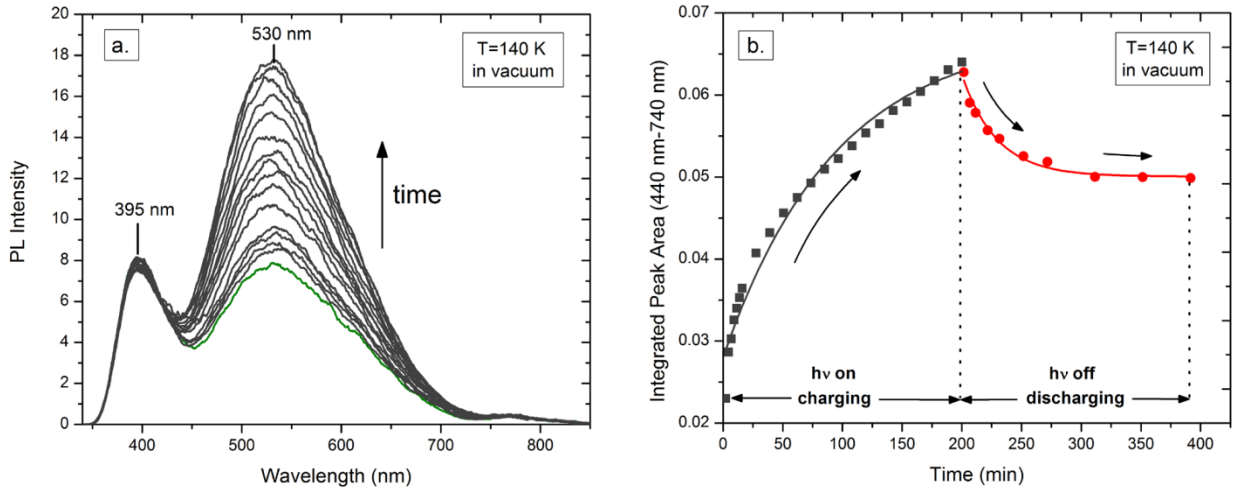

Figure 2. a. Development of a 530 nm TiO_2 photoluminescence feature during continuous UV irradiation in vacuum at 140 K. b. Change in PL intensity during and upon discontinuation of UV irradiation in vacuum at 140 K: Gray curve shows an exponential increase in PL intensity upon irradiation of TiO_2 particles indicating a decrease in the surface negative charge due to electron hopping from particle to particle, charging the interior of the TiO_2 network. The red curve shows a decrease in the PL intensity of the TiO_2 particles as negative charge transports from the interior of the TiO_2 powder back to the surface, partially restoring upward band bending.

B. Electron Migration from Particle to Particle.

Figure 3 shows several consecutive charging/discharging cycles of the TiO_2 network at 140 K in vacuum. During the UV irradiation cycles, the PL intensity increases (shown by gray curves) as negative surface charge diffuses deeper into the network of TiO_2 particles leaving less charge on the surface and causing upward-bent bands to flatten (point 2). As previously discussed, the bands flatten as UV light causes electrons to leave the surface of the TiO_2 particles located on the outermost surface of the powder. Upon discontinuation of UV irradiation (shown by red curve), partial relaxation occurs as the PL intensity exponentially decreases as electrons diffuse back from the bulk onto the TiO_2 surface. The rate of charge diffusion from the surface into the TiO_2 powder bed by UV irradiation ***increases*** as higher levels of PL intensity are produced in successive experiments (gray curves) with rate constants $k_{1\text{-}2}= 2 \times 10^{-4}\ s^{-1}$, $k_{3\text{-}4}= 3 \times 10^{-4}\ s^{-1}$ and $k_{5\text{-}6}=3 \times 10^{-3}\ s^{-1}$. On the other hand, the rate of charge diffusion from the bulk to the surface of the TiO_2 network in the dark in vacuum, ***decreases*** as time passes with discharge time rates $k_{2\text{-}3}= 7 \times 10^{-4}\ s^{-1}$, $k_{4\text{-}5}= 4 \times 10^{-4}\ s^{-1}$and $k_{6\text{-}7}= 3 \times 10^{-4}\ s^{-1}$. The reason for the decreasing rate of discharge is that during the passage of time in the experiment, electronic charge penetrates more deeply into the bulk, and becomes unavailable for back diffusion.

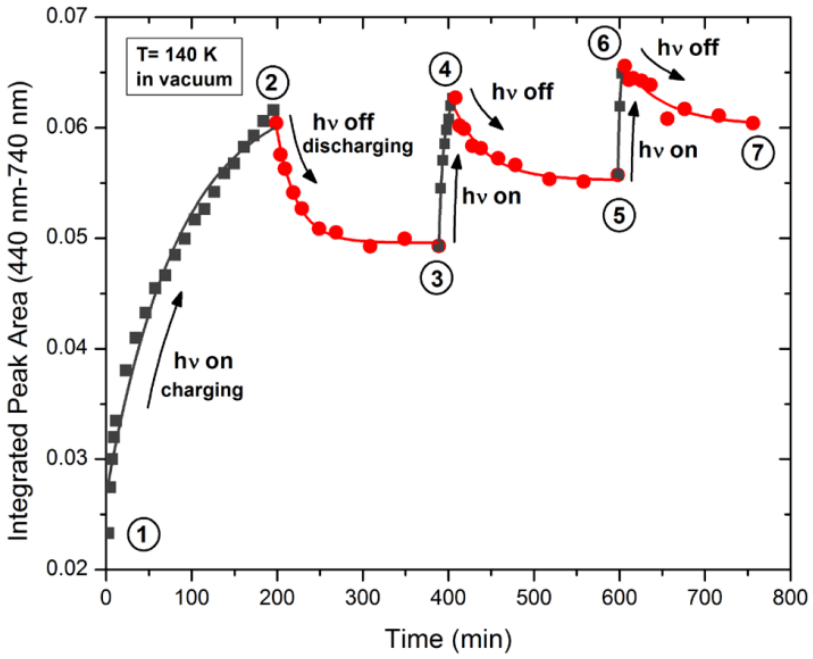

Figure 3. Photoluminescence development upon UV irradiation (gray squares) and relaxation in the dark (red circles) at 140 K in vacuum. During the three UV irradiation cycles (shown by gray squares), the rate of photoluminescence intensity increase yields the slowest (k_{1-2}= 2 x 10^{-4} s^{-1}); development in the first cycle and faster (k_{3-4}= 3 x 10^{-4} s^{-1} and k_{5-6}= 3 x 10^{-3} s^{-1}) development during the second and third irradiation cycle, respectively. Upon interruption of UV light (shown by red circles), the rate of change of the PL intensity decreases as time passes giving PL decay rates of k_{2-3}= 7 x 10^{-4} s^{-1}, k_{4-5}= 4 x 10^{-4} $s^{-1}$and k_{6-7}= 3 x 10^{-4} s^{-1}.

C. Adsorbed NH_3 - Immobilization of Surface Charge in Interconnected TiO_2 Particles.

We studied the adsorption of the electron donor molecule NH_3 on TiO_2 particles to determine if the deposition of an immobile charged chemical species would show different behavior from the displacement of mobile electrons. Adsorption of NH_3 is performed at 120 K which is a temperature where electrons are mobile in TiO_2. In Figure 4, the green point shows the PL intensity from a clean n-type TiO_2 surface in vacuum at 120 K which represents an initial upward band bending condition of the n-type material. Upon admission of ~ 8 x 10^{16} NH_3 molecules in

the dark, the PL intensity initially rises as a result of the flattening of the band. Chemisorbed NH_3 causes the partial cancellation of the local negative-outward surface dipole on the outer TiO_2 n-type particle (as shown by red points). Following NH_3 adsorption in the dark at 120 K, the PL intensity remains constant in vacuum for 130 min which implies the presence of a stable surface charge on the TiO_2 particles in the outermost surface.

This experiment strikingly demonstrates the contrasting behavior of mobile electrons as they hop between TiO_2 particles and immobile electrons as they remain attracted by positively charged adsorbate molecules which do not move into the interior of the TiO_2 powder at the temperature employed[36]. The sign of the behavior of the PL intensity and the rate of PL intensity change is a measure of the mobility and the direction of motion of electrons contrasted to the immobility of electrons upon adsorption of positively charged molecules.

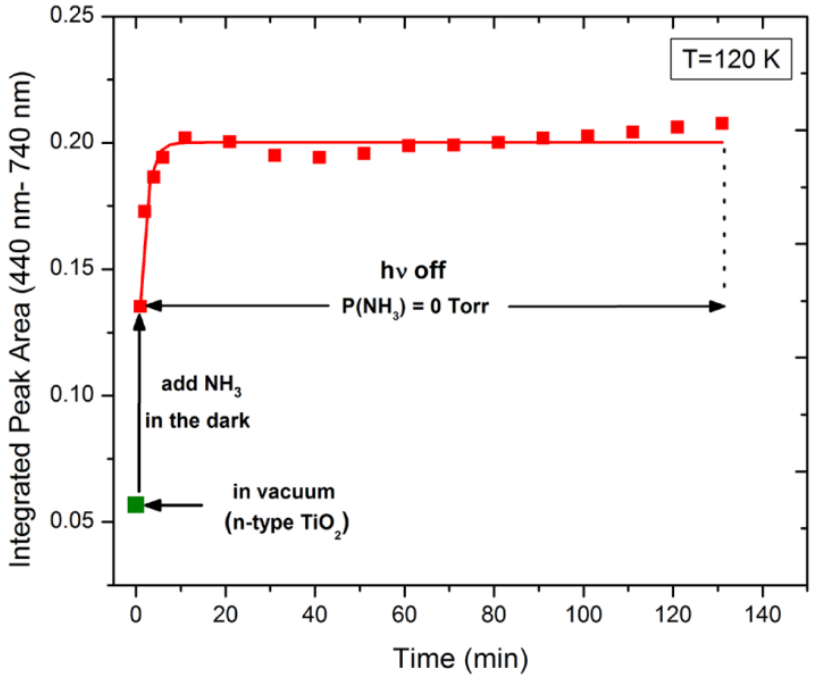

Figure 4. A. Immobilization of charges by chemical means. Adsorption of NH_3 on n-type TiO_2 surface with upward bent bands at 120 K in the dark. Upon admission of ~$8x10^{16}$ molecules of NH_3 (electron

donor molecule), the PL intensity increases quickly as the upward bent bands of TiO_2 flatten and the PL intensity then remains invariant over time in the dark.

D. Temperature Dependence of Charge Migration between TiO_2 Particles.

In Figure 5, the gray points show the normalized PL development under UV irradiation for ~ 184 min in vacuum. Here, the irradiated surface is initially brought to a near-flat band condition. At 184 min the UV light is blocked for 120 min at different temperatures: 84 K; 100 K; 110 K; and 140 K. In the dark, the PL intensity exponentially decreases and the rate of the discharging process increases with rate constants of $k_{84K}= 1.9 \times 10^{-4}\ s^{-1}$; $k_{100K}= 3.5 \times 10^{-4}\ s^{-1}$; $k_{110K}= 3.9 \times 10^{-4}\ s^{-1}$ and $k_{140K}=4.6 \times 10^{-4}\ s^{-1}$ as the temperature is increased from 84 K to 140 K, respectively. Comparing data at all four temperatures, one sees that the rate of charge migration from the TiO_2 interior to the surface is reduced at lower temperatures as judged by the rate of decay of the PL intensity in vacuum in the dark. The inset b. shows the natural logarithm of the rate of charge migration between particles as a function of T^{-1}. Here, the error bar represents a ± 20 % estimated error of the charge migration rate. The activation energy for the electron transfer process is determined from the plot, $E_a= 0.015 \pm 0.008$ eV.

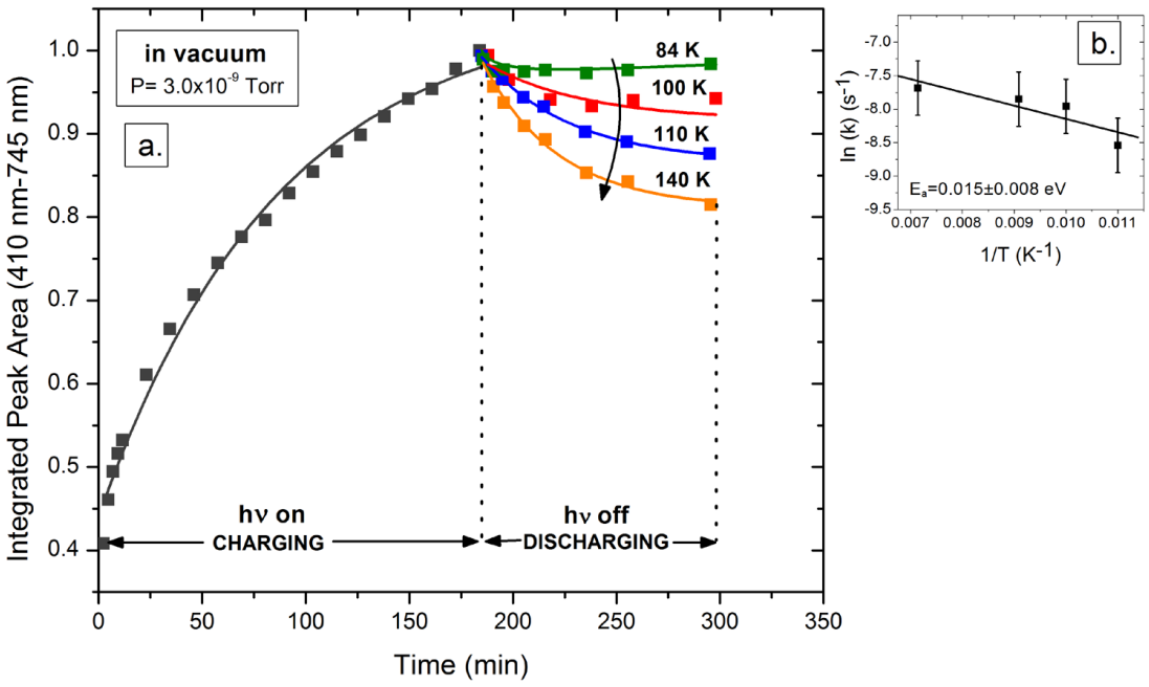

Figure 5. Photoluminescence decay in the dark in vacuum at different temperatures. Gray points represent the PL development upon UV irradiation. The TiO_2 surface is prepared to a near-flat band condition as a saturation PL intensity plateau is almost achieved. Upon interruption of UV light, the PL decrease is observed at different temperatures: 84 K (green); 100 K (red); 110 K (blue) and 140 K (orange). Inset b. shows the natural logarithm of the rate of charge migration in the dark as a function of temperature where the extracted activation energy is 0.015 ± 0.008 eV. The data are normalized at the maximum PL intensity.

IV. Discussion

A. Diffusion of Electrons in TiO_2 Powder.

The planar powdered TiO_2 sample is pressed into rectangular units of dimension 0.022 cm x 0.022 cm x 0.0095 cm thickness inside a tungsten grid. Each small unit is a rectangular block of semiconducting powder with a back and front face exposed to vacuum and with the four edges connecting to tungsten-oxide-coated-W boundaries. This corresponds to a material suspended with vacuum interfaces on the front and back, and with insulating interfaces at the four edges.

The tungsten grid holding the TiO_2 may be considered as an insulating support due to its thick oxide coating[42]. The geometry of each of the TiO_2 units is that of a suspended rectangular-shaped powder matrix without external contact, and it may therefore be considered to be an isolated unit in vacuum.

UV light, incident on the front surface of the powdered matrix, and mainly absorbed by the outermost-TiO_2 particles, causes electron transport into the interior producing a positive surface photovoltage (Figure 1) which serves to flatten the upward bent bands of the outermost particles. This is associated with a PL intensity increase [exponential with time and UV flux (F_{hv})] during long UV light exposures[32] in vacuum as shown in Figure 2. Upon turning the light off, the flattened bands start bending upwards again as negative charge inside the TiO_2 powder senses the more "positively" charged surface, and electrons return by slow hopping back to the surface. Due to the slow electron hopping throughout the powder matrix, the rate constant of decay in Figure 3 of the photovoltage in the dark is slow and is of order 4×10^{-4} s^{-1} at 140 K. The slow hopping of trapped electrons during discharging in the dark in anatase TiO_2 powder was also observed by both EPR spectroscopy[43, 44] and DRIFT-FTIR[45] under high vacuum conditions. This rate constant yields an electron mobility which is seven orders of magnitude smaller than the electron mobility associated with *in situ* electron transport processes in TiO_2 single crystals[25] and must correspond therefore to charge redistribution due to electron hopping over the surface of the TiO_2 particles and/or between TiO_2 particles. The electron transport to the interior particles of the powdered matrix when UV light is on is accompanied by back diffusion of charge to the surface. Hence, the measured rate of change in the PL intensity is the sum of the rate of forward diffusion, driven by UV light, and the rate of back diffusion of electrons. **When UV light is off, the observed PL behavior is directly related only to back diffusion of electrons from the**

interior of the TiO_2 matrix back to the outermost TiO_2 particles which then experience upward band bending and an associated reduction of PL intensity. Here, only a fraction of the bulk electrons migrates back to the TiO_2 surface, as judged by the 20% reduction in PL intensity at 140 K, as most of the electrons are distributed deeper in the powder where long hopping distances reduce electron back diffusion rates to the surface. Most importantly, in the cyclical experiment of Figure 3, electrons are constantly diffusing into the interior as time passes. Figure 6 shows a distribution of electron density, n_e, as time passes and electrons penetrate by diffusion deeper and deeper into the porous TiO_2 particle bed. The inward electron diffusion rate decreases as the gradient of electron density decreases with time. A back diffusion rate component also exists in this picture and as time passes, despite the gradient behavior, the back diffusion rate component will also decrease as electron density spreads to the interior due to the longer diffusion path lengths involved. Since the net rate of electron transport is the sum of the forward component and backward component rates, as time passes for charging experiments with the UV irradiation on, the rate of charging (and hence the rate of increase in the PL intensity) will increase, reflecting the decrease in the back diffusion rate for electrons which have penetrated more deeply into the TiO_2 matrix. Thus, in Figure 3, $k_{5\text{-}6} > k_{3\text{-}4} > k_{1\text{-}2}$. Conversely, as time passes and deeper electron penetration occurs, where the electron path length for back diffusion increases, the rate of back diffusion in Figure 3 will decrease and $k_{2\text{-}3} > k_{4\text{-}5} > k_{6\text{-}7}$. The rate component of back diffusion is a convolution of the electron density gradient and the distances of electron diffusion to reach the surface at $x = 0$.

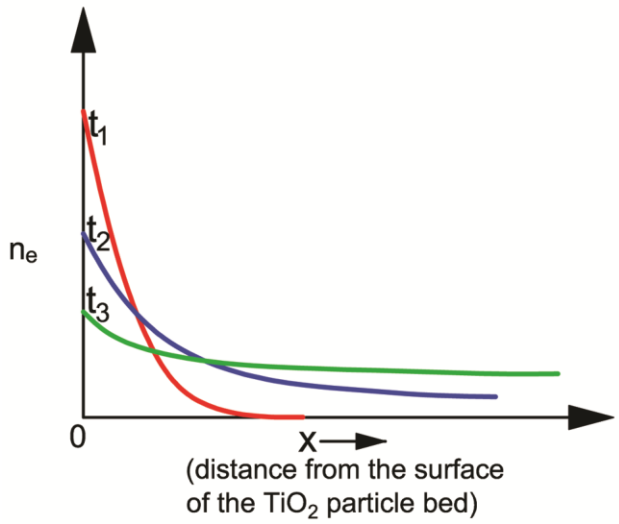

Figure 6. Diffusion of electrons over time in a TiO_2 network. The density of electrons (n_e) at the surface decreases as electrons diffuse deeper into the TiO_2 matrix. As time passes ($t_3>t_2>t_1$) more electrons are distributed into the TiO_2 matrix as shown.

The behavior of mobile electrons is not observed when immobile adsorbate is used to produce surface charging. Thus in Figure 4, the adsorption of NH_3, a donor molecule causing band flattening, is comparable to the production of a positive photovoltage and causes an enhancement of the PL intensity. However, since at 120 K, NH_3 is immobile and does not diffuse or desorb away from the surface of the outermost TiO_2 particle[36], the PL decay effect is not observed since "charge" mobility is absent due to the attraction of immobile NH_3 molecules to interior electrons and a constant surface charge is present. This molecule has the expected effect on the PL intensity and is unlike mobile electrons in dynamical behavior.

B. Temperature Dependence of Electron Hopping through TiO_2 Particles.

An approximate estimate of the effect of temperature on hopping transport has been obtained by measuring the discharge decay behavior of the charged TiO_2 surface at various temperatures.

Figure 5 shows that after charging to a near maximum condition, the decay rate of the discharge process increases as temperature is increased in the range 84 K – 140 K. The Arrhenius plot of these data show that the activation energy for the decay rate is 0.015 ± 0.008 eV. This activation energy relates to the barrier for particle-to-particle transport of electrons where 0.030-0.100 eV activation energies have been found for such transport process in capped CdSe quantum dots and capped silver nanocrystals[46, 47]. Our measurements cannot discriminate an activated process for transport from electron-trap to trap-site on the TiO_2 particle surfaces compared to electron hopping from TiO_2 particle to TiO_2 particle.

C. Estimates of Electron Mobility in Hopping through TiO_2 Particles.

An approximate estimate can be made of the mobility of the electrons using the time constants for decay of charge and crude estimates for the diffusion lengths and electrostatic potential between the fully-charged front face of the TiO_2 powder and the back face. For the fully-charged TiO_2 surface in Figure 5, we measure a discharge rate constant at 140 K of k= 4.6 x 10^{-4} s^{-1}. Assuming that the electrical potential at the TiO_2 front surface is of order of 0.1 V[31, 48], and the thickness of the powder layer is 9.5 x 10^{-5} m, and the dielectric constant of powdered TiO_2 is 100 [49], we estimate that the electric field across the depth of our TiO_2 sample is of order 10^3 V m^{-1}. By extrapolation of the Arrhenius plot in Figure 5, we estimate that the 300 K electron mobility is 1 x 10^{-10} $m^2V^{-1}s^{-1}$. This value is in satisfactory agreement with Nelson's et al. value for electron mobility (1 x 10^{-11} $m^2V^{-1}s^{-1}$ - ~1 x 10^{-10} $m^2V^{-1}s^{-1}$) in a porous TiO_2 network obtained under vacuum conditions by time-of-flight measurements at 300 K[27].

V. Summary of Results

The following results have been obtained from this study of the production and decay of photoluminescence in a compressed TiO_2 powder of n-type material, working in high vacuum with relatively clean surfaces:

1. Discharging rates have been measured as a function of temperature. It has been found that TiO_2 powder, when charged by the surface photovoltage effect on its outer surface by exposure to UV light (3.88 eV), will discharge in the dark as electrons originally transported into the TiO_2 bulk are allowed to back diffuse to the surface.

2. The data obtained from cyclical experiments of charging and discharging indicate that the charge transport can be understood by simple considerations of the behavior of a planar slab of TiO_2 powder.

3. The activation energy for the electron transport process has been measured to be 0.015 ± 0.008 eV in the 84 – 140 K temperature region.

4. An estimate of the electron mobility of 1×10^{-10} $m^2V^{-1}s^{-1}$ has been made for the transport process and the process observed here is very slow compared to *in situ* electron transport processes in crystalline TiO_2. It is assigned to electron hopping either from TiO_2 surface site to surface site, or from nanocrystallite to nanocrystallite in the TiO_2 matrix.

5. Although expected changes in PL intensity are achieved by adsorption of an immobile donor molecule, charge mobility effects in the TiO_2 are not seen as for mobile electrons.

ACKNOWLEDGEMENTS

We acknowledge with thanks the support of this work by the Army Research Office under grant number 55748CH as well as a fellowship for Ana Stevanovic from AES Corp. through the AES Graduate Fellowships in Energy Research Program at the University of Virginia.

References:

1. Hagfeldt, A.; Gratzel, M., Light-Induced Redox Reactions in Nanocrystalline Systems. *Chem. Rev.* **1995,** 95, 49-68.
2. Law, M.; Greene, L. E.; Johnson, J. C.; Saykally, R.; Yang, P. D., Nanowire Dye-Sensitized Solar Cells. *Nat Mater* **2005,** 4, 455-459.
3. Kamat, P. V., Tio2 Nanostructures: Recent Physical Chemistry Advances. *J. Phys. Chem. C* **2012,** 116, 11849-11851.
4. O'Regan, B.; Gratzel, M., A Low-Cost, High-Efficiency Solar-Cell Based on Dye-Sentisized Collodial Tio_2 Films. *Nature* **1991,** 353, 737-740.
5. Bach, U.; Lupo, D.; Comte, P.; Moser, J. E.; Weissortel, F.; Salbeck, J.; Spreitzer, H.; Gratzel, M., Solid-State Dye-Sensitized Mesoporous Tio2 Solar Cells with High Photon-to-Electron Conversion Efficiencies. *Nature* **1998,** 395, 583-585.
6. Gratzel, M., Photoelectrochemical Cells. *Nature* **2001,** 414, 338-344.
7. Linsebigler, A. L.; Lu, G. Q.; Yates, J. T., Photocatalysis on Tio2 Surfaces - Principles, Mechanisms, and Selected Results. *Chem. Rev.* **1995,** 95, 735-758.
8. Mills, A.; LeHunte, S., An Overview of Semiconductor Photocatalysis. *J. Photochem. Photobiol. A-Chem.* **1997,** 108, 1-35.
9. Fujishima, A.; Zhang, X.; Tryk, D. A., Tio(2) Photocatalysis and Related Surface Phenomena. *Surf. Sci. Rep.* **2008,** 63, 515-582.
10. Thompson, T. L.; Yates, J. T., Surface Science Studies of the Photoactivation of Tio2-New Photochemical Processes. *Chem. Rev.* **2006,** 106, 4428-4453.
11. Crossland, E. J. W.; Noel, N.; Sivaram, V.; Leijtens, T.; Alexander-Webber, J. A.; Snaith, H. J., Mesoporous Tio2 Single Crystals Delivering Enhanced Mobility and Optoelectronic Device Performance. *Nature* **2013,** 495, 215-219.
12. Ducati, C., Materials Science Porosity in a Single Crystal. *Nature* **2013,** 495, 180-181.
13. Gratzel, M., Dye-Sensitized Solid-State Heterojunction Solar Cells. *MRS Bull.* **2005,** 30, 23-27.
14. Duzhko, V.; Timoshenko, V. Y.; Koch, F.; Dittrich, T., Photovoltage in Nanocrystalline Porous Tio_{2}. *Phys. Rev. B.* **2001,** 64, 075204.
15. Schroder, D. K., Surface Voltage and Surface Photovoltage: History, Theory and Applications. *Meas. Sci. Technol.* **2001,** 12, R16-R31.
16. Dittrich, T.; Weidmann, J.; Koch, F.; Uhlendorf, I.; Lauermann, I., Temperature- and Oxygen Partial Pressure-Dependent Electrical Conductivity in Nanoporous Rutile and Anatase. *Appl. Phys. Lett.* **1999,** 75, 3980-3982.
17. Forro, L.; Chauvet, O.; Emin, D.; Zuppiroli, L.; Berger, H.; Levy, F., High-Mobility N-Type Charge-Carriers in Large Single-Crystals of Anatase (Tio2). *J. Appl. Phys.* **1994,** 75, 633-635.
18. Yagi, E.; Hasiguti, R. R.; Aono, M., Electronic Conduction above 4 K of Slightly Reduced Oxygen-Deficient Rutile Tio2-X. *Phys. Rev. B.* **1996,** 54, 7945-7956.
19. Benzaquen, R.; Benzaquen, M.; Charbonneau, S.; Poole, P. J.; Rao, T. S.; Lacelle, C.; Roth, A. P.; Leonelli, R., Evidence from Electrical-Transport and Photoluminescence Spectroscopy of a Band of Localized Deep Donors in High-Purity N-Type Inp Grown by Chemical-Beam Epitaxy. *Phys. Rev. B.* **1994,** 50, 16964-16972.
20. Nelson, J.; Chandler, R. E., Random Walk Models of Charge Transfer and Transport in Dye Sensitized Systems. *Coord. Chem. Rev.* **2004,** 248, 1181-1194.
21. Barzykin, A. V.; Tachiya, M., Mechanism of Charge Recombination in Dye-Sensitized Nanocrystalline Semiconductors: Random Flight Model. *J. Phys. Chem. B* **2002,** 106, 4356-4363.

22. Anta, J. A.; Nelson, J.; Quirke, N., Charge Transport Model for Disordered Materials: Application to Sensitized Tio2. *Phys. Rev. B.* **2002,** 65.
23. Eppler, A. A.; Ballard, I. N.; Nelson, J., Charge Transport in Porous Nanocrystalline Titanium Dioxide. *Physica E-Low-Dimensional Systems & Nanostructures* **2002,** 14, 197-202.
24. Cao, F.; Oskam, G.; Meyer, G. J.; Searson, P. C., Electron Transport in Porous Nanocrystalline Tio2 Photoelectrochemical Cells. *J. Phys. Chem.* **1996,** 100, 17021-17027.
25. Hendry, E.; Koeberg, M.; O'Regan, B.; Bonn, M., Local Field Effects on Electron Transport in Nanostructured Tio2 Revealed by Terahertz Spectroscopy. *Nano Lett.* **2006,** 6, 755-759.
26. Dittrich, T.; Lebedev, E. A.; Weidmann, J., Electron Drift Mobility in Porous Tio2 (Anatase). *Phys. Status Solidi A* **1998,** 165, R5-R6.
27. Aduda, B. O.; Ravirajan, P.; Choy, K. L.; Nelson, J., Effect of Morphology on Electron Drift Mobility in Porous Tio2. *Int. J. Photoenergy* **2004,** 6, 141-147.
28. Kopidakis, N.; Schiff, E. A.; Park, N. G.; van de Lagemaat, J.; Frank, A. J., Ambipolar Diffusion of Photocarriers in Electrolyte-Filled, Nanoporous Tio2. *J. Phys. Chem. B* **2000,** 104, 3930-3936.
29. Solbrand, A.; Lindstrom, H.; Rensmo, H.; Hagfeldt, A.; Lindquist, S. E.; Sodergren, S., Electron Transport in the Nanostructured Tio_2-Electrolyte System Studied with Time-Resolved Photocurrents. *J. Phys. Chem. B* **1997,** 101, 2514-2518.
30. Muraoka, Y.; Takubo, N.; Hiroi, Z., Photoinduced Conductivity in Tin Dioxide Thin Films. *J. Appl. Phys.* **2009,** 105.
31. Zhang, Z.; Yates, J. T., Jr., Band Bending in Semiconductors: Chemical and Physical Consequences at Surfaces and Interfaces. *Chem. Rev.* **2012,** 112, 5520-5551.
32. Stevanovic, A.; Buttner, M.; Zhang, Z.; Yates, J. T., Jr., Photoluminescence of Tio2: Effect of Uv Light and Adsorbed Molecules on Surface Band Structure. *J. Am. Chem. Soc.* **2012,** 134, 324-32.
33. Eagles, D. M., *J. Phys. Chem. Solids* **1964,** 25, 1243.
34. Cardona, M. H., G., Optical Properties and Band Structure of Wurtzite-Type Crystals and Rutile. *Phys. Rev. B.* **1964,** 137, A1467.
35. Ghosh, G., *Handbook of Optical Constants of Solids*. Academic Press: 1985.
36. Stevanovic, A.; Yates, J. T., Jr., Probe of Nh(3) and Co Adsorption on the Very Outermost Surface of a Porous Tio(2) Adsorbent Using Photoluminescence Spectroscopy. *Langmuir : the ACS journal of surfaces and colloids* **2012,** 28, 5652-9.
37. Kronik, L.; Shapira, Y., Surface Photovoltage Spectroscopy of Semiconductor Structures: At the Crossroads of Physics, Chemistry and Electrical Engineering. *Surf. Interface Anal.* **2001,** 31, 954-965.
38. Jing, L. Q.; Sun, X. J.; Shang, J.; Cai, W. M.; Xu, Z. L.; Du, Y. G.; Fu, H. G., Review of Surface Photovoltage Spectra of Nano-Sized Semiconductor and Its Applications in Heterogeneous Photocatalysis. *Sol. Energy Mater. Sol. Cells* **2003,** 79, 133-151.
39. Lantz, J. M.; Corn, R. M., Electrostatic-Field Measurements and Band Flattening During Electron-Transfer Processes at Single-Crystal Tio2 Electrodes by Electric-Field-Induced Optical 2nd-Harmonic Generation. *J. Phys. Chem.* **1994,** 98, 4899-4905.
40. Hollingsworth, R. E.; Sites, J. R., Photo-Luminescence Dead Layer in P-Type Inp. *J. Appl. Phys.* **1982,** 53, 5357-5358.
41. Ando, K.; Yamamoto, A.; Yamaguchi, M., Surface Band Bending Effects on Photoluminescence Intensity in N-Inp Schottky and Mis Diodes. *Jpn. J. Appl. Phys.* **1981,** 20, 1107-1112.
42. King, D. A.; Madey, T. E.; Yates, J. T., Interaction Oxygen with Polycrystalline Tungsten .2. Corrosive Oxidation. *J. Chem. Phys.* **1971,** 55, 3247-&.
43. Berger, T.; Sterrer, M.; Diwald, O.; Knozinger, E.; Panayotov, D.; Thompson, T. L.; Yates, J. T., Light-Induced Charge Separation in Anatase Tio2 Particles. *J. Phys. Chem. B* **2005,** 109, 6061-6068.
44. Ke, S. C.; Wang, T. C.; Wong, M. S.; Gopal, N. O., Low Temperature Kinetics and Energetics of the Electron and Hole Traps in Irradiated Tio2 Nanoparticles as Revealed by Epr Spectroscopy. *J. Phys. Chem. B* **2006,** 110, 11628-11634.
45. Szczepankiewicz, S. H.; Moss, J. A.; Hoffmann, M. R., Slow Surface Charge Trapping Kinetics on Irradiated Tio2. *J. Phys. Chem. B* **2002,** 106, 2922-2927.

46. Yu, D.; Wang, C. J.; Wehrenberg, B. L.; Guyot-Sionnest, P., Variable Range Hopping Conduction in Semiconductor Nanocrystal Solids. *Phys. Rev. Lett.* **2004,** 92.
47. Doty, R. C.; Yu, H. B.; Shih, C. K.; Korgel, B. A., Temperature-Dependent Electron Transport through Silver Nanocrystal Superlattices. *J. Phys. Chem. B* **2001,** 105, 8291-8296.
48. Rothschild, A.; Komem, Y.; Levakov, A.; Ashkenasy, N.; Shapira, Y., Electronic and Transport Properties of Reduced and Oxidized Nanocrystalline Tio2 Films. *Appl. Phys. Lett.* **2003,** 82, 574-576.
49. Parker, R. A., Static Dielectric Constant of Rutile (Tio_{2}), 1.6-1060°K. *Phys. Rev. B* **1961,** 124, 1719-1722.

Chapter 6.

Effect of Single Wall Carbon Nanotubes and Au Nanoparticles on Electron Hopping between Photoactive TiO_2 Particles

Unpublished work: (1) **Stevanovic, A**.; Yates, J. T., Jr.,"Molecular Conductor Wires and Electron Hopping between Photoactive TiO_2 Particles", **in preparation.**
(2) **Stevanovic, A**.; Ma, S.; Yates, J. T., Jr.,"Effect of Au nanoparticles on Electron Hopping between TiO_2 Particles", **in preparation.**

I. Introduction

In the optimization of inorganic photovoltaic devices, a major challenge is to enhance the rate of charge transport between semiconductor particles to improve the efficiency of collecting photogenerated electrons by the back electrode[1]. The charge transport phenomenon in metal-oxide semiconductor particles (TiO_2, ZnO and others) has been extensively studied due to the capability of these materials to be photo-activated by sunlight[2-4]. Upon absorption of the light from the solar spectrum that has energy higher than their band gap energy (E_{bg} ~ 3 eV), these metal-oxide semiconductors can be electronically excited. Hence, the charge transport induced by ultraviolet irradiation has been studied by surface photovoltage spectroscopy[5-7], photoluminescence (PL) spectroscopy [8-10] and modeling[11-14]. It was found that photoexcited electrons in the semiconductor particle can move freely in the conduction band or become trapped at a defect site. For such trapped electrons, hopping from a site to a neighbor site or from a particle to a neighbor particle takes place. We previously demonstrated that continuous UV irradiation on n-type TiO_2 electrically charges the TiO_2 powder by distributing photoexcited electrons deep into the TiO_2 powder bed causing the surface photovoltage to become more

positive. However, in the dark, the powder discharges as negative charge relaxes back to the TiO_2 surface, as the charged capacitor discharges by the slow electron hopping process partially restoring negative surface charge[15]. The relaxation of negative charge back to the surface is found to be a very slow process on the minute's time scale at 100 K in contrast to *in situ* transport processes within a single TiO_2 particle which occur on a picosecond time scale in crystalline TiO_2[16].

One way to amplify the rate of charge transport between TiO_2 particles is to link semiconductor particles together with highly conjugated molecules or metal nanoparticles. The addition of these molecules is expected to enhance electrical conductance between TiO_2 particles. The unique electronic properties of single wall carbon nanotubes (SWNT), a highly conjugated molecule with enormous specific surface area, suggests that SWNTs are good candidates for enhancement of the conductance between TiO_2 particles. Its conductivity is related to electron delocalization through its conjugated sp^2 orbitals and thus, this molecule is capable of withdrawing photoexcited charges from TiO_2 particles and possibly assisting in charge conduction between particles[17-19]. Figure 8 shows a SWNT schematically interacting with a TiO_2 particle. The alignment of the bandgap of a semiconductor SWNT molecule to the TiO_2 bandgap is schematically shown and it may be seen that SWNT molecules are expected to behave as acceptor molecules for TiO_2 electrons which have been excited by UV light into the TiO_2 conduction band (CB). The experimentally obtained charge carrier mobility in SWNTs is 10^8 m^2 V^{-1} s^{-1} at room temperature [20, 21]and is strongly governed by the density of defects and by electron scattering by phonons in the material [22]. The carrier mobility controlled by electron hopping between TiO_2 particles[23] is 10^{-10} m^2 V^{-1} s^{-1}, ~18 order of magnitude below SWNT mobility, suggesting the vastly improved conduction should be achieved by doping TiO_2 by SWNTs. It

was reported that SWNTs and other fullerenes enhance inter-particle conduction between TiO_2 particles. Kamat et al.[24-28] studied several nanostructures where molecules such as SWNT, C_{60} and graphene oxide were employed to link TiO_2 semiconductor particles together. Their findings measuring the photocurrent of the TiO_2 that contained SWNT show that carbon nanotube molecules act as electron acceptors and also as conductors as they are capable of withdrawing charge and transporting it away from TiO_2 particles. It should be pointed out that the Kamat's studies are carried in solutions (ethanol or toluene) where our studies involve SWNT-TiO_2 mixtures which have been mechanically prepared and processed at elevated temperatures in vacuum. Another method to enhance the inter-particle charge transport is to decorate TiO_2 powder with Au nanoparticles by their attachment to TiO_2 particles from solution[26].

We present experiments that involve a new photoluminescence decay method developed in our laboratory to measure the enhancement of particle-particle conductivity in vacuum, under well-controlled surface conditions, employing different concentrations of SWNTs to explore their electron accepting and conducting abilities when mixed with TiO_2 particles[23]. This method involves charging of the TiO_2 powder by continuous UV irradiation at 3.88 eV which causes a redistribution of electrons within the TiO_2 powder bed inducing changes in surface photovoltage as observed by an increase of the PL intensity of TiO_2 as shown in Figure 1 (a). In contrast to charging by UV light, upon discontinuation of irradiation, the distributed electrons tend to return back to the surface, partially restoring the surface photovoltage as observed by decrease in the PL intensity as shown in Figure 1(b). The charging and discharging of the TiO_2 powder bed is governed by equations shown in the Figure 1. By employing this method we are able to distinguish between electron acceptor and electron conducting properties of a linker molecule. We found that photoluminescence due to electron-hole recombination in TiO_2 is suppressed as

concentration of SWNTs increases, implying that SWNTs possess electron acceptor capabilities. In addition, we found that incorporation of 1-5 % of SWNTs by weight produced no change in the PL development rate upon continuous UV irradiation. This indicates that the SWNTs do not influence the rate of charging or the rate of the surface photovoltage effect. The rate constants for charging the SWNT-TiO_2 composite and pure TiO_2 are the same. In addition, upon discontinuation of UV excitation, we observe that electrons tend to return to the TiO_2 surface (discharging) without the rate being affected by SWNT molecules. We measured the rate of discharge to be the same for all samples that contained SWNTs, compared to clean TiO_2. In addition, we observed that Au nanoparticles dramatically suppress the electron-hole recombination process in TiO_2 and also significantly reduce the electron hopping rate between TiO_2 particles.

The effect of adsorbed oxygen and other species such as organic molecules and water can be neglected in our experiments as they all are performed under high vacuum conditions, after vacuum processing at high temperatures.

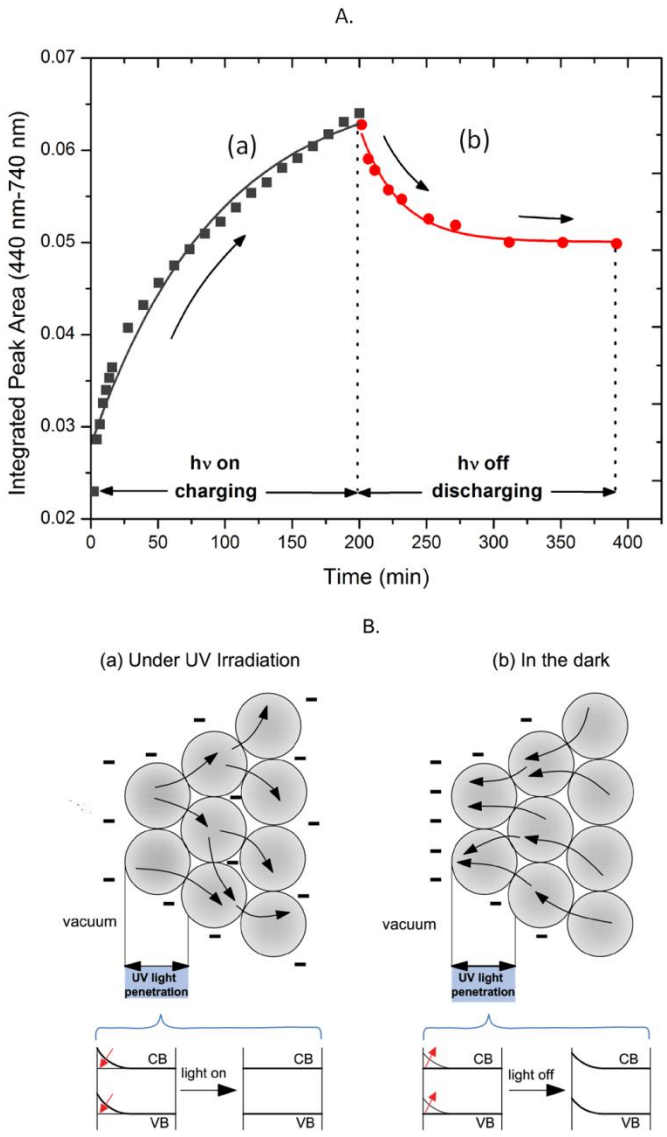

Figure 1. A. Photoluminescence development (a) during continuous irradiation and (b) in the dark; B. Schematic of charging the TiO_2 powder by continuous irradiation induces charge redistribution toward a flat-band condition and discharging in the dark restores upward band bending. Both charging and discharging curves were fitted by single exponential curve with time constants for charging $k_c = 1.6 \times 10^{-4}$ s^{-1} and discharging $k_d = 3.3 \times 10^{-4}$ s^{-1}.

II. Experimental Methods

Photoluminescence and infrared measurements of powdered samples were performed in a continuously pumped high vacuum cell as described previously[8] . In brief, the stainless steel optical cell with two CaF_2 windows allowing both PL and IR measurements, can be moved from a purged IR spectrometer to an adjacent PL spectrometer. The base pressure in the cell after bakeout was ~ 2.0×10^{-9} Torr as measured by a cold cathode gauge or residual gas analyzer (RGA SRS 200). The samples were pressed as 7 mm diameter pellets with 0.095 mm thickness into a tungsten grid with 0.022 cm × 0.022 cm square openings. The mass of each sample was ~ 5.9×10^{-3} g. The grid was clamped to a Cu (OFHC) sample holder which was connected to electrical feedthroughs and mounted on the end of a re-entrant Dewar. The temperature of the samples was monitored by with a K-type thermocouple spot-welded on the center top of the grid and was programable to 0.1 K in the range of 84 and 1000 K using liquid-N_2 cooling and electrical heating.

The PL measurements employed a 320 ± 10 nm (3.88 eV) incident light from a pulsed Xe source with continuous power 9.1×10^{-5} J cm^{-2} s^{-1} (1.5×10^{14} photons cm^{-2} s^{-1}) measured at the sample position. The PL spectra were measured 15° off the specular direction to minimize reflection of incident light from the sample surface and the windows. A cutoff filter at 390 nm was employed on the detector side to minimize the further influence of reflected incident light. During experiments, the sample was continuously exposed to the incident UV radiation unless a shutter was used to block the radiation.

The TiO_2/SWNT composites were synthesized by mixing TiO_2 powder (Evonic Industries, formerly Degussa P-25) and a mixture of metallic (60 %) and semiconducting (40%) SWNT (South West Nanotechnology). Typically, 0.1 g of SWNT was dispersed into deionized

water and sonicated for 10 minutes. To obtain composites with different mass ratios of SWNT to TiO_2, various amounts of TiO_2 were added into the SWNT water slurry and then sonicated for another 10 minutes to better disperse the nanotubes in the TiO_2 slurry. The slurry was dried under vigorous stirring at 353 K and dried TiO_2/SWNT composites with 100:1, 100:3 and 100:5 ratios were produced. Also, the reference sample, pure TiO_2, was suspended in deionized water, sonicated and dried at 353 K. The pure TiO_2 sample was pressed into the upper section of the grid while the TiO_2/SWNT was pressed into the lower section. The two samples were studied on the same grid under identical conditions, by adjusting the vertical position of the grid.

For Au particles, the well-known reduction of $HAuCl_4$ (hydrogen tetrachloroaurate trihydrate) in urea solution was used[29] , giving controlled Au cluster growth located on the admixed TiO_2 particles in the range from a few nanometers in diameter. This method provided Au nanoparticles supported on TiO_2 with the average Au particle size of ~ 3 nm[30].

Before PL and IR measurements, the samples were heated in vacuum to 680 K in 0.1 Torr of research-grade O_2 (99.99%) for 40 min to remove surface impurities and to partially oxidize the sample. The sample was then evacuated at 680 K for 10 min, and then cooled down to 84 K for PL and IR measurements.

An electron micrograph of the TiO_2/SWNT composite is shown in Figure 2 (a) for the 5% mixture. It may be seen that the SWNTs exist primarily in bundles, bonded by van der Waals forces, as they interact with multiple TiO_2 particles. Figure 2 (b) shows an electron micrograph of Au-TiO_2 with a Au particle size distribution that indicates a most probable Au diameter of 3 nm.

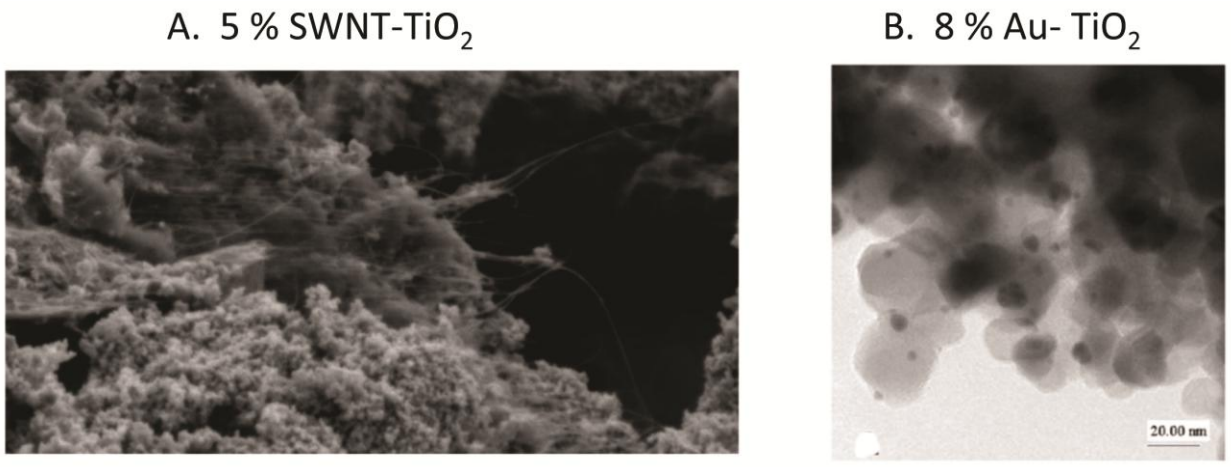

Figure 2. TEM Micrograph of A. 5 % SWNT-TiO_2 composite; B. 8 % Au- TiO_2 composite.

III. Experimental Results

A. SWNT Effect on Electron Hopping between TiO_2 Particles.

Figure 3 shows that PL intensity of TiO_2 when different concentrations of single wall carbon nanotubes are mixed together with TiO_2. The PL peak intensity of clean TiO_2 powder (red spectrum) is compared with PL emission of TiO_2 powders that contain A. 1 %; B. 3 % and C. 5 % of SWNTs (gray spectra). All spectra show the same PL emission peak at ~ 525 nm (2.36 eV) . The small feature at 390 nm is an artifact that originates from the reflection of the incident UV beam off the CaF_2 window and tungsten grid and this is disregarded. The mixed TiO_2-SWNT composites show a decrease in PL intensity to 82 %, 55 % and 40 % respectively, of the PL intensity of the pure TiO_2 sample. The decrease in PL intensity of TiO_2 indicates that a very small amount of SWNTs have a significant effect on electron-hole recombination in TiO_2 particles as carbon nanotubes efficiently delocalize electrons from photoexcited TiO_2 particles. The withdrawing of photogenerated electrons by SWNT reduces the magnitude of electron-hole recombination and hence the photoluminescence intensity.

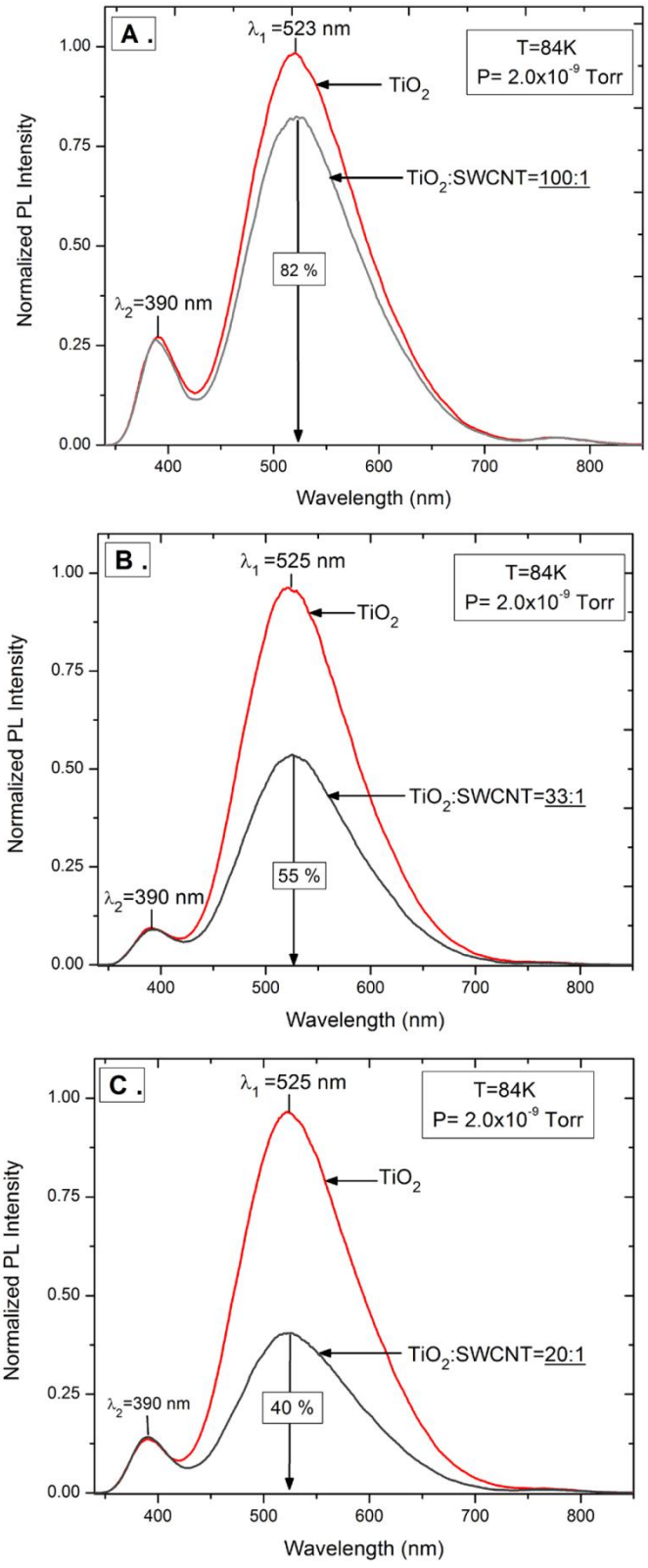
A .
λ1 =523 nm
T=84K
P= 2.0x10-9 Torr
TiO2
TiO2:SWCNT=100:1
82 %
λ2=390 nm
Normalized PL Intensity
Wavelength (nm)
B .
λ1 =525 nm
T=84K
P= 2.0x10-9 Torr
TiO2
TiO2:SWCNT=33:1
55 %
λ2=390 nm
Normalized PL Intensity
Wavelength (nm)
C .
λ1 =525 nm
T=84K
P= 2.0x10-9 Torr
TiO2
TiO2:SWCNT=20:1
40 %
λ2=390 nm
Normalized PL Intensity
Wavelength (nm)

Figure 3. Photoluminescence spectra of clean TiO_2 (red curve) and TiO_2-SWCNT composites (gray curves). The mixed TiO_2-SWNT composites contain: A. 1 %; B. 3 % and C. 5 % of SWNTs in TiO_2 powder. All samples show an emission maximum at ~ 525 nm upon excitation by 3.88 eV (320 nm) irradiation in vacuum at 84 K. Spectra from TiO_2 that contain SWNTs are normalized to the spectrum of the clean TiO_2 reference sample present in each experiment; the two measurements are carried out by sample transition in the cell.

Figure 4 shows the charging and discharging rates for several TiO_2 samples that contain 0%, 1%, 3% and 5% of SWNT at 110 K under vacuum. Our previous finding[23]indicated that electrons show hopping mobility at this temperature where electron hopping occurs with an activation energy of 15 meV. During continuous UV irradiation with 3.88 eV photons for 185 min in vacuum, the PL intensity of all TiO_2-SWNT composites is enhanced with very similar PL development rates related to the increase of surface photovoltage in the powdered samples. On the other hand, when the UV irradiation was discontinued, the PL intensity shows a decrease. These measurements show that TiO_2-containing single wall carbon nanotubes, while acting as electron acceptors by reducing the PL intensity, show the same charging/discharging rates as pure TiO_2 powder at a constant temperature. The inset shows the charging/discharging rates as the concentration of SWNTs increases. The average charging rate at 110 K is $k_c \sim 1.4 \times 10^{-4}\ s^{-1}$, while the average discharging rate at 110 K is $k_d \sim 3.4 \times 10^{-4}\ s^{-1}$. This result implies that SWNTs which connect TiO_2 particles absorb electrons or interfere with electron-hole recombination, but do not have any measurable effect on discharge rate of electrical conduction between TiO_2 particles. Since the time constants for charging are very similar for all samples, we show only one charging curve (gray squares) in Figure 4 which is an average of all charging curves.

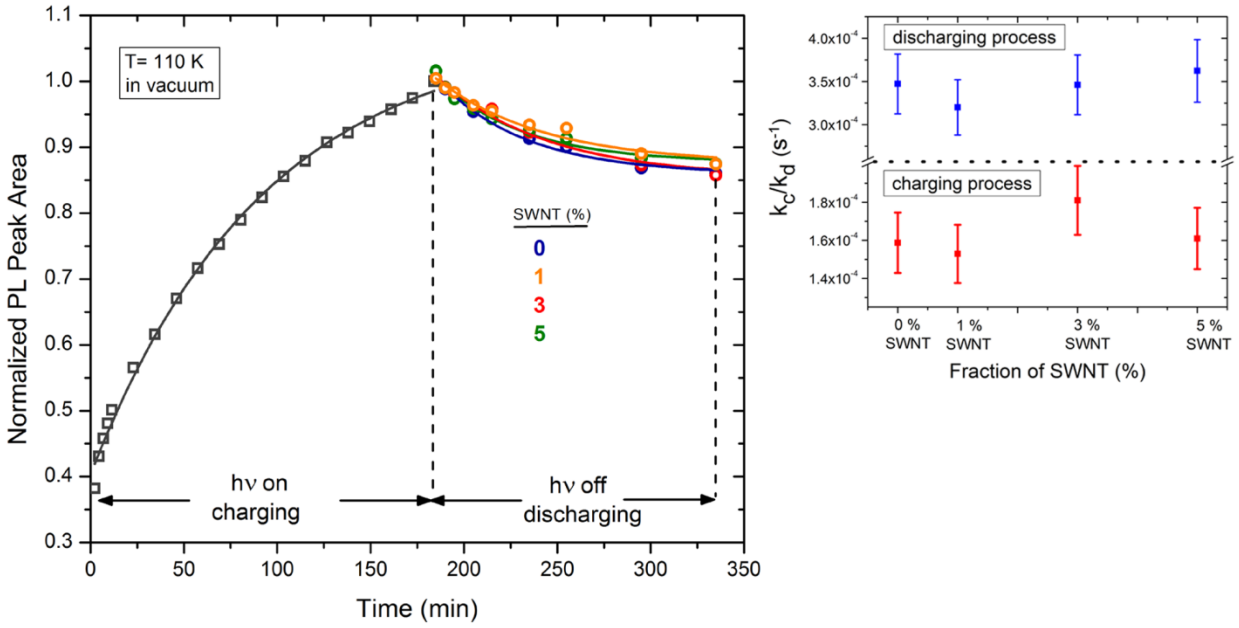

Figure 4. Charging curve (gray squares) is obtained upon continuous UV irradiation for 185 min in vacuum. Discharging curves for: clean TiO_2 (blue), 1% SWNT (orange), 3% SWNT (red) and 5 % SWNT (green) upon discontinuation of UV light for 150 min. Inset shows the rates for both charging (red squares) and discharging (blue squares) processes. All data were collected at 110 K in vacuum.

B. Au Effect on Electron Hopping between TiO_2 Particles.

Figure 5 shows the PL spectra of pure TiO_2 and Au/TiO_2 in vacuum measured at 110 K. At 110 K the PL intensity from TiO_2 is smaller than at 84 K (see Figure 3) due to plasmon excitation and subsequent electron scattering. The TiO_2 sample shows a PL peak maximum at about 540 nm (red curve). The PL emission of Au/TiO_2 sample is significantly suppressed compared to the pure TiO_2, and the PL peak almost disappears (gray curve). This result is evidence of Au nanoparticles capturing photoexcited electrons from TiO_2. As a result, the probability for electrons to recombine with holes to generate photoluminescence is suppressed leading to significantly small PL intensity of TiO_2. There are also two peaks observed at 390 and 780 nm in Figure 5. The peak at 390 nm is due to a small amount of reflected incident radiation off the CaF_2 window and the tungsten grid while the peak at 780 nm is a second-order feature of

the 390 nm reflected light. Both peaks remained invariant during the experiment. In addition, the two peaks are obsereved when the PL spectrum of an empty portion of the W- grid was recorded.

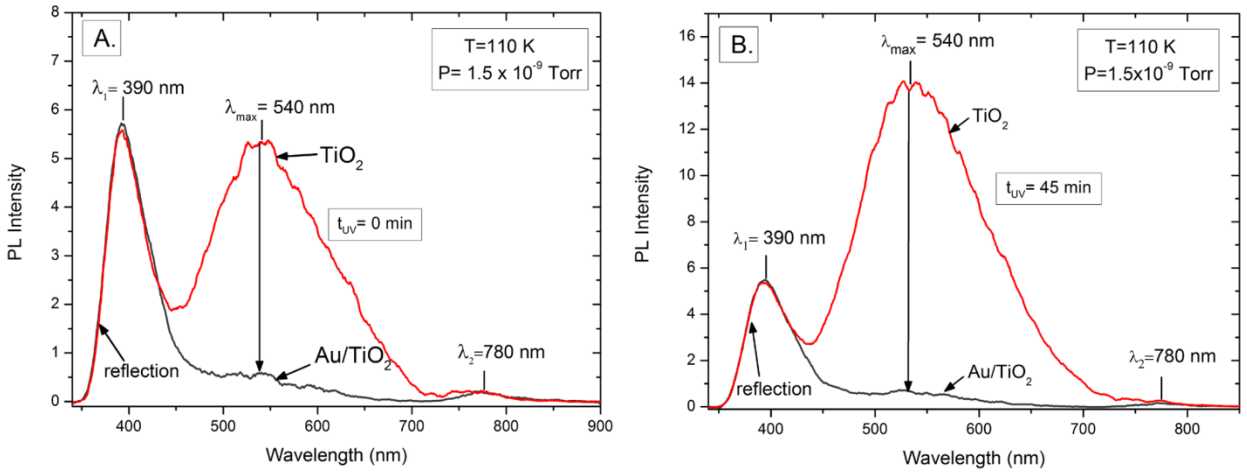

Figure 5. Photoluminescence spectra of pure TiO_2 (red spectra) and Au/TiO_2 (gray spectra) in vacuum at 110 K. The PL emission shows maximum at ~ 540 nm when excited by 320 nm (3.88 eV) light. A. PL spectra before UV irradiation; B. PL spectra after 45 min of continuous UV irradiation. The PL intensity of TiO_2 is significantly suppressed in the Au/TiO_2 sample. The peak at 390 nm and a second-order feature at 780 nm is due to reflection of the incident light from both CaF_2 window and the tungsten grid.

Figure 6 shows the PL development behavior during continuous 320 nm irradiation in vacuum at 110 K for both TiO_2 (red squares) and Au/TiO_2 (gray squares) samples. For TiO_2, the PL signal increases exponentially with continuous exposure to UV irradiation. This PL development is associated with a decrease in the degree of upward band bending in n-type TiO_2 [8] as holes from the valence band diffuse to the surface causing an increase in positive surface photovoltage. As a result, the depletion layer contracts, providing more PL active sites and the PL emission is enhanced. Unlike TiO_2, the Au/TiO_2 sample shows very low PL emission which is invariant during continuous UV irradiation for 95 min.

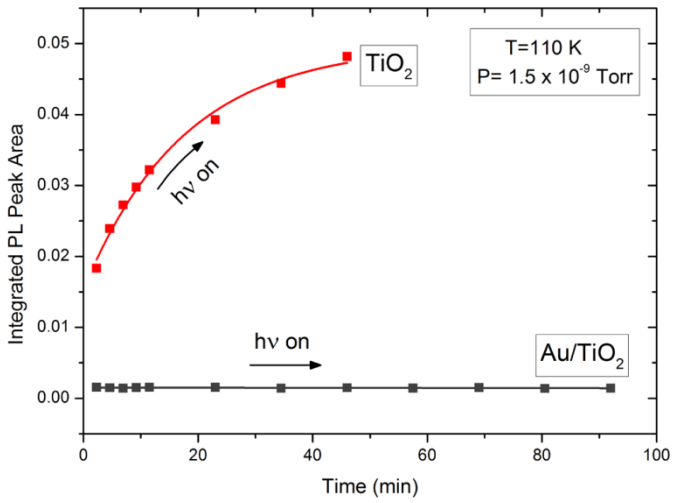

Figure 6. Photoluminescence development of TiO_2 (red curve) and Au/TiO_2 (gray curve) upon continuous UV irradiation of 3.88 eV ($\lambda_{exc.}$= 320 nm) in vacuum at 110 K. Upon continuous UV irradiation, the PL development for TiO_2 shows an exponential increase in the PL signal. The PL emission of Au/TiO_2 sample is diminished and the PL development completely suppressed.

Figure 7 shows schematic of charge transfer between TiO_2 and Au nanoparticles. The Au particles are capable of accepting negative surface charge and also photoexcited electrons from the conduction band or a defect site in TiO_2 particle. During the continuous UV irradiation, the excited electrons favorably transfer to Au particles where they are trapped for long periods of time (Figure 7D). As a result, the recombination process of electrons and holes in TiO_2 is strongly suppressed as indicated by very low PL intensity for the Au/TiO_2 sample. Because of the band bending, the holes may migrate to the surface of TiO_2. However, the holes in the TiO_2 particle tend to reach the interface where they may recombine with the trapped electrons in Au nanoparticles emitting heat. There are two important processes: (1) electrons are trapped by Au nanoparticles; and (2) photogenerated holes in TiO_2 recombine with trapped electrons in Au.

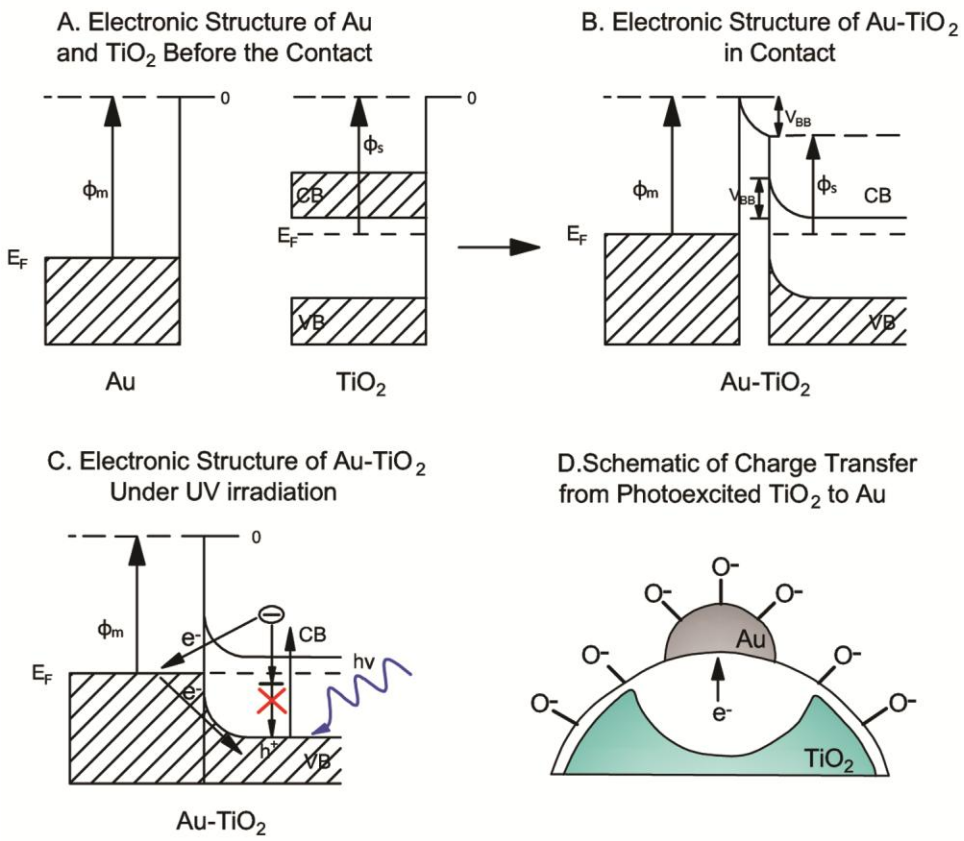

Figure 7. A. Electronic structure of Au and TiO_2 before the contact; B. Electronic structure of Au and TiO_2 after the contact; C. Electronic structure of Au -TiO_2 upon photoexcitation of TiO_2. Gold nanoparticles are capable of accepting negative surface charge and also electrons from the conduction band resulting in suppressed PL signal. Possible channel for the Au nanoparticles to discharge is through recombination of trapped electrons in the Au particles with holes in TiO_2. This recombination process results in heat emission; D. Schematic of photoexcited charge withdrawal from TiO_2 to Au nanoparticles.

IV. Discussion

As shown in Figure 8, the energy of the conduction band of TiO_2 when coupled with metallic or semiconductor nanotubes is always higher than the energy of the conduction band of a SWNT which results in energetically favorable transfer of photoexcited electrons from TiO_2 to the conduction band of carbon nanotubes. Upon excitation of TiO_2 by UV irradiation, photogenerated electrons in the conduction band of TiO_2 can evolve in one of the following

ways: (1) de-excite to the bottom of the conduction band and quickly find a defect site within TiO_2 where they can recombine with a hole, emitting PL light or heat; or (2) de-excite by transferring to the lower energy conduction band of a carbon nanotube resulting in suppressed PL emission from TiO_2 particles. We observe that SWNTs behave as electron acceptor molecules as all samples which contained different fraction of SWNT in TiO_2 powder show systematically suppressed PL intensity relative to the pure TiO_2 powder. The PL suppression scales with the SWNT fraction.

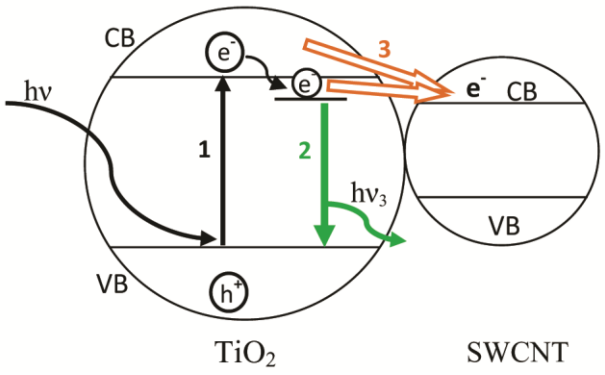

Figure 8. Schematic diagram of proposed mechanism for electron transfer from TiO_2 to SWNT. The electrons from the valence band in TiO_2 are promoted to the conduction band by absorption of photon energy of $h\nu \geq 3.2eV$ (process 1); then they either relax to a TiO_2 defect site recombining with a hole and emitting PL light $h\nu_2$ (process 2) or they transfer to an adjacent SWNT (process 3), where PL at 525 nm does not occur.

During continuous UV irradiation of both the pure TiO_2 and the SWNT-TiO_2 sample, we observed that charging rates for samples that contained SWNT do not differ from the charging rate of a pure TiO_2 sample. Here, the average charging rate is $k_c = 1.6 \times 10^{-4}\ s^{-1}$. Hence, the SWNT have no influence on the charge hopping between TiO_2 particles. In addition, upon discontinuation of UV irradiation, the discharging rates for both SWNT samples and pure TiO_2 are similar with an average time constant $k_d = 3.3 \times 10^{-4}\ s^{-1}$. The increase in SWNT fraction in

powdered samples had no influence, and does not produce a change in the charging/discharging rates. This result implies that SWNT show only electron accepting properties but do not influence the charge conductance between TiO_2 particles.

In addition, the contact between Au nanoparticles and TiO_2 particles induces a Schottky barrier between the metal and the semiconductor as shown in Figure 7A and 7B. The maximum potential energy of electrons in Au particles (the Au Fermi energy) is lower than that the potential energy of conduction band (CB) electrons in TiO_2 which results in electron flow from TiO_2 to Au particles. This electron transfer causes Fermi level shifting until the equilibrium is reached and the Schottky barrier is established upon Fermi energy alignment. As a result, the conduction and valance bands in TiO_2 bend upwards.

The photoluminescence observes the charge recombination in TiO_2 particles and provides an insight about the location of the photoexcited electrons in the Au-TiO_2 sample. Here, the electron-hole recombination in TiO_2 is dramatically suppressed when Au nanoparticles are in contact with TiO_2 compared to the pure TiO_2 sample. This result implies that Au nanoparticles act as electron acceptors trapping nearly all the excited electrons causing strong suppression of the PL signal in TiO_2 particles. During continuous UV irradiation, photoexcited electrons in the pure TiO_2 are displaced deeply into the bulk of the material causing a decrease in the surface photovoltage and enhanced PL intensity emission as bands flatten. However, continuous UV irradiation of the Au-TiO_2 sample shows significantly low PL emission and almost no change in the PL intensity during irradiation indicating that Au nanoparticles trap negative charge away from TiO_2. Here, the electron hopping between TiO_2 particles is inhibited by Au nanoparticles as photoexcited electrons are scavenged away by gold. Ultimately, Au nanoparticles will be electron saturated after long UV exposures and the discharge of Au particles may occur through

a recombination channel where electrons in the Au recombine with holes in TiO_2 emitting heat instead of light.

V. Conclusion

By employing photoluminescence spectroscopy which observes charging/discharging processes in photoexcited TiO_2 we found the following results:

(1) SWNT exhibit electron accepting behavior as the PL intensity of TiO_2-SWNT composites systematically decrease with the increase of the fraction of SWNT in TiO_2 powder.

(2) SWNT do not affect electron hopping between TiO_2 particles as charging/discharging rates are similar to those for pure TiO_2 sample and they are also independent of the fraction of the SWNT in TiO_2 powder.

(3) Gold nanoparticles strongly suppress the PL intensity as they are excellent electron acceptors.

(4) Because Au traps photogenerated electrons the surface photovoltage phenomenon is not observed on Au-TiO_2 , and charging/discharging phenomena do not occur.

References:

1. Gratzel, M., Dye-Sensitized Solid-State Heterojunction Solar Cells. *MRS Bull.* **2005,** 30, 23-27.
2. Linsebigler, A. L.; Lu, G. Q.; Yates, J. T., Photocatalysis on Tio2 Surfaces - Principles, Mechanisms, and Selected Results. *Chem. Rev.* **1995,** 95, 735-758.
3. Diebold, U., The Surface Science of Titanium Dioxide. *Surf. Sci. Rep.* **2003,** 48, 53-229.
4. Fujishima, A.; Zhang, X.; Tryk, D. A., Tio(2) Photocatalysis and Related Surface Phenomena. *Surf. Sci. Rep.* **2008,** 63, 515-582.
5. Kronik, L.; Shapira, Y., Surface Photovoltage Spectroscopy of Semiconductor Structures: At the Crossroads of Physics, Chemistry and Electrical Engineering. *Surf. Interface Anal.* **2001,** 31, 954-965.
6. Duzhko, V.; Timoshenko, V. Y.; Koch, F.; Dittrich, T., Photovoltage in Nanocrystalline Porous Tio_{2}. *Phys. Rev. B.* **2001,** 64, 075204.
7. Jing, L. Q.; Sun, X. J.; Shang, J.; Cai, W. M.; Xu, Z. L.; Du, Y. G.; Fu, H. G., Review of Surface Photovoltage Spectra of Nano-Sized Semiconductor and Its Applications in Heterogeneous Photocatalysis. *Sol. Energy Mater. Sol. Cells* **2003,** 79, 133-151.
8. Stevanovic, A.; Buttner, M.; Zhang, Z.; Yates, J. T., Jr., Photoluminescence of Tio2: Effect of Uv Light and Adsorbed Molecules on Surface Band Structure. *J. Am. Chem. Soc.* **2012,** 134, 324-32.
9. Anpo, M.; Chiba, K.; Tomonari, M.; Coluccia, S.; Che, M.; Fox, M. A., Photocatalysis on Native and Platinum-Loaded Tio2 and Zno Catalysts-Origin of Different Reactivities on Wet and Dry Metal-Oxides. *Bull. Chem. Soc. Jpn.* **1991,** 64, 543-551.
10. Idriss, H.; Andrews, R. M.; Barteau, M. A., Application of Luminescence Techniques to Probe Surface-Adsorbate Interactions on Oxide Single-Crystals. *Journal of Vacuum Science & Technology a-Vacuum Surfaces and Films* **1993,** 11, 209-218.
11. Nelson, J.; Chandler, R. E., Random Walk Models of Charge Transfer and Transport in Dye Sensitized Systems. *Coord. Chem. Rev.* **2004,** 248, 1181-1194.
12. Barzykin, A. V.; Tachiya, M., Mechanism of Charge Recombination in Dye-Sensitized Nanocrystalline Semiconductors: Random Flight Model. *J. Phys. Chem. B* **2002,** 106, 4356-4363.
13. Anta, J. A.; Nelson, J.; Quirke, N., Charge Transport Model for Disordered Materials: Application to Sensitized Tio2. *Phys. Rev. B.* **2002,** 65.
14. Vanmaekelbergh, D.; de Jongh, P. E., Driving Force for Electron Transport in Porous Nanostructured Photoelectrodes. *J. Phys. Chem. B* **1999,** 103, 747-750.
15. Stevanovic, A.; Yates, J. T., Jr., Probe of Nh(3) and Co Adsorption on the Very Outermost Surface of a Porous Tio(2) Adsorbent Using Photoluminescence Spectroscopy. *Langmuir : the ACS journal of surfaces and colloids* **2012,** 28, 5652-9.
16. Hendry, E.; Wang, F.; Shan, J.; Heinz, T. F.; Bonn, M., Electron Transport in Tio2 Probed by Thz Time-Domain Spectroscopy. *Phys. Rev. B.* **2004,** 69.
17. Biercuk, M. J.; Ilani, S.; Marcus, C. M.; McEuen, P. L., Electrical Transport in Single-Wall Carbon Nanotubes. *Carbon Nanotubes* **2008,** 111, 455-493.
18. Ilani, S.; McEuen, P. L., Electron Transport in Carbon Nanotubes. In *Annual Review of Condensed Matter Physics, Vol 1*, Langer, J. S., Ed. 2010; Vol. 1, pp 1-25.
19. McEuen, P. L.; Park, J. Y., Electron Transport in Single-Walled Carbon Nanotubes. *MRS Bull.* **2004,** 29, 272-275.
20. Dresselhaus, M. S.; Dresselhaus, G.; Saito, R., Physics of Carbon Nanotubes. *Carbon* **1995,** 33, 883-891.
21. R.Sait;; M.S.Dresselhaus;; G. Dresselhaus, *Physical Properties of Carbon Nanotubes*. Imperial Collegc Press: 1998.
22. Park, J. Y.; Rosenblatt, S.; Yaish, Y.; Sazonova, V.; Ustunel, H.; Braig, S.; Arias, T. A.; Brouwer, P. W.; McEuen, P. L., Electron-Phonon Scattering in Metallic Single-Walled Carbon Nanotubes. *Nano Lett.* **2004,** 4, 517-520.

23. Stevanovic, A.; Yates, J. T., Jr., Electron Hopping through Tio2 Powder: A Study by Photoluminescence Spectroscopy. *J. Phys. Chem. C* **2013,** 117, 24189-24195.
24. Kamat, P. V., Tio2 Nanostructures: Recent Physical Chemistry Advances. *J. Phys. Chem. C* **2012,** 116, 11849-11851.
25. Kongkanand, A.; Dominguez, R. M.; Kamat, P. V., Single Wall Carbon Nanotube Scaffolds for Photoelectrochemical Solar Cells. Capture and Transport of Photogenerated Electrons. *Nano Lett.* **2007,** 7, 676-680.
26. Subramanian, V.; Wolf, E. E.; Kamat, P. V., Catalysis with Tio2/Gold Nanocomposites. Effect of Metal Particle Size on the Fermi Level Equilibration. *J. Am. Chem. Soc.* **2004,** 126, 4943-4950.
27. Vietmeyer, F.; Seger, B.; Kamat, P. V., Anchoring Zno Particles on Functionalized Single Wall Carbon Nanotubes. Excited State Interactions and Charge Collection. *Adv. Mater.* **2007,** 19, 2935-+.
28. Williams, G.; Kamat, P. V., Graphene-Semiconductor Nanocomposites: Excited-State Interactions between Zno Nanoparticles and Graphene Oxide. *Langmuir* **2009,** 25, 13869-13873.
29. Zanella, R.; Giorgio, S.; Henry, C. R.; Louis, C., Alternative Methods for the Preparation of Gold Nanoparticles Supported on Tio2. *J. Phys. Chem. B* **2002,** 106, 7634-7642.
30. Green, I. X.; Tang, W.; Neurock, M.; Yates, J. T., Jr., Spectroscopic Observation of Dual Catalytic Sites During Oxidation of Co on a Au/Tio(2) Catalyst. *Science* **2011,** 333, 736-739.

Appendices

Appendix A. Depletion Layer Thickness in TiO_2 Particles.

Calculations of the depletion layer thickness, D, in 30 nm- anatase and 80 nm-rutile TiO_2 nanoparticles using equation (3):

$$V_{bb}(r_0) = -\frac{k_B T}{2e}\left(\frac{D}{L_D}\right)^2 = \frac{eN_d D^2}{2\varepsilon_r \varepsilon_0}$$

$$D^2 = \frac{V_{bb}(r) 2\varepsilon_r \varepsilon_0}{eN_d}$$

$$V_{bb}(r) = 0.1 - 0.4\,V$$

$$\varepsilon_r = 31 \quad \text{(for anatase)}$$

$$\varepsilon_r = 100 \quad \text{(for rutile)}$$

$$\varepsilon_0 = 8.85 \cdot 10^{-12}\,\frac{F}{m}$$

$$e = 1.6 \cdot 10^{-19}\,C = 1.6 \cdot 10^{-19}\,FV$$

$$N_d = 10^{25}\,m^{-3} \quad \text{(assumed dopant concentration)}$$

Where V_{bb} is band bending in TiO_2; ε_r is relative permittivity; ε_0 is vacuum permittivity; e is elementary charge; N_d is dopant concentration in TiO_2.

$$D = \frac{0.1\,V \cdot 2 \cdot 31 \cdot 8.85 \cdot 10^{-12}\,\frac{F}{m}}{1.6 \cdot 10^{-19}\,F \cdot V \cdot 10^{25}\,\frac{1}{m^3}}$$

or

$$D = \frac{0.4\,V \cdot 2 \cdot 100 \cdot 8.85 \cdot 10^{-12}\,\frac{F}{m}}{1.6 \cdot 10^{-19}\,F \cdot V \cdot 10^{25}\,\frac{1}{m^3}}$$

$$D = 6\,nm - 12\,nm \quad \text{(for **anatase** } TiO_2 \text{ particles)}$$

$$D = 10\,nm - 21\,nm \quad \text{(for **rutile** } TiO_2 \text{ particles)}$$

Appendix B. Electron Mobility at 300 K

The electron hopping rate at 300 K was estimated from the inset in Figure 5 (Chapter 5).The inset is the natural logarithm of the rate of charge migration in the dark as a function of temperature

$$k = k_0 e^{-\frac{E_a}{k_B T}}$$

$$\ln k = \ln k_0 - \frac{E_a}{k_B T}$$

Where interception of the linear plot is $k_0 = -6.16$ and the slope $\tan\alpha = -198.2$.

The activation energy for the electron hopping process was obtained from the slope of the k =f (T):

$$\tan\alpha = -\frac{E_a}{k_B} = -198.2$$

$$k_B = 1.38 \cdot 10^{-23}\frac{J}{K}$$

$$E_a = 0.015\ eV$$

Finally, the electron hopping rate at 300 K is:

$$k = 1.2 \cdot 10^{-3} s^{-1}$$

Electron mobility is:

$$\mu = \frac{\vartheta}{E}$$

Where ϑ- the electron mobility; E -electric field.

Electric field in the TiO_2 powder:

$$E = \frac{V}{d}$$

$V = 0.1\ V$ (typical band bending in TiO_2 particles)

$d = 9.5 \cdot 10^{-5} m$ (thickness of the sample)

$E = 1 \cdot 10^3 \frac{V}{m}$ (electric field within the TiO_2 sample)

Electron mobility at 300 K is:

$$\mu = \frac{9.5 \cdot 10^{-5} m \cdot 1.2 \cdot 10^{-3} s^{-1}}{10^3 \frac{V}{m}}$$

$$\mu = 1 \cdot 10^{-10} \frac{m^2}{Vs}$$

Appendix C1. Dependence of the Photoluminescence Signal on Distance, Δy, from a Focal Point.

A reference fluorescence standard (purchased from Labsphere) was mounted on an XYZ stage as shown in Figure 1. The sample was excited by selecting 340 nm light from the Xe source and using a 340 nm band pass filter. This sample shows two emission peaks at 464 nm and 520 nm. Continuous irradiation of the sample for 120 min (see inset of Figure 1) caused no change in the PL intensity of both peaks. The reference sample was tilted by ~ 15° relative to the front face of the PL spectrometer. Figure 2 shows the change of PL signal with distance, Δy, from the focal point.

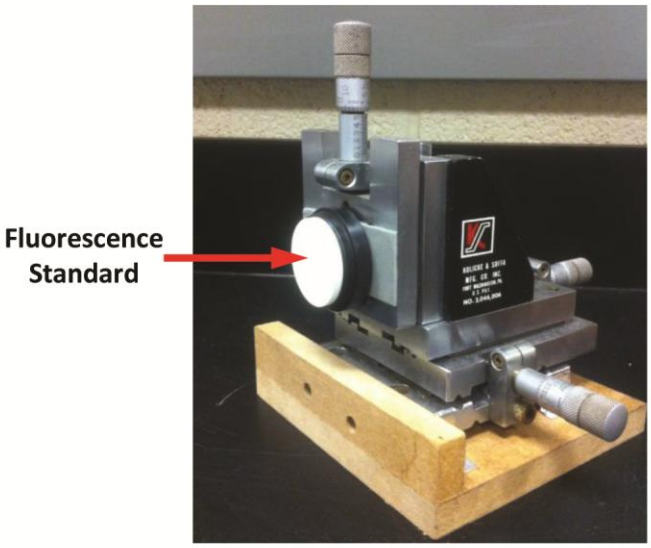

Figure 1. The xyz-stage for holding the reference fluorescence standard.

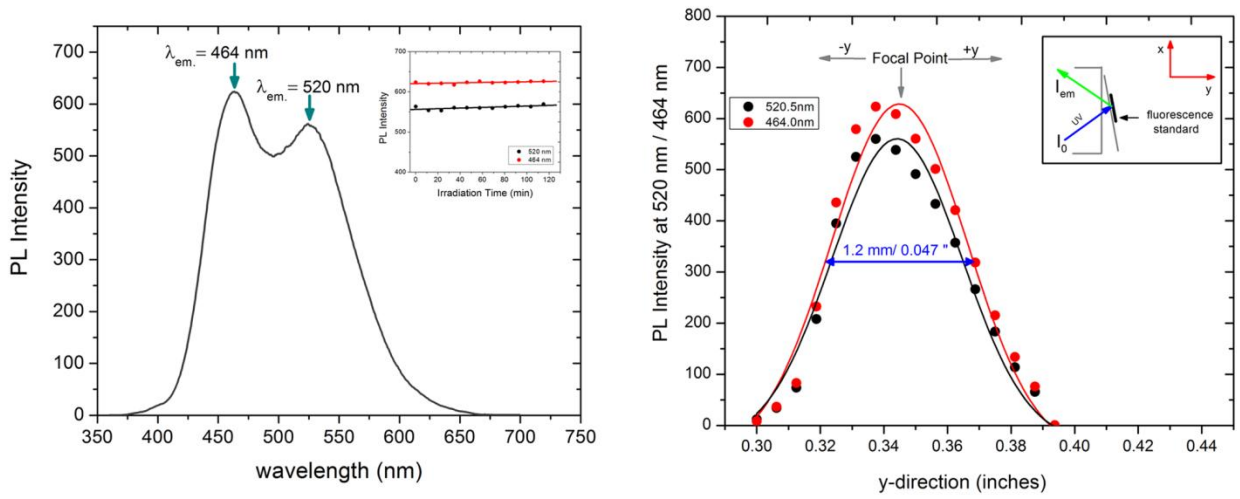

Figure 2. A. Photoluminescence spectra of a reference standard emitting at 464 nm and 520 nm at room temperature. Inset shows that both PL signals are invariant in time during continuous UV irradiation for 120 min. B. PL intensity shows maximum intensity when the sample is placed in the focal point. Moving the sample away from the focal plane by ±1.2 mm causes a 50% decrease in the PL signal.

Sample positioning for PL measurements

Once the high vacuum cell is placed in front of the PL spectrometer, the visible green light (500 nm) from the Xe source is used to position the PL beam on the sample. When the beam is visually positioned, we employ 320 nm light to adjust the angle of the sample by using a screw driven adjustment installed on the back of the high vacuum apparatus. The change in the angle was detected by observing the change in the position of a laser beam that was installed on the high vacuum cell. The maximum change in the angle is ~ 2° and one turn of the screw causes an angular change of 0.0072°. The fine adjustment is achieved by moving the sample with the XYZ manipulator inside the cell until maximum PL intensity is obtained, as shown in Figure 3.

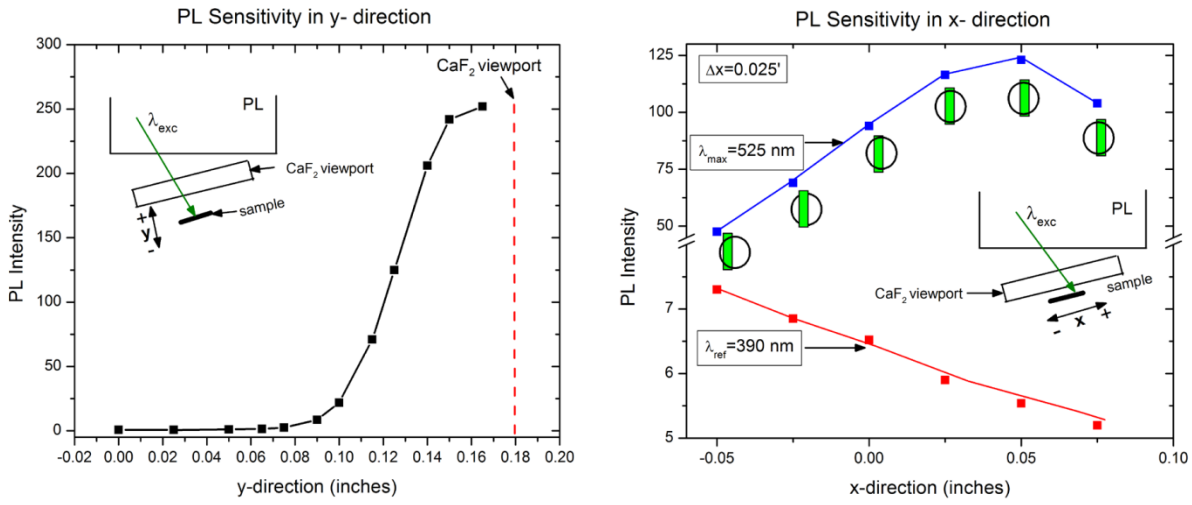

Figure 3. Photoluminescence emission sensitivity on the position in both y and x –directions (right and left hand side graphs). The peak at 390 nm originates from the reflected incident light.

Appendix C2. Calibration of the Manifold and Gas Handling System.

We connected a reference bulb filled with nitrogen gas that has known volume V_0=503.5 cm^3 to the system. Both the manifold and gas handling system are calibrated by N_2 gas expansion into different regions in the system and by reading the pressure by a Baratron gauge (0.001 -10 Torr) in certain volumes, V_f , and using the ideal gas *Boyle–Mariotte law* (see equation 1 and 2*),* we were able to determine all the unknown volumes, V_f, in the system. The gas expansion was performed 3 times.

$$PV = k \qquad for\ T, n = const. \qquad (1)$$

where T is temperature and n is number of molecules.

$$P_i V_i = P_f V_f \qquad (2)$$

1. V_{ref} = 505.3 cm^3 (reference bulb volume)
2. V_0= (2.8 ± 0.1) cm^3 (volume between valve #1 and #2)
3. V_1= (147 ± 1) cm^3
4. V_2= (96 ± 1) cm^3
5. V_3= (51.2 ± 0.4) cm^3
6. V_4 = (1590 ± 40) cm^3

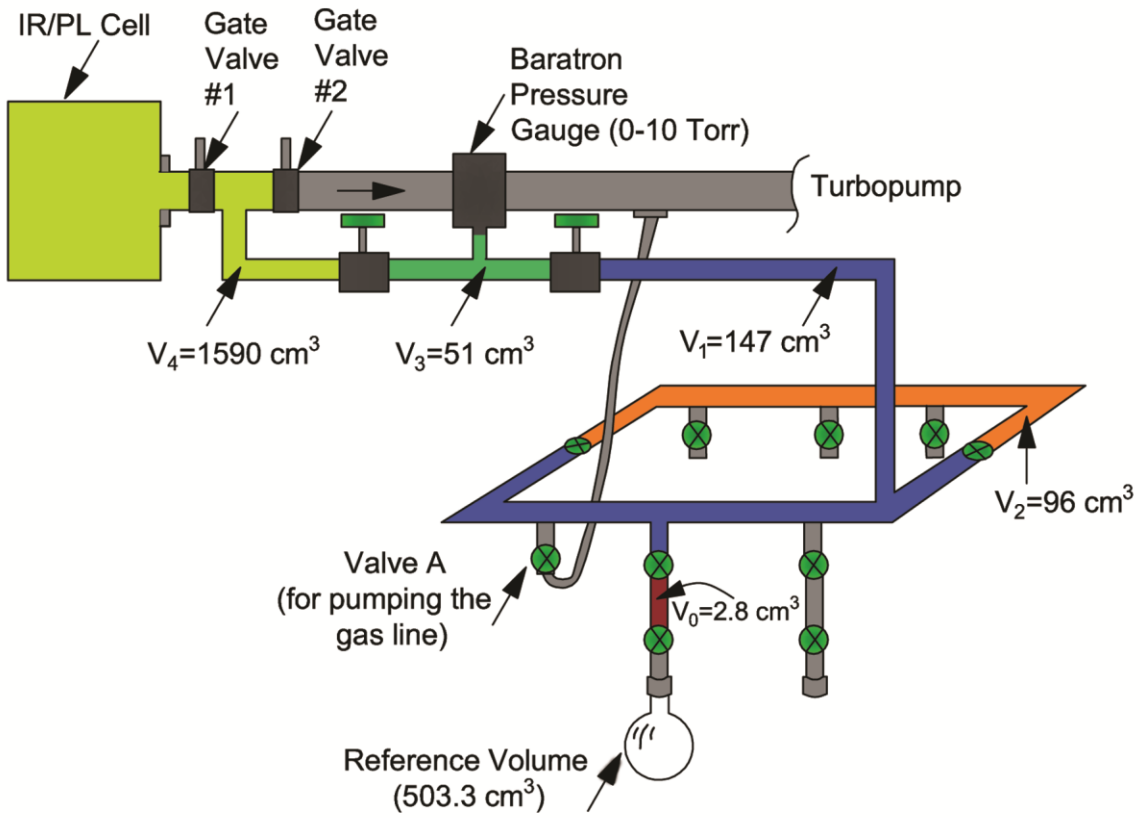

Figure 1. shows the gas handling system and the manifold. The volume in the system was divided in the following sections: V_0-purple; V_1-blue; V_2-orange; V_3-green; and V_4-yellow.

Appendix C3. The Pore Size Distribution and Surface Area of TiO_2.

To determine the pore size distribution and surface area of TiO_2 powder (P-25 Degussa) samples, nitrogen adsorption-desorption measurements were performed at 77 K. The pore size and specific surface area were determined by using Quantachrome Autosorb Automated Gas Sorption System. The sample was previously heated to 680 K for 30 min in vacuum to remove surface contaminants. Once the sample was cleaned, it is brought to a constant temperature by placing it into an external bath (a Dewar flask filled with liquid nitrogen). Then, small amounts of a N_2 gas were admitted in steps into the evacuated sample chamber and the change in its partial pressure was monitored. The surface area is calculated from a monolayer amount using the BET method. The isotherms permit the pore size distribution to be calculated as shown in Figure 2 (right hand side graph). The average pore sizes determined from the shape of the hysteresis loop for TiO_2 powder is ~ 9 nm with a BET surface area of 62 m^2/g.

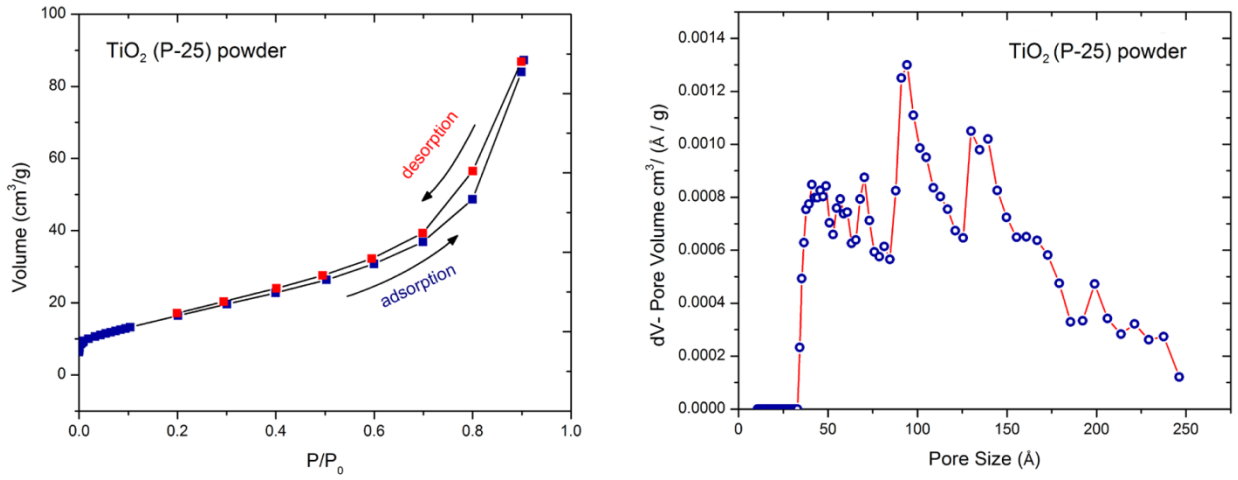

Figure 2. Hysteresis and pore size distribution of TiO_2- P-25 powder heated to 680 K in vacuum for 30 min.

Appendix C4: Monolayer of Gas on Powdered TiO_2 Surface.

Mass of TiO_2 sample: $m(TiO_2) = 6.0\ x10^{-3}\ g$

Powder specific surface area measured by BET: $S(TiO_2) \sim 60\ \frac{m^2}{g}$

Area occupied by one molecule: $A_{molecule} = 10\ Å^2$

Number of molecules to achieve a monolayer on powdered TiO_2 is:

$$n = \frac{surface\ area}{surface\ occupied\ by\ one\ molecule}$$

$$n = \frac{60\ \frac{m^2}{g}\ x\ 6.0\ x10^{-3}\ g}{10\ Å^2}$$

$$n = 3.6\ x\ 10^{18}\ \ molecules$$

Appendix C5. Sample Positioning for the IR Measurements.

Positioning the sample for infrared measurements is obtained by sliding the high vacuum cell into the spectrometer compartment. The cell holder design to hold the cell inside the IR compartment places the cell such that the IR beam passes through the sample grid stretched between the Cu bars (sample holder). Fine positioning is achieved by monitoring the energy of the IR beam that passes through the tungsten grid and the sample. Adjusting the z-direction, the IR beam moves along the grid sensing both the portion of empty W-grid and the powder-filled grid. Figure 1 shows that the amount of energy that reaches the detector after the IR beam passes through the W-grid which is ~ 70 % transparent, is significantly higher than when the IR beam passes through the powdered sample. We use the smallest beam size (J=1.6 mm) to obtain finer spatial resolution.

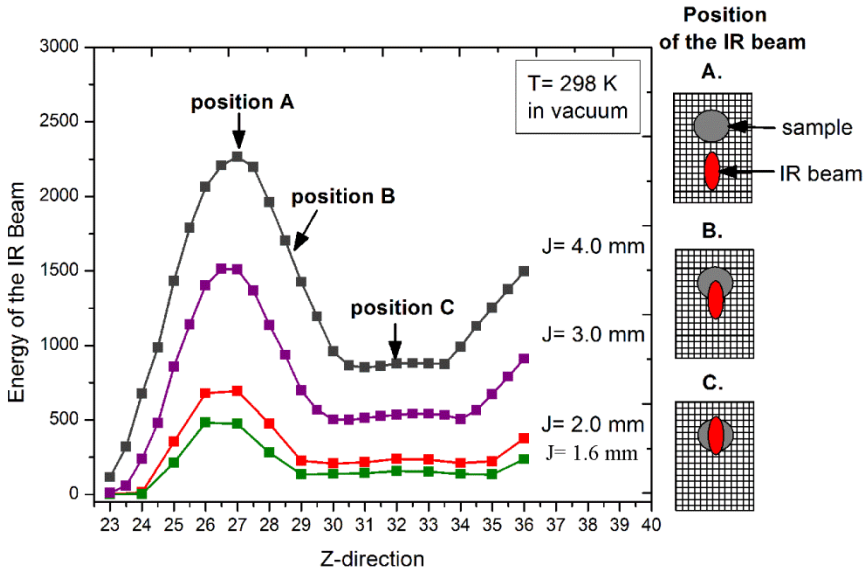

Figure 1. IR beam energy dependence on the transparency of the empty and powdered filled W-grid.

Appendix C6. Temperature-Dependence of the Photoluminescence Emission of TiO_2

The change in photoluminescence intensity of TiO_2 as a function of temperature is shown in Figure 1. Temperature was changed from 87 K to 243 K with an increment of 5 K using 1 K/s heating rate. The PL emission decreases as the temperature of the TiO_2 increases. Inset of Figure 1 shows the plot of the PL peak maximum as a function of temperature. Figure 2 shows the change of PL intensity as a function of reciprocal temperature. An activation energy of 72 meV was extracted from the data that fit equation (1).

$$[PL] = \frac{[PL]_0}{(1+Be^{-\frac{E_a}{k_B T}})} \qquad (1)$$

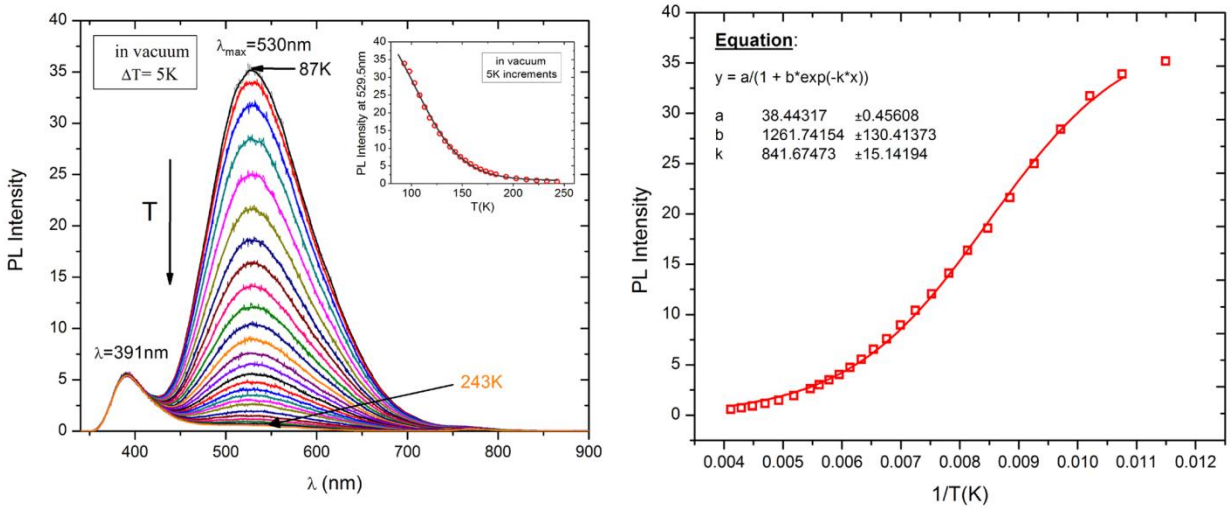

Figure 1. Temeprature-dependence of the photoluminescence intensity of TiO_2 obtained under high vacuum conditions. The PL intensity decreases as temperature is raised from 87 K to 243 K.

Figure 2 shows thermally activated increase of the full width at half-maximum (FWHM) as a function of temperature (left) and reciprocal temperature (right). This thermally activated increase of FWHM is due to the: (1) trap site distribution and (2) electron-phonon interaction.

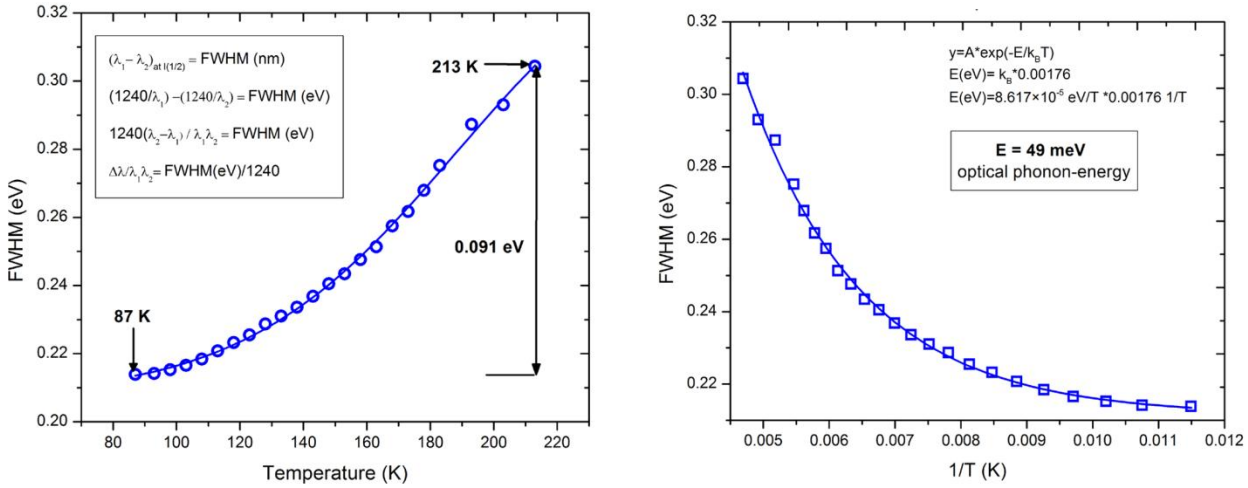

Figure 2. The change of FWHM as a function of temperature (right) and reciprocal temperature (left).

Appendix C7. Calibration of the Perkin-Elmer Xenon Source in Photoluminescence Spectrometer at NIST.

We used a bolometer PM 100D (Thermal Power Sensor S302C, Thorlabs) as a calibrating instrument to measure the flux of the Xe source. Radiation of was captured in an 11 mm dia. "black body" absorber. The beam width of 2 mm in width and 11 mm in length fit across the sensor of the bolometer. The bolometer head was placed in the focal point of the optical path. The bolometer and bench were shielded for outside light by plastic panels. First the background irradiation was collected when the source light was turned off. Then, the light was turned on and irradiation at 320 nm was collected over time while employing a 320 nm band pass filter. From this data, we are able to calculate the flux of light at 320 nm:

$$F_{h\nu}(320\ nm\ ) = \frac{0.02\ x\ 10^{-3}\frac{J}{s}}{0.22\ cm^2}\ x\ \frac{1}{3.88\ eV\ x\ 1.60\ x\ 10^{19}\frac{J}{eV}} =$$

$$F_{h\nu}(320\ nm\ ) = 1.46\ x\ 10^{14}\ \frac{photons}{cm^2 s}$$

If we assume ~ 10 nm penetration depth of 320 nm light, the influenced volume of TiO_2 is:

$$dV = 1cm^2 x10\ nm\ x\ 10^{-9}\ \frac{m}{nm} x\ 10^2\ \frac{cm}{m} =\ 10^{-6}cm^3$$

Density of TiO_2 and molecular weight is: $\rho = 4.2\ \frac{g}{cm^3}$ and $M(TiO_{2)} = 80\frac{g}{mole}$

Number of TiO_2 units in the volume of 10^{-6} cm^3 is:

$$\#(TiO_2\ units) = \frac{4.2\frac{g}{cm^3} x10^{-6}cm^3}{80\frac{g}{mole}} x6.02\ x10^{23}\ \frac{1}{mole}$$

$$\#(TiO_2\ units) = 3.2\ x\ 10^{16}\ TiO_2\ units$$

Number of photons per 68 sec scan is:

$$n_{h\nu} = 1.46\ x\ 10^{14} x\ 68\ s = 9.4\ x\ 10^{15}\ \frac{photons}{cm^2}$$

Hence, during our studies of PL decay in the dark, each measured point involves about 0.3 photon/TiO_2 unit in the irradiated volume. The level of exposure caused almost no change in the PL intensity.

Appendix C8. Sample Position Relative to the Incident Light.

Both the IR/PL cell and the sample in front of the PL spectrometer are tilted by 15° relative to the front face of the PL spectrometer in order to minimize specular reflection of the incident light. The geometry of the sample relative to the PL instrument is shown in Figure 1A. In addition, Figure 1B shows the photoluminescence of clean TiO_2 and the tungsten grid after the heating procedure in O_2 at 680 K. The PL spectra were recorded at 84 K. It is shown that slightly oxidized tungsten grid (WO_x) does not affect the PL spectrum of the TiO_2 sample. Two peaks at 390 nm and 780 nm originate from the reflected incident light from the grid and CaF_2 window.

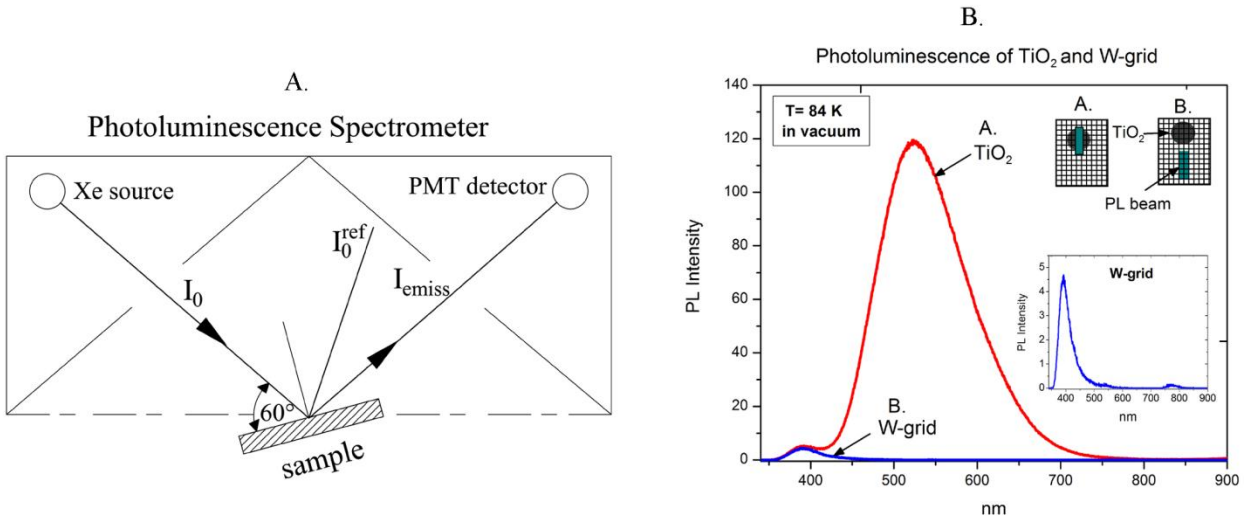

Figure 1. A. The geometry of the sample relative to the incident light; B. Photoluminescence spectra of TiO_2 and W- grid.

Appendix C9. Purging of the IR beam and Spectrometer.

Purging the IR beam by dried-air free of IR-active water and carbon dioxide was obtained by purifying the supplied compressed air using an installed gas line that contains a heater, several oil filters and a purging unit as shown in Figure 1. The purged dried-air is further brought to the IR spectrometer. The purging unit consists of two towers filled with beads that act as adsorbent for CO_2 and H_2O as shown in Figure 2. When ~ 120 psi of the compressed air enters the first tower, most of the CO_2 and H_2O from the compressed air is adsorbed inside the tower. Partially purged air is then sent to a second tower where most of CO_2 and H_2O are removed. The purged gas alternates between the two towers where the portion of the gas is sent into the IR spectrometer. This insures high quality purged air.

Figure 3A shows the IR cell inside of the IR compartment in the spectrometer. The rubber sleeves are held on the window flanges by band clamps and they are compressed against the inner walls of the IR compartment providing a gas-tight seal between the walls and the cell. Figure 3B shows the performance of purging CO_2 and H_2O. The red curve shows the purging performance of the entire compartment when it is sealed with the original lid while the blue curve shows the purging performance of the IR beam line sealed by rubber sleeves. By measuring the decrease in absorbance of H_2O and CO_2, we found that, it takes ~ 500 s to purge the entire compartment. In contrast to that, to purge the much smaller volume within the rubber sleeves, takes only 18 s. Therefore, by using the rubber sleeves we enhanced the purging efficiency by 30 fold.

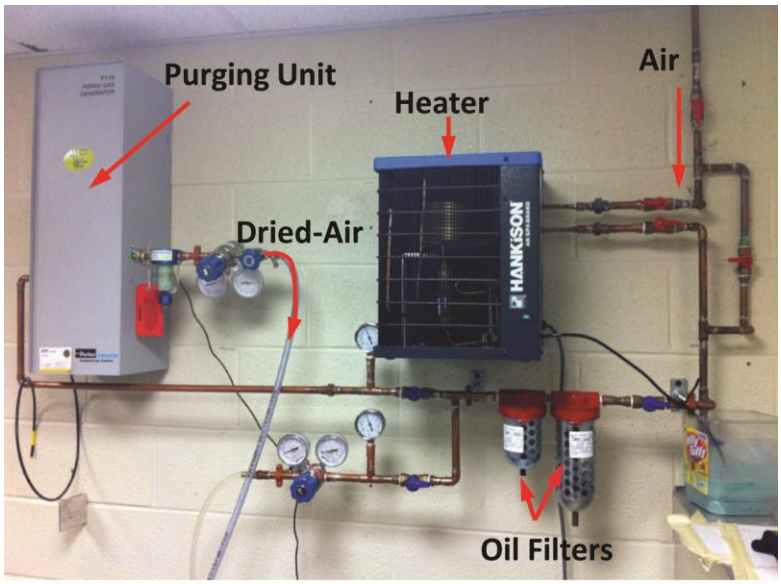

Figure 1. Gas line for making H_2O and CO_2–free dried-air that serves for purging the optics inside the IR spectrometer and IR beam.

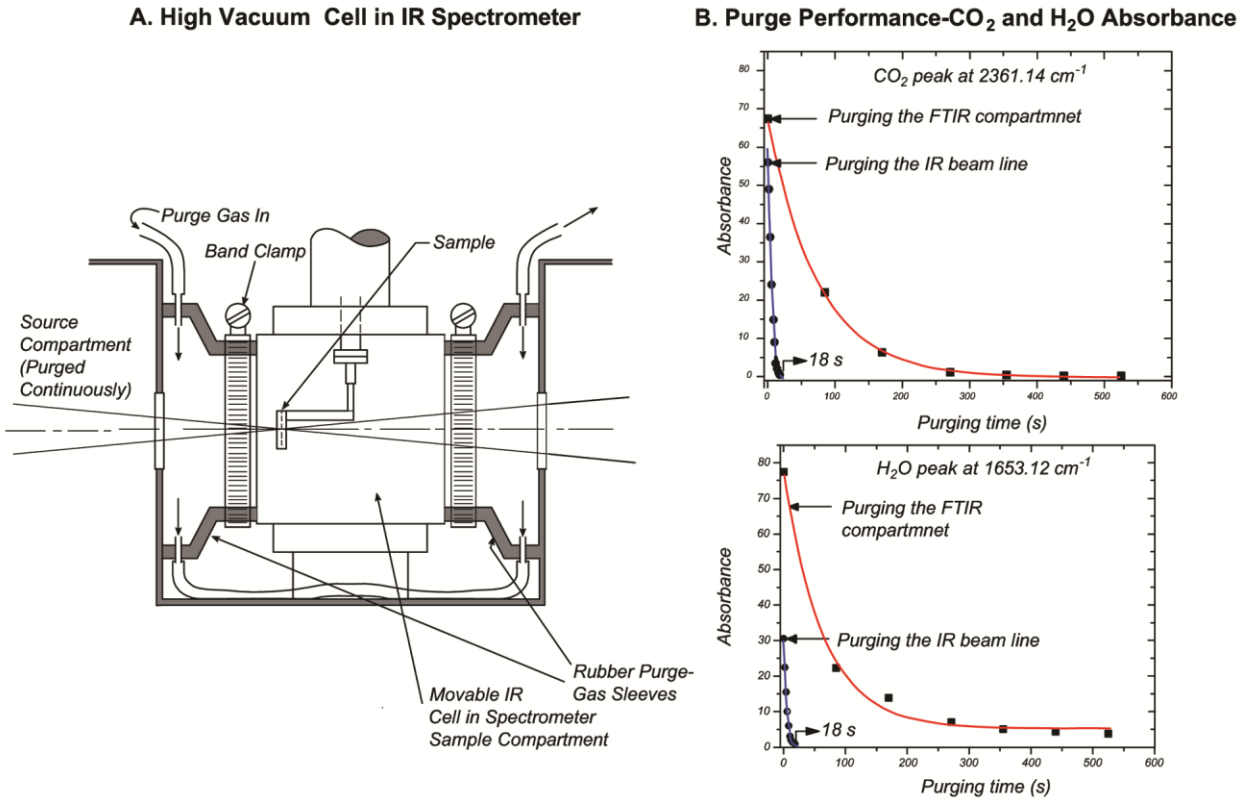

Figure 3A. Purging of the IR beam when high vacuum cell is inside of the IR compartment. B. Purging performance of the IR beam pass through the compartment (red curve) and rubber sleeves (blue curve).

Appendix C10. Number of Sites in TiO_2 Powder Probed by UV and IR Irradiation.

Mass of TiO_2 sample: $m(TiO_2) = 6.0\ x10^{-3}\ g$

Powder specific surface area measured by BET: $S(TiO_2) \sim 60\ \frac{m^2}{g}$

Area occupied by one molecule: $A_{molecule} = 10\ Å^2$

Thickness of TiO_2 sample: $\ell = 0.095\ cm$

UV irradiation (320 nm) penetration depth: $s = 20\ nm$

Number of sites **in a full depth** of TiO_2 powder that are probed by IR irradiation:

$$Surface\ Area = m(TiO_2)xS(TiO_2) = 6.0\ x\ 10^{-3}x\ 60\ \frac{m^2}{g} = 0.36\ m^2$$

$$\#\ of\ sites\ in\ the\ full\ depth\ of\ TiO_2 = \frac{m(TiO_2)xS(TiO_2)}{A_{molecule}} =$$

$$= \frac{0.36\ m^2}{10Å^2} = \frac{0.36\ m^2}{10x10^{-20}m^2}$$

$$\#\ of\ sites\ in\ \boldsymbol{the\ full\ depth}\ of\ TiO_2 = 3.6\ x10^{18}\ sites$$

Number of sites **in the 20 nm region** of TiO_2 powder exposed to UV irradiation:

$$fraction\ of\ illuminated\ sites\ in\ TiO_2 = \frac{s}{l} = \frac{20\ nm}{0.0095\ cm} = 2.10\ x\ 10^{-4}$$

$$\#\ of\ sites\ exposed\ to\ UV\ irradiation\ in\ the\ TiO_2 =$$
$$= (\#\ of\ sites\ in\ the\ full\ depth\ of\ TiO_2)x\ (fraction\ of\ illuminated\ sites\ in\ TiO_2)$$
$$= 2.10\ x\ 10^{-4}x\ 3.6\ x10^{18}$$

$$\#\ of\ UV\ \boldsymbol{illuminated\ sites}\ in\ TiO_2 = \ 7.6\ x\ 10^{14}\ sites$$

Appendix D. List of Publications

1. **Stevanovic, A.**; Buttner, M.; Zhang, Z.; Yates, J. T., Jr., "Photoluminescence of TiO_2: Eeffect of UV Light and adsorbed molecules on surface band structure" **Journal of the American Chemical Society,** 2012, 134, (1), 324-32.

2. **Stevanovic, A**.; Yates, J. T., Jr., "Probe of NH_3 and CO Adsorption on the Very Outermost Surface of a Porous TiO_2 Adsorbent Using Photoluminescence Spectroscopy" **Langmuir** 2012**,** 28, (13), 5652-9.

3. **Stevanovic, A.**; Yates, J. T., Jr., "Electron Hopping Through TiO_2 Powder- A Study by Photoluminescence Spectroscopy" **J.Phys. Chem. C, DOI:** 10.1021/jp407765r.

4. **Stevanovic, A.**; Yates, J. T., Jr.,"Molecular Conductor Wires and Electron Hopping between Photoactive TiO_2 Particles", **in preparation.**

5. **Stevanovic, A.**; Ma, S.; Yates, J. T., Jr.,"Effect of Au nanoparticles on Electron Hopping between TiO_2 Particles", **in preparation.**

6. McEntee M.; **Stevanovic A.;** Yates, J. T., Jr.," Spectroscopic Detection of Adsorbate Induced Charge Transfer between Au Nanoparticles and TiO_2 Support", **in preparation.**